ISBN 978-82-326-2172-9 (printed ver.)
ISBN 978-82-326-2173-6 (electronic ver.)
ISSN 1503-8181

Amir Hayati-Soloot

Doctoral thesis

Doctoral theses at NTNU, 2017:50

Amir Hayati-Soloot

Resonant Overvoltages in Offshore Wind Farms

Analysis, modeling and measurement

Doctoral theses at NTNU, 2017:50

NTNU
Norwegian University of Science and Technology
Thesis for the Degree of
Philosophiae Doctor
Faculty of Information Technology
and Electrical Engineering
Department of Electric Power Engineering

NTNU

NTNU
Norwegian University of
Science and Technology

NTNU
Norwegian University of
Science and Technology

Amir Hayati-Soloot

Resonant Overvoltages in Offshore Wind Farms

Analysis, modeling and measurement

Thesis for the Degree of Philosophiae Doctor

Trondheim, March 2017

Norwegian University of Science and Technology
Faculty of Information Technology and Electrical Engineering
Department of Electric Power Engineering

NTNU
Norwegian University of
Science and Technology

NTNU
Norwegian University of Science and Technology

Thesis for the Degree of Philosophiae Doctor

Faculty of Information Technology and Electrical Engineering
Department of Electric Power Engineering

ISBN 978-82-326-2172-9 (printed ver.)
ISBN 978-82-326-2173-6 (electronic ver.)
ISSN 1503-8181

Doctoral theses at NTNU, 2017:50

Printed by NTNU Grafisk senter

Preface

The thesis is part of the requirements for the Philosophiae Doctor degree at the Norwegian University of Science and Technology (NTNU). The thesis represents four years of my research at NTNU in 2009-2013. The research has been done under the supervision of professor Hans Kristian Høidalen.

I would like to thank Norwegian Research Center for Offshore Wind Farm (NOWITECH) which has been source of funding. Thanks to the great support of NOWITECH, a research-oriented 500 kVA wind turbine transformer is designed and manufactured with which the high-value measurement-based study is carried out. The NOWITECH meetings (*work package 4 meetings*, *DeepWind conferences* and *NOWITECH day*) have been great opportunities to obtain constructive feedbacks on the thesis work. The author appreciates also the great work of Møre Trafo AS for the production of the transformer.

I would like to express my gratitude and sincere thanks to my supervisor, Professor Hans Kristian Høidalen, who have guided me during these years thoroughly so that I could accomplish this task. He has always been supportive and responsive. He provided me with valuable and timely advices. I wish him the very best in his life.

Also, I kindly appreciate Dr. Bjørn Gustavsen, my co supervisor, for giving valuable advice and assistance. He provided me the black box model of 300 kVA 11/0.23 kV transformer which was beneficial as the initial step of my PhD. Furthermore, special thanks should be given to faculty members and fellow PhD students at the electric power engineering department due to energetic and plentiful assistance.

I appreciate the endless support of my parents and finally, I thank my beloved wife, Nazanin Davari, who gave me support, confidence, and hope to carry out my research. Her enthusiasm has been contagious and motivated me to work with full energy.

Trondheim, February 2017

Amir Hayati-Soloot

Abstract

In this thesis, the resonant overvoltages at the terminal and inside wind turbine transformers are studied. The motivation of this study is the requirement for improved transformers for wind farms, especially Offshore Wind Farms (OWF). Compared to conventional medium voltage transformers, these transformers should operate in more onerous conditions; switching operation, harmonics and spikes from converters at LV side, loading cycles and operation under fault conditions. In addition, access for condition monitoring and maintenance is restricted.

The main sources of the resonant overvoltages are energization of transformers with short cables and close-up earth faults. In the case of Wind Turbine Transformers (WTTs), high frequency spikes from power converters can also cause resonant overvoltages, which is out of scope of this thesis.

The first goal is to study resonant overvoltages at the terminal of WTTs. Both energization of a typical offshore wind farm and close-up earth faults are modeled and simulated. The model used for WTT (in this part) is a black-box model based on swept frequency admittance measurements on the transformer terminals. The other important components to be modeled are cables, power converters, Vacuum Circuit Breakers (VCBs) and platform transformer. It is found that resonant overvoltages occur when the frequency of a sustained voltage oscillation at the transformer MV terminals matches with a resonant frequency in the WTT voltage transfer function. Furthermore, this research shows that the appropriate protection scheme against resonant overvoltages is Resistive-Capacitive (RC) filter. The simulation results for a 11/0.230 kV 300 kVA transformer shows that energizing the transformer with a 23 m cable may lead to resonant overvoltage at the LV terminal with a rate of rise of voltage (*du/dt*) equal to 93 p.u./µs if there is not any type of protection installed on the LV terminal. The installation of surge arrester or RC filter can decrease the *du/dt* to 27 or 11 p.u./µs, respectively. Therefore, RC filter is superior to surge arrester as a protection measure against resonant overvoltages. Surge arresters just limit the overvoltage amplitudes while the rate of rise of overvoltages are still high and this can lead to internal resonant overvoltages as reported by other researchers. It should be noted that the main duty of surge arrester is to protect the transformer against lightning overvoltages.

The other goal of this thesis is the investigation of internal resonances. Since the cable lengths in wind turbines are pre-known, the quarter wave frequency of these cables can be obtained. This frequency is the dominant resonant frequency during energization. In this way, the effect of winding designs on the internal resonant overvoltages can be assessed. A 500 kVA 11/0.23 kV with three different windings, i.e. disc, layer and pancake, on three limbs is designed and manufactured for this purpose. Frequency response of the windings for input HV and LV impedances and transferred voltages are measured and compared. The amplitude of transferred voltages to LV terminal at dominant resonant frequencies is more critical for layer and pancake windings compared

to disc winding. Meanwhile, the transferred voltages inside disc winding have many resonant frequencies in the range 100kHz-1MHz.

To draw general conclusions about resonant frequencies of these windings, an analytical lumped-parameter model is developed and verified with measurements. It is observed that the calculations results from the model follow the trend of the measurement for input HV impedance in the case of Layer winding. The resonant frequency at 10kHz is not represented since flux linkage with other phases is not included in the model. This resonant frequency is not also represented for disc and pancake windings. The shortcoming of the model result for layer winding is that the resonant frequencies at 100 and 300 kHz for the measured HV winding is presented with a shift in the calculated model at 50 and 130 kHz.

Except from 10 kHz, the calculation result for HV input disc impedance is in good agreement with measurement for disc winding. The shortcoming is the shift in the resonant frequencies and slight higher amplitude of the calculated results. For the pancake winding, the calculated results for HV impedance has the same decreasing trend and same amplitude range of the measurement results. Same as disc and layer windings, shift in the frequency response is the drawback. The double resonant frequencies at 40 and 50 kHz in the measurement results is only represented with one resonant frequency at 30 kHz in the calculation results. In addition, the resonant frequency at 600 kHz is not represented in the calculation results.

In the case of induced voltage to LV, the model results for layer winding are in good agreement with measurements for f<1MHz. But, for f>1MHz, it only follows the decreasing trend of the measurements. The dominant resonant frequency in 1.6 MHz is not well represented. In the case of disc winding, the model is capable of good calculation of induce LV amplitude for resonant frequencies around 100 kHz. It however deteriorates the trend of induced LV voltage for higher frequencies. In the case of pancake winding, the amplitude of resonant frequencies around 1 MHz is considerably lower than measurements and it requires improvement.

Base on the FRA measurements performed for transferred voltages inside three winding types, disc winding has critical resonant behavior in the range 65 kHz to 1.5 MHz. In this range, there are several resonant frequencies where Disc winding reaction is such as standing wave with several nodes. The internal resonant frequencies for layer and pancake windings are sporadic. Considering the repair and accessibility costs of offshore wind farms, the design and characteristics of wind turbine transformers should be improved. Pancake windings with their modular designs can be proposed as a proper solution.

Contents

Preface ..... **iii**

Abstract ..... **v**

1 Introduction **1**

1.1 Motivation 1

1.2 State-of-the-art 1

1.3 Scope of work 2

1.4 Contributions 3

1.5 List of pulications 4

1.6 Thesis outline 5

2 Background **9**

2.1 Development of wind farms 9

2.2 Transient phenomena in wind famrs 11

2.2.1 Switching operation in wind farms 11

2.2.2 Harmonics and spikes inwind farms 12

2.2.3 Loading cycle in wind farms 13

2.2.4 Fault ride-through in wind farms 13

2.3 Overvoltages in wind farms 14

2.4 Wind turbine transformer modelling 15

2.4.1 Black-Box model 15

2.4.2 White-Box model 16

2.4.2.1.Distributed-parameter model based on Multiconductor Transmission Line (MTL) 16

2.4.2.2. Lumped-parameter model from network analysis 17

2.5 Protective and preventive measures against overvoltages 20

3 Methods 21

3.1 Simulation of transferred resonant overvoltages 21

3.2 Measurement and white-box model of internal resonance 21

4 Selected papers 25

5 Result & Discussion 29

5.1 Transferred resonant overvoltages 29

5.1.1 Parametric wide band model 29

5.1.2 Winding comparison 32

5.1.3 Protection schemes 33

5.2 Internal resonant overvoltages 35

5.3 Modeling transformer windings 43

5.3.1 Limitation of analytical RLC formula in Lumped-Parameter Model 46

6 Conclusions and future work 49

6.1 Conclusions 49

6.2 Future work 50

References 53

Appendix 59

1 Introduction

1.1 Motivation

Among the renewable energy technologies, wind and solar photovoltaics (PV) are leading in terms of newly installed power capacities. In recent years, onshore wind power installation has become quite price-competitive with conventional fossil fuel-based power plants. Offshore wind power requires more investment per kWh compared to onshore wind power. However, offshore wind velocity is more robust. One of the key factors, which can help offshore wind to be more competitive in the future, is to increase availability of wind farm components and lower maintenance costs.

Offshore wind farms are composed of wind turbines which are interconnected with Medium Voltage (MV) submarine cables in rows or branches. The rows are then connected to a medium voltage switchgear and platform transformer, and from there to the power grid via a HV cable.

Transient overvoltages, more specifically resonant overvoltages, are among the challenges offshore wind farms encounter and may result in failure of interconnecting cables, transformers or power converters. In the context of the availability of offshore wind farms, studies in the area of protective and preventive measures against transient overvoltages are beneficial. Installation of surge arresters and resistive-capacitive filters as a protective measure for the components is assessed in the literature, while there has been little focus on the preventive measures.

The wind turbine transformer, as the vital joint between the LV side of each wind turbine and the MV collection grid, has a high impact on the reliability and availability of wind farms. From the MV collection side, switching transients and close-up earth faults may lead to resonance overvoltages at terminals and inside wind turbine transformers. And from the LV side, these transformers are connected to frequency converters. The output sinusoidal voltage of the frequency converters is superimposed with high frequency spikes, which can also excite internal resonant overvoltages. These overvoltages can cause insulation failures and shorten the life time of wind turbine transformers. This has been motivated the author to study the resonant overvoltages in wind farm with the emphasis on how wind turbine transformers can be protected and prevented against them.

1.2 State-of-the-art

Switching transients in offshore wind farms has been among a number of interesting research topics recently. In the literature, overvoltage due to switching transients in offshore wind farms has been studied by means of performing measurements, simulations and modeling in Electro-Magnetic Transient Program (EMTP) softwares such as PSCAD, ATP-EMTP and

Power Factory. High frequency modeling of the offshore wind farm components, i.e. transformers, cables and circuit breakers has been the focus of various research studies, specifically in PhD projects in Technical University of Denmark and Chalmers University of Technology. Among literature studies relevant to switching transients, the following can be highlighted:

- Comparison of measured switching transient overvoltage in the Collection Grid of Nysted Offshore Wind Farm with EMT Simulations.
- Energizing operations of the export cable, reactor and filter in the onshore substation on Walney Offshore Windfarm 1.
- Validation of a Switching Operation in the External Grid of Gunfleet Sand Offshore Wind Farm by Means of EMT Simulations.
- Transient Recovery Voltages at the Main 132kV Line Bay GIS Circuit Breaker in a Windfarm
- Voltage dip caused by the sequential energization of wind turbine transformers.
- The effect of wind farm topology, e.g. collection cables with conductors of different cross-sectional area, line bifurcation or branches.
- Protective measures such as surge arresters and resistive-capacitive filters
- Resonant overvoltage due to energization

In the context of resonant overvoltage in the system level, there has been less focus on close-up earth faults, which is going to be studied in this thesis. Furthermore, the resonant overvoltages for a wider power range of wind turbine transformers is introduced in this thesis, which gives an insight into the resonant overvoltages for future wind farms.

Resonant overvoltage inside wind turbine transformers, which can be seen as a component-level study, has also been assessed in the literature. In the PhD thesis of Tarek Abdulahovic, turn-to-turn voltage stress obtained during very fast transients (VFT) is compared with the turn-to-turn voltage stress measured during the basic lightning impulse level (BIL) in order to find if current transformer standards account for the voltage stress that appears during VFT, especially in wind farms. Internal resonant overvoltages have been widely studied in power systems and the application of surge protection devices, improvement of winding insulation level and modification of part of the winding structure are introduced as protective measures against resonant overvoltages. However, the comparison of winding types, e.g. disc, layer, pancake, with the aim of selecting the least vulnerable to the internal resonant overvoltages has not yet been studied. It is highlighted and assessed in this thesis with the objective of providing insights into preventive measures that can be taken during the design stage of offshore wind farms.

1.3 Scope of work

The focus of this work is to study resonant overvoltages in wind turbine transformers with the help of analytical modeling, experiment and simulation. As mentioned in the state-of-the-art section, the study can be both on the system-level and on the component-level. Therefore, the scope considered for the system-level study is:

- The simulation of a typical wind farm by means of high frequency modeling of the involved components. Then, studying switching transients and close-up earth faults and scenarios which result in resonance overvoltages.
- To introduce a parametric black-box model of wind turbine transformers in order to study resonant overvoltage for a wider power range of wind turbine transformers. And to study the effect of protective measures such as surge arresters and RC filters against resonant overvoltages.

The scope of work for the component-level, i.e. transformer-level:

- To design and follow-up production of a 11/0.230kV 500 kVA transformer with three different winding types, i.e. disc, pancake and layer, on the three limbs, with the aim of comparing their frequency responses and resonant frequencies.
- To measure HV/LV and LV/HV voltage ratios, input HV and LV impedances and last but not least the voltages transferred to internal taps.
- To carry out a white-box model for the above-mentioned 500 kVA transformer windings and verify the model via FRA measurements.

1.4 Contributions

The thesis contributions are as follows:

- By introducing the parametric black box model of the 300 kVA transformer, it is found that energization transients can lead to resonant overvoltages at the LV terminal if:
  (a) The input impedance of the WTT at resonant frequency is much higher than the cable surge impedance.
  (b) Quarter-wave resonant frequency of the cable is in the vicinity of a transformer resonant frequency.

  In the case of standalone transformer energization with variable cable length, it is found that the maximum du/dt can reach up to 460 p.u/µs for a 11/0.23 kV 300 kVA transformer (shift factor = 1) if no surge arrester and resistive-capacitive filters are applied.

- Thanks to the introduced parametric model, the pattern of cable length vs. shift factor shows that du/dt is more than 100 p.u/µs for fictitious transformers with the shifted frequency responses of the 300 kVA transformer. Surge arresters on the HV and LV terminals of the transformer cannot reduce du/dt significantly. Therefore, resistive-capacitive filters should be installed at HV and LV terminals. In this way, du/dt is decreased to <20 p.u/µs.

- It is found that resonant overvoltages produced by close-up earth faults are similar to those produced by energization transients since they can be interpreted as switching to earth. Their main modeling difference is that close-up earth faults

occur while the wind farm is producing power (steady state mode), i.e. the power converter at the LV side of the WTT is connected and is in operation. On the other hand, energization occurs when the wind farm is out of operation and the power converter is disconnected. The amplitude and du/dt of resonant overvoltages due to close-up earth faults are lower than those due to switching resonance thanks to the presence of the power converter and DC link capacitor.

- Resonant overvoltage in transformer windings occurs when the incident transient at the HV terminal of transformer has a frequency component matching one of the resonant frequencies of the winding. This presents itself as excessive voltage-to-ground (terminal resonance) or voltage drops (internal resonance). The first one is critical at resonant frequencies where the associated anti-nodes in the HV winding are close to the LV winding or yoke. The second one is critical at resonant frequencies where the associated out-of-phase anti-nodes are located close together in the HV winding.

- Between the studied windings in the 500 kVA transformer, internal resonance is most likely to happen in disc winding especially in frequency range (0.1-1 MHz) which wind turbine energization or close-up earth faults could excite. Thus, wind turbine transformers with disc windings can experience more gassing and insulation failures.

- The thesis describes the analytical high frequency model of the windings in detail. It is based on a white-box RLC ladder model. The outputs of this model can contribute to drawing general conclusions regarding protection of wind turbine transformers against resonant overvoltages.

1.5 List of publications

The research work has resulted in publications in peer-reviewed conferences and journals. Selected papers, inserted in this thesis, are as following:

1. **A. H. Soloot**, H. K. Hoidalen and B. Gustavsen, ”Resonant overvoltage assessment in offshore wind farms via a parametric black-box wind turbine transformer model”, *Wind Energy*, *Vol. 18, issue 4, pp. 1061-1074, June 2015*.
2. **A. H. Soloot**, H. J. Bahirat, H. K. Høidalen, B. Gustavsen and B. A. Mork,” Investigation of Resonant Overvoltages in Offshore Wind Farms- Modeling and Protection”, *in proc. of International Power System Transients (IPST2013)*, Vancouver, Canada, July 2013.
3. **A. H. Soloot**, H. K. Hoidalen and B. Gustavsen, “Internal Resonant Overvoltage in Wind Turbine Transformers- Sensitivity Analysis of Measurement Techniques”, *in proc. of International Conference on Electrical Machines and Systems*, Busan, Korea, Oct. 2013.
4. **A. H. Soloot**, H. K. Hoidalen and B. Gustavsen,” Influence of the winding design of wind turbine transformers for resonant overvoltage vulnerability”,

IEEE transaction on Dielectric and Electrical Insulation, Vol.22, Issue 2, pp. 1250-1257, April 2015.

5. **A. H. Soloot**, H. K. Hoidalen and B. Gustavsen, "Modeling of Wind Turbine Transformers for the Analysis of Resonance Overvoltages", *Elecrical Power System Research,Vol. 115, pp. 26-34, Oct. 2014.* (selected paper from *International Power System Transients (IPST2013)*, Vancouver, Canada, July 2013.)

The followings are additional papers, which is published for this study while not inserted in the thesis.

1. **A. H. Soloot**, H. K. Hoidalen and B. Gustavsen, "The Assessment of Overvoltage Protection within Energization of Offshore Wind Farms", *Energy Procedia (Elsevier)*, Volume 24, pp. 151-158, 2012.
2. **A. H. Soloot**, H. K. Hoidalen and B. Gustavsen," The Effect of Winding Design on Transformer Frequency Response with Application on Offshore Wind Farm Energization", *in proc. of International Conference on Renewable Energy Research and Applications (ICRERA2012)*, pp. 1-5, Nagasaki, Japan, November 2012.
3. **A. H. Soloot**, H. K. Hoidalen and B. Gustavsen," A Study of Switching Overvoltages In Offshore Wind Farm", *in proc. of International Symposium on High Voltage Engineering (ISH)*, pp. 336-343, Germany, August 2011.
4. **A. H. Soloot**, H. K. Hoidalen and B. Gustavsen," Frequency Domain Investigation of Switching Transients in Offshore Wind Farms", *in proc. of IEEE Powertech conference*, pp. 1-5, Norway, June 2011.
5. **A. H. Soloot**, H. K. Hoidalen,"Analysis of Switching Transients in Offshore Wind Parks with Focus on Prevention of Destructive Effects", *in proc. of 6th PhD seminar on Wind Energy in Europe*, 30 Sep.-1 Oct. 2010, pp. 188-192, Trondheim, Norway.
6. **A. H. Soloot** and H. K. Høidalen, "High Frequency Modeling of Transformers in ATP for Investigation of Resonances in Offshore Wind Park", *in Porc. of the EEUG Meeting 2010,European EMTP-ATP Conference*, PP 164-175,Finland, August, 2010.

1.6 Thesis outline

The thesis contains the following chapters:

Chapter 1: Introduction

In this chapter, the motivation for the research study is described. The research studies in the literature are briefly outlined in the state-of-the-art section. Resonant overvoltages in offshore wind farms can be studied with system-level or component-level approaches. The cutting edge of research for both of the approaches is mentioned in the state-of-the-art section. Then, the goal-setting and scope of work of the thesis is briefly introduced for

both approaches in the next sub-section. The main contributions to the two corresponding study approaches are outlined afterwards. All of the publications for this PhD research are listed in the next sub-section. The five selected publications represent the methods, results and contributions, which are going to be discussed in detail in this thesis. In the following, the focus of the selected papers is briefly outlined.

Chapter 2: Background

The history and statistics of wind farm development is explained in this chapter. The brief review of research works on overvoltages in wind farms and protective measures is detailed. Also wind turbine transformer modeling is explained briefly in this chapter. The two branches of transformer models, i.e. black-box and white-box, have been seen as the core elements during system- and component-oriented studies, respectively. Finally, the protective and preventive measures are brought in.

Chapter 3: Methods

This chapter addresses the methods used in this research work to study resonant overvoltages.

- Simulation of an offshore wind farm, as a system-level approach, to study resonant overvoltage.
- Measurement and white-box modeling, as a component-level approach, to study resonant overvoltages inside WTT.

In this chapter, the contribution of each of the selected papers is explained.

Chapter 4: Selected Papers

In this chapter, the selected papers are summarized. The main findings of this research work are detailed in these papers. It should be mentioned that papers I and II contribute to the system-level approach of this thesis, which can be seen as the first paper package. Papers III-V contribute to the component-level approach of this thesis, which can be seen as the second paper package.

Simulations of a typical wind farm system for switching transients and close-up earth faults are presented in paper I and II, respectively. These papers clarify the conditions in which resonant overvoltage occurs in the system, how the exposure of the WTT as the key joint is affected, and last but not least the effect of protective measures.

Paper III discusses the sensitivity analysis of the measurement equipment with the aim of obtaining appropriate measurements results. In this way, it paves the way for paper IV to present the SFRA measurements for transferred voltages inside windings and consequently the comparison of internal resonance between windings. The white box model to calculate the transferred voltages inside windings and internal resonance is introduced in paper V. The verification of the model is performed with the help of measurements in paper IV. As one can see, papers III-V have chronologically introduced and discussed the transformer internal resonance.

The interface of these two paper packages are the transferred resonant overvoltages at the LV side of the wind turbine transformer. In the first paper package, the black-box of the 300 kV transformer with layer winding is the core of the study, while in the second paper package, the white-box of the 500 kV transformer with three different winding types is the core of the study. As this PhD research started with the first paper package and system-oriented study, it was intriguing to investigate how the terminal resonances at LV could be followed and related with resonances inside the transformer. This led to the second paper packages and component-oriented study.

Chapter 5: Result & Discussion

Chapter 5.1 presents the results and discussion for the system-level study with the title of transferred resonant overvoltages.

Chapter 5.2 and 5.3 presents the results and discussion for the component-level study with the title of internal resonant overvoltages.

Chapter 6: Conclusions and future work

Appendix: presents the selected papers included in this thesis.

2 Background

2.1 Development of Wind Farms

The wind power has been utilized for many centuries. Until the early twentieth century, wind power was used to provide mechanical power to pump water or to grind grain. At the beginning of modern industrialization, the use of the fluctuating wind energy resource was substituted by fossil fuel fired engines or the electrical grid, which provided a more consistent power source. In the early 1970s, with the first oil price shock, interest in the power of the wind re-emerged. However, the main focus was on wind power providing electrical energy instead of mechanical energy. The technology was improved step by step in such a way that by the end of the 1990s, wind energy has emerged again as one of the most important sustainable energy resources. During the last decade of the twentieth century, worldwide wind capacity was doubled approximately every three years. The cost of electricity from wind power had fallen to about one sixth of the cost in the early 1980s, and the trend seems to continue [1].

Fig. 2-1 shows the comparison between fuel share of electricity generation in 1973 and 2011[2]. As one can see, the share of renewable energies has increased approximately by a factor of 8. The increasing tendency to install wind power in Europe can be observed in Fig. 2-2. Wind energy has had the most installation in Europe in the last fourteen years[3].

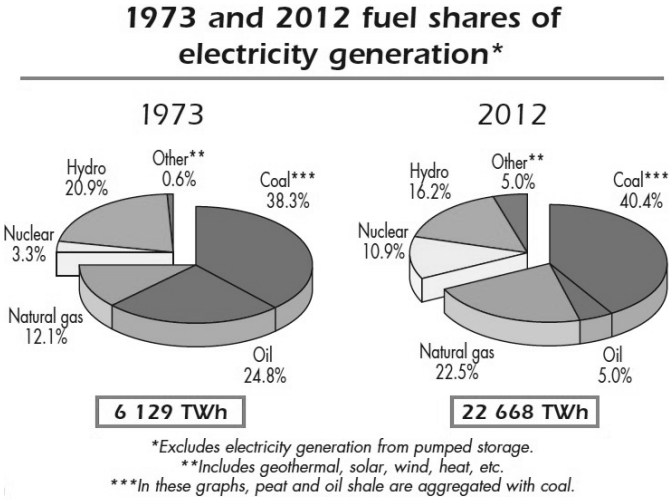

Figure 2–1. Comparison between fuel share of electricity generation in 1973 and 2012 in the world[2].

The scarcity of land in Europe and opposition to visual and noise pollution [4-5] lead the planners and developers to offshore wind installation with the additional advantage of better wind conditions [6]. The researchers and planners envisage a European super-grid that would integrate the renewable resources much more efficiently and increase their penetration into the energy mix [7]. Although the first OWF was installed in Vindeby, Denmark in 1991, the development of OWF was not significant during 1990-2000. However, the share of OWF in wind power annual has later been drastically increased from 1% (2001) to 14% (2013) (see Fig. 2-3) [3].

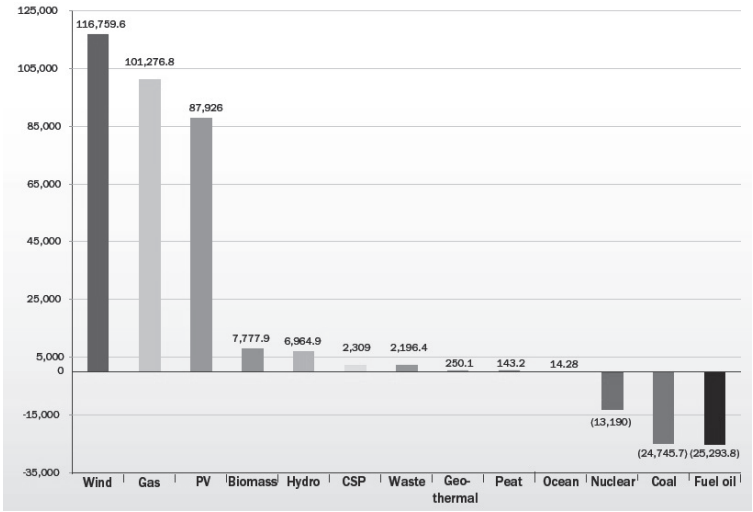

Figure 2–2. Net electricity generating installations in the Europe 2000-2014 (MW) [3].

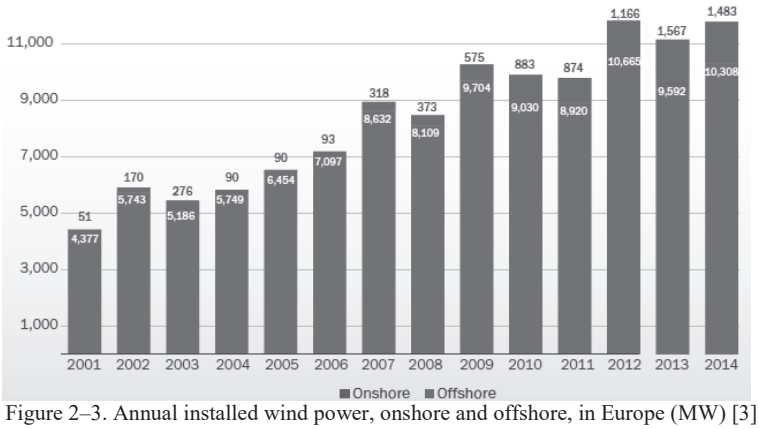

Figure 2–3. Annual installed wind power, onshore and offshore, in Europe (MW) [3]

2.2 Technical challenges in wind power systems

Distributed generation incorporated with the increasing installation of renewable energies, has made the wind energy more visible in power generation. Wind energy has different types of energy conversion systems, ranging from generators equipped with gearbox to gearless generators connected to power converters. Today, variable speed wind turbine generators, which are connected through a full power converter; defined as the Type 4 converters, are increasingly implemented in wind farms [8]. In this type, the generators feed their output to Back-to-Back (BtB) converters, which in turn feed the step-up Wind Turbine Transformers (WTT) that are connected to collection grids. Although this arrangement adds the controllable characteristics and decouples the generator from the grid by a DC-link, it necessitates certain considerations in the design of transformers and cables in its vicinity. Fig. 2-4 shows a single-line diagram of a typical wind power plant.

According to the average age of this type of wind energy generation (type 4), the problems of WTTs are relatively new and transformer manufacturers are still attempting to keep the records and causes of any undisclosed failures. Therefore, there is very little published data about the detailed analysis of such failures. Meanwhile, a large number of gassing problems is reported in recent publications [9-12]. This fact merely indicates that WTTs should be more robust and should not be just off-the-shelf distribution transformers in comparison with conventional transformers. To prevent these failures, a number of transformer manufacturers proposed a series of modifications [13-14].

Different manufacturers [15-16] discuss the current state of the art and the factors, which should be taken into account in the design of wind turbine transformers, and a comprehensive summary is given below.

2.2.1 Switching operation in wind farms

Switching operations affect the transformer insulation significantly. As it can be seen in Fig. 2-4-a, typically a WTT is connected to vacuum circuit breakers (VCB) via cables with lengths of few hundred meters. These VCBs disconnect the transformer in cases of very high or very low wind speed and also in the events of severe fault in the grid. In other words, VCB action can occur quite a few times in one day. Oscillatory overvoltages due to switching of these VCBs traverse through transformers and can excite one or more of the winding's natural resonance frequencies resulting in severe internal voltage amplification and insulation system damages [17]. The internally amplified voltages can degrade transformer insulation without having a significant overvoltage at transformer terminals.

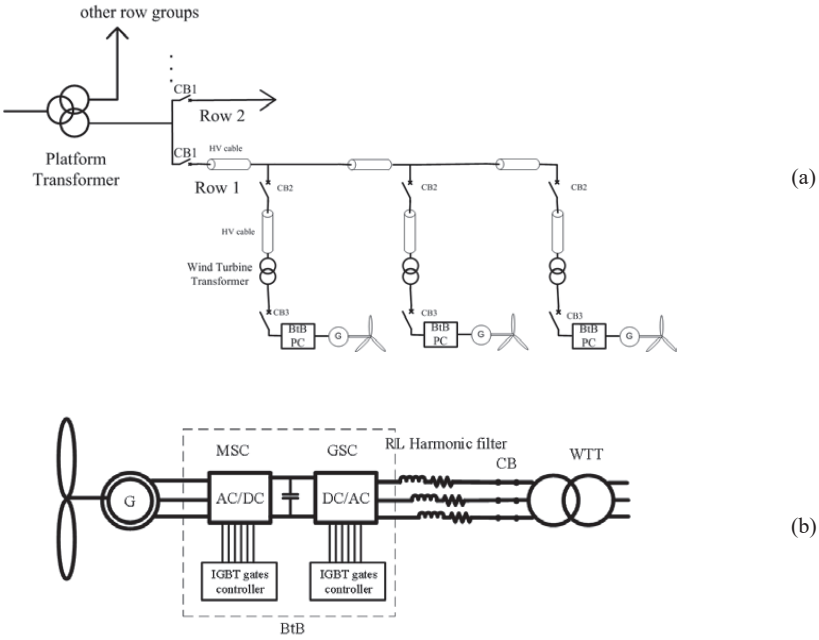

Figure 2-4: (a)- A typical wind farm single-line diagram, (b)-BtB converter.

2.2.2 Harmonics and spikes in wind farms

Step-up WTTs are supplied by power converters. The output voltage of the converter after filtering is a sinusoidal waveform with spikes repeating at the switching frequency of the converter. These spikes are very fast transients containing high frequency components in the range of 100 kHz up to MHz due to high rate of rise/fall of voltage (*du/dt*), which impose additional electrical stresses on transformer insulation system. These stresses are caused by internal resonances and travelling of voltage surge along the windings. This should be considered in the design of wind turbine transformers.

Other than voltage spikes, power converters also produce harmonics in the range of kHz, which inserts additional eddy, and dielectric losses in transformers compared to that in 50/60 Hz. At critical spots in the winding, these additional losses may result in hot spots and consequently generation of more gases, partial discharge (PD) and insulation deterioration.

To reduce the amount of high-frequency contents delivered to the secondary winding, the use of electrostatic shields is reported in [18]. These shields act as a capacitive filter to prevent the transfer form critical voltage components at the secondary side. Meanwhile, implementation of an electrostatic shield can shift resonance frequencies of the windings and potentially increase the amplification factor at some other frequencies. Therefore,

more work should be done on the design of electrostatic shield to improve its applicability.

2.2.3 Loading cycle in wind farms

Distribution transformers typically experience a constant pattern of loading cycle (two times a day for most of the regions). Step-up transformers in wind farms may experience several ups and downs in the power generation, even in a short time period, depending on the fluctuations in wind speed. High numbers of loading cycles together with fast rate of changes impose excessive thermal stresses on transformer structure. Besides, temperature variations of transformer oil change considerably the absolute values of the gas content [19], which can increase partial discharge probability.

2.2.4 Fault ride-through in wind farms:

This fault ride-through capability places larger electrical, thermal and mechanical demands on the wind step-up transformer while conventional transformers are not normally subjected to or designed to survive [20]. As an instance, the requirement for fault ride-through is sets by Federal Energy Regulatory Commission (FERC) in 2004 [21]. The curve is shown in Fig. 2-5 and is taken verbatim from the German E.ON Netz requirement. It is reported in [20] that wind farms installed from 2007 had to meet the fault ride-through requirement down to 15 percent of rated voltage (see. Fig. 2-5). For units installed after 2007, the fault ride-through requirement is down to zero voltage.

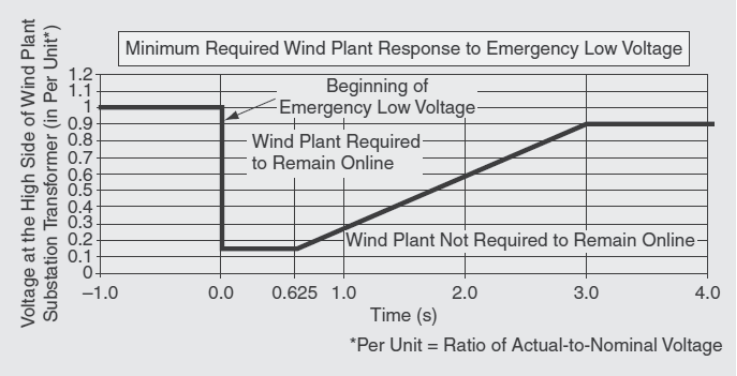

Figure 2-5. Proposed low-voltage ride-through requirement for wind plants [21].

In another study in the NOWITECH group [22], the authors showed that the collection gird voltage can drop down to 0.2 p.u. for a three phase short circuit occurred 0.5 km away from wind turbine terminal. Simulations showed that the wind turbines could operate stable through three phase short circuits in the collection grid. This is due to the action of the DC-chopper, which absorbs excess energy in the DC-link when the collection grid voltage drops.

Typically, wind farms use grounding transformers to contribute to the fault detection capability of the protection system during Single Line to Ground (SLG) faults and limit temporary overvoltages. Without grounding transformers, overvoltages can damage collector system cables, arrestors, and the wind turbine transformer [23].

From the aforementioned discussions, it can be concluded that many factors should be considered in the design of wind farm transformers. Although it is evident that transformer gassing problems and failures are consequences of combination of many factors together, the implementation of new design criteria for the transformer insulation will only become possible when the distribution of overvoltages and ageing of transformer insulation at higher frequencies are thoroughly examined.

2.3 Transient overvoltages in wind farms

Overvoltages can be categorized according to the IEC60071-1 classification; continuous operating voltage, temporary overvoltages, slow front (switching), fast front (lightning) and very fast front transients. Some of the recent studies of overvoltages in wind farms are reviewed as following;

Transient overvoltages are analyzed in [24] during inadvertent cable feeder deenergization and fault clearing scenarios on the collection grid of a large wind farm (300 MW). The impact of wind turbine transformer configuration, Δ/Yn or Yn/Yn**,** is evaluated and solutions to suppress the overvoltage, i.e. grounding transformer and fast grounding switch, are proposed. In [25], the energization (switching) overvoltages of cable feeders are simulated while other feeders are not connected and compared with the case where other feeders are connected. Arana performed measurements and simulations for slow front transient overvoltages in his PhD thesis [26]. The capabilities of the simulation tools are tested, analyzed and compared in order to find the limitations of the different models and methods to estimate correctly the switching overvoltages in offshore wind power grids. As an extension to the study in [26], the author in [27] shows how to develop a wide-band, linear black-box model of a linear multiport system using commercial off-the-shelf sweep frequency response analyser.

The switching overvoltages at MV collection grid can also be studied with the consideration of the impact of restrikes and reignitions of vacuum circuit breakers on wind transformer terminals [28-29]. The high-frequency properties of a 3.14 MVA 35/1.0/0.4 kV WTT, commonly used for the doubly fed asynchronous generator are investigated and it is shown that the voltage transfer from the 35 kV side to either of the two low-voltage taps is strongly dependent on the loading of the other tap [30]. It is also shown that the use of a simplified transformer model based on lumped capacitances gives unrealistic results.

Resonant overvoltages have been studied in literature thoroughly for transformer switching [31-34]. The resonant overvoltages can occur due to both energization transients [35] and close-up short circuits [36], when the frequency of a sustained voltage

oscillation at the transformer MV terminals matches a resonant frequency in the WTT voltage transfer function. Internal resonance will not necessarily result in immediate breakdown, but may very often only develop partial discharges, causing accelerated ageing of the winding insulation [36-37]. In [39] resonant overvoltages along the winding of wind turbine transformers are studied. It is found that during switching of dry-type transformers with short cable, severe turn-to-turn voltages can appear. Consequently, the critical voltage as a function of rise time is proposed.

2.4 Wind turbine transformer modelling

Transformer modeling can be categorized to black-box and white-box models;

2.4.1 Black-box model

If the computation of internal stresses along the windings is not required, a transformer terminal model can be used. This model is described in the frequency domain (ω) in terms of transformer admittance matrix as [40]:

$$I_t(j\omega) = Y_t(j\omega)V_t(j\omega) \tag{1}$$

where I_t and V_t are nodal current and voltage, respectively. Considering a transformer with n terminals, Y_t is the admittance matrix of size $n \times n$. If a 1 p.u. voltage is applied at node j of the transformer while the remaining terminals are short circuited, the j^{th} column of Y_t will be equivalent to the currents measured from ground to each terminal. The measurements are based on Sweep Frequency Response Analysis (SFRA). Applying this procedure, direct measurement of all elements of Y_t can be completed (Fig. 2.6)

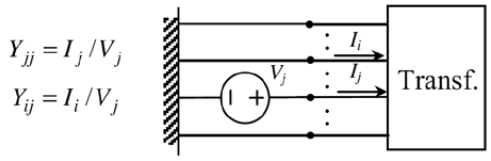

Figure 2.6. Measurement procedure for the j^{th} column of the admittance matrix [40].

To obtain the time-domain response of the system, the modified admittance matrix is approximated with rational functions [41]. The output of this approximation will be matrices A, B, C, D, and E, which define a Space Equation Realization (SER) of the form

$$I_t(s) \cong Y_{fit}(s)V_t(s) = [C(sU - A)^{-1}B + D + sE]V_t(s) \tag{2}$$

where Y_{fit} represents the rational approximation of the modified admittance matrix, U is the unitary matrix and s is the Laplace operator. If a set of N poles is used, with n = 6 for

the 3-phase 2-winding transformer, the matrix dimensions are *A: N × N*, *B: N × 6*, *C = 6 × N*, *D: 6 × 6*, *E: 6 × 6*. Next, Y_{fit} is represented in the form of an electrical network, whose branches are calculated as follows:

$$y_i = \sum_{j=1}^{n} Y_{fit,ij}, \quad y_{ij} = -Y_{fit,ij} \tag{3}$$

where y_i and y_{ij} represent admittance branches between node *i* and ground and between nodes *i* and *j*, respectively. Each branch in Equation (3) is described as a rational function:

$$y(s) = \sum_{m=1}^{N} \frac{C_m}{s - a_m} + d + s.e \tag{4}$$

where C_m and a_m are residuals and poles, respectively, which can either be real quantities or complex conjugate pairs. Finally, each branch can be represented by an electrical network [42]. The model sensitivity to measurement errors and the rational approximation was found to be very high when one or more terminals were open-circuited on both sides of the transformer [40]. Thus, a transformer model may, in general, produce accurate results in one situation and inaccurate results in a different situation. To detect such conditions, analysis of the measurements using matrix condition number and redundant measurements are useful. It was found that the sensitivity due to measurement errors could be strongly reduced by introduction of measured transferred voltages. It was also found that the sensitivity decreased when reducing the voltage ratio of the transformer [40].

2.4.2 White-box model

White-box models are based on the calculation of the impedance matrix from the geometrical design data of the transformer while black-box models obtain this matrix from terminal measurement. The white-box models can be used by the transformer designer to study the transformer windings resonance and voltage distribution along the transformer windings. The two main white-box models are classified as distributed and lump parameter models.

2.4.2.1. Distributed-Parameter Model Based on Multi-conductor Transmission Line (MTL)

As shown in Fig. 2.7, in this model each conductor represents a winding section (disc or turn). To preserve continuity, the end of each conductor is topologically connected to the beginning of the next conductor, resulting in a zigzag connection [43–48]. This is defined simply as

$$v_{ri} = v_{s(i+1)} \quad i_{ri} = -i_{s(i+1)} \quad i = 1 \dots N - 1 \tag{5}$$

where v_{ri}, i_{ri} are voltage and current at receiving point i, respectively. $v_{s(i+1)}$ and $i_{s(i+1)}$ are voltage and current at sending point $i+1$. The winding model is obtained from the telegrapher's equations of an MTL, which are defined in the Laplace domain as

$$\frac{dV(z,s)}{dz} = -Z(s)I(z,s) \tag{6}$$

$$\frac{dI(z,s)}{dz} = -Y(s)V(z,s) \tag{7}$$

Z and Y are the $N \times N$ matrices of series impedances and shunt conductances per unit length, where N is the number of conductors (discs or turns). $V(z,s)$ and $I(z,s)$ are the vectors of voltages and currents at point z of the winding. In Fig 2.7, the equivalent impedance Z_{eq} connected at the end of the N^{th} element can be used to represent the remaining part of the winding, when only a section of the winding needs to be modeled in detail. Z_{eq} can also represent the neutral impedance.

Numerical solutions to (6) and (7) are the Bergeron method [49] and finite-differences methods [50-51] in time domain, as well as the direct solution in the frequency domain, and subsequent numerical frequency–time transformation [52-53].

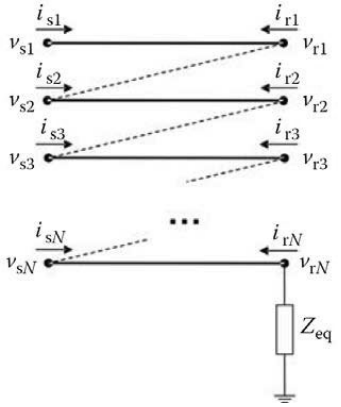

Figure 2.7. Multi-conductor transmission line model for the transformer winding [41].

2.4.2.2. Lumped-Parameter Model from Network Analysis

In this model, the transformer winding is divided to units (see Fig. 2.8) with one or several wire turns. Each of these units are then modeled with RLC components. The core of transformer for frequencies higher than 10 kHz does not contribute to flux coupling between phases since the eddy currents in hinder the magnetic flux to circulate inside core. This phenomenon is challenging for mutual inductance calculation. The following methods are introduced in literature for the parameter calculation of Lumped-Parametet (RLC ladder) model:

- Modeling based on self and mutual inductance

This method is first proposed by Robins [54] and it has been developed further in other works, e.g. [55]-[56]. This model is applied for internal resonance study in this work.

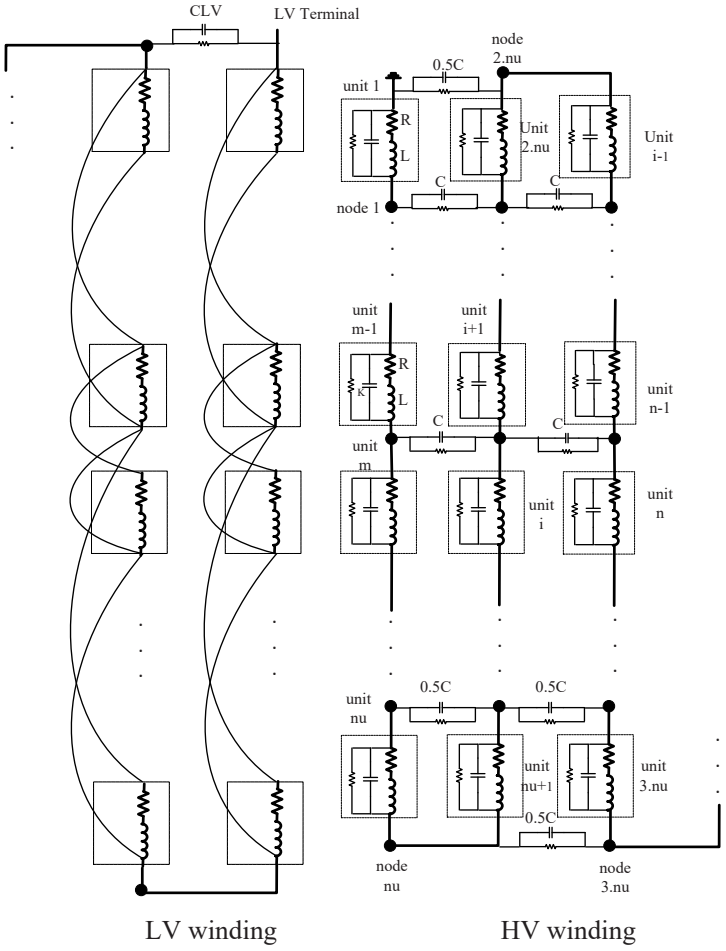

Figure 2.8. RLC ladder model of LV foil and HV layer winding.

Let us consider *nu* number of units in each layer of HV layer winding. *nH* is the number of HV layers and therefore *nu*×*nH* is the total number of units. Besides, the LV foil winding has *nL* layers, and we take each layer as one unit. The total order of *R*, *L*, *C* and *G* matrices becomes $m=nL+nu\times nH$.

Performing the Kirchhoff's Voltage Law (KVL) and Kirchhoff's Current Law (KCL) for all units results in (8) and (9), respectively. In Appendix *A* of paper V, KCL and KVL for an arbitrary unit, *i*, is performed.

$$[A]_{m\times m}[V]_{m\times 1} = ([R]_{m\times m} + j2\pi f[L]_{m\times m})[I_b]_{m\times 1} \quad (8)$$

$$[I]_{m\times 1} - [A]^t_{m\times m}[I_b]_{m\times 1} = ([G]_{m\times m} + j2\pi f[C]_{m\times m})[V]_{m\times 1} \quad (9)$$

Matrices V, I and I_b representing nodal voltages, injected nodal currents, the currents of inductive branches, respectively. A is a connectivity matrix describing the topology, linking branches and nodal quantities. The diagonal elements in A matrix are equal to 1 and sub-diagonal elements are equal to -1 and the rest is zero. Exceptionally, the first row and the row number $nL+1$, which are for first units in LV and HV winding respectively, have only the diagonal element, since the other nodes of these units are grounded.

The nodal admittance matrix Y can be calculated by reforming (8) to obtain I_b based on V and inserting this in (9). This gives (10).

$$[I] = [Y][V] \quad (10)$$

$$[Y] = [G] + j2\pi f[C] + [A]^t([R] + j2\pi f[L])^{-1}[A]$$

The analytical equations for the components of the R, L, C and G matrices are explained in paper V. These matrices are symmetrical, the admittance matrix also becomes symmetrical. To obtain the equation for the transferred voltage to LV, impedance matrix, Z, should be calculated from (10) by inverting Y. Since only the last element of I vector is none-zero due to the connection of last unit to the HV terminal, the last column of Z multiplies with the terminal current, I_m, and gives the nodal voltage in (11). Therefore, the transferred voltage to LV terminal is according to (12).

$$[Z(:,m)]I_m = [V] \quad (11)$$

$$V_{LV}/V_{HV} = Z(nL,m)/Z(m,m) \quad (12)$$

The other methods for the parameter calculation of RLC ladder model are briefly explained and referenced here:

- Modeling based on leakage inductance

This method is proposed by Blume et al. in [57] and improved in [58-59]. The leakage impedance is properly calculated. Though, the iron core is not considered with suitable accuracy.

- Modeling based on duality principle

The magnetic equivalent circuit of the transformer core can be modeled to an electric circuit based on duality principle [60]. Meanwhile, the duality-based models have shortcoming for calculation of leakage inductances. In [61], this problem is solved by introducing negative inductances.

- Modeling based on numerical field calculations

Numerical field calculation methods can be based on Finite Element Method (FEM) [62], Finite Difference Method (FDM) [63], Fredholm integral equations [64] or Equivalent Magnetization Surface Current Approach [65]. Authors in [66] employed finite element computation for parameter estimation of 100 kVA dry type wind transformer to study internal resonance. It is mentioned that detailed geometrical design of transformer and material properties is necessary for these methods. There should be considered a compromise between the accuracy of the model and computation time.

2.5 Protective and preventive measures against overvoltages

As discussed in section 2.3, there are two types of resonant overvoltages for wind turbine transformers; internal resonant overvoltages and transferred resonant overvoltages. In the case of transferred resonant overvoltages, surge arresters and Resistive-Capacitive (RC) filters are the protective devices. In Paper I, it is shown that RC filters have a considerable effect on both overvoltage amplitudes and maximum rate of rise (or fall) of overvoltages (du/dt). It is found that the implementation of RC filters alone can securely protect WTTs MV and LV terminal from resonant overvoltages.

Appropriate protective measures for internal resonances depend on the power rating and voltage level of transformers. For power transformers with High Voltage (HV) and Extra High Voltage (EHV) and some hundred MVA power ratings, the application of internal surge protection devices, improvement of insulation level of winding and modification of part of winding structure can be applied [67-71]. However, for wind turbine transformers with powers up to some MVA, none of abovementioned measures would be applicable. They are massively produced according to standards and considerations about distribution networks and performing the aforementioned measures would not be cost-efficient. As a preventive measure, resonance behavior of winding type can be compared for distribution transformers and the least vulnerable can be suggested for wind turbine applications.

3 Methods

3.1 Simulation of transferred resonant overvoltage

A detailed high frequency model of an OWF row in Alternative Transients Program-Electromagnetic Transients Program (ATP-EMTP) is presented. This model includes interconnecting cables, a wind turbine transformer, surge arresters and resistive-capacitive filters. Energization transients in the OWF row are discussed in detail with the focus on the occurrence of resonant overvoltage at the LV terminal of the transformer.

In order to represent the wind turbine transformer, the black-box model of 300 kVA 11/0.23 kV YNyn0 is pre-made by Gustavsen [17] and applied in this work. It has been employed for both simulations of switching transients and close-up earth faults. The model is improved to a parametric black-box model of a WTT, which includes scaling and shifting factors for impedance and frequency, respectively. In this way, resonant overvoltage for a wider power range of wind turbine transformers is studied in paper I. Energization topology is defined as,

- The position of the WTT; in the base or in the nacelle.
- The priority of the energization of the raw circuit breaker or turbine circuit breaker

The effect of this energization topology on the occurrence of resonant overvoltages and their characteristics is also investigated in paper I.

To simulate resonant overvoltages due to close-up earth faults, the modeling of the power converter at the LV terminal of the WTT is required. It is modeled as two back-to-back voltage source converters. The RL harmonic filters and snubber circuits are also included. The details are explained in paper II. This model can simulate the steady state operation as well as the resonant overvoltage due to an earth fault in the ATP-EMTP software. The shortcoming is that it requires a long simulation time. A simplified model, which has the same accuracy as the first model for resonant transient only, is also presented.

3.2 Measurement and white-box model of internal resonance

Investigation into internal resonant overvoltage is carried out in this work through measurements and white-box modeling of a 500 kVA 11/0.23 kV transformer with three winding types, i.e. layer, disc and pancake, on its three limbs as shown in Fig. 3.1-left. Along each of the windings 25 taps are implemented, with the tap positions shown in Fig. 3.2. The transferred voltage inside windings are measured by means of an Agilent network analyzer E5061B and Sweep Frequency Response Analysis (SFRA) method. To obtain measurements with appropriate quality and accuracy, sensitivity analysis of the measurements of the effect of foil, voltage and current probes are carried out and

discussed in paper III. Concluding the current transformer CM-100-6L-IR50 as the current probe, Tektronix P2220 probes (at x10 mode) as the voltage probe, the appropriate measurement setup is selected for the foiled transformer.

Then, the results of the SFRA measurements of the transferred voltages along the three windings are presented in paper IV. Transferred voltages are presented in the patterns of voltage-to-ground and voltage drop. In the context of the terminal resonance and internal resonance, the comparison of the measured results for the three windings are highlighted in this paper. The effect of a short-circuited or open-circuit LV winding is also investigated.

In Paper V, the proposed white-box model of the 500 kVA transformer, which is coded in MATLAB, is introduced and verified. As mentioned in sub-section 2.4.2.2, the lumped-parameter model based on self and mutual inductance calculations is selected for this research. Equation (12) defines the transferred voltages, in which the calculation requires the calculation of the Z matrix. The analytical equations for the components of the Z matrix, i.e. R, L, C and G matrices, are explained in paper V. To work on the model, the author should have had visual access to the windings. Thus, the transformer is set up out of tank. To investigate the effect of the tank, aluminum foil is used around the transformer.

The measurements in paper IV, along with input impedance measurements represented in paper V, are employed to verify the white box model. The verification of the model, agreements with measurement results and limitations assist us to draw general conclusions.

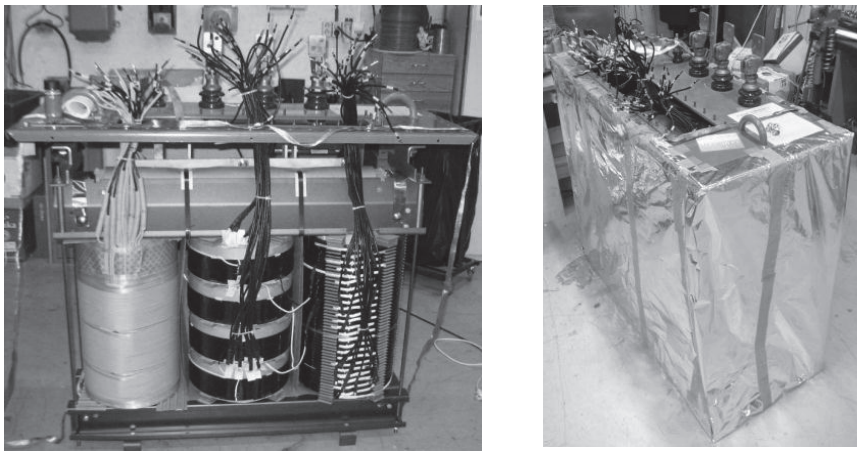

Figure 3.1. The photo of the 500 kVA transformer- left: without foil- right: with foil.

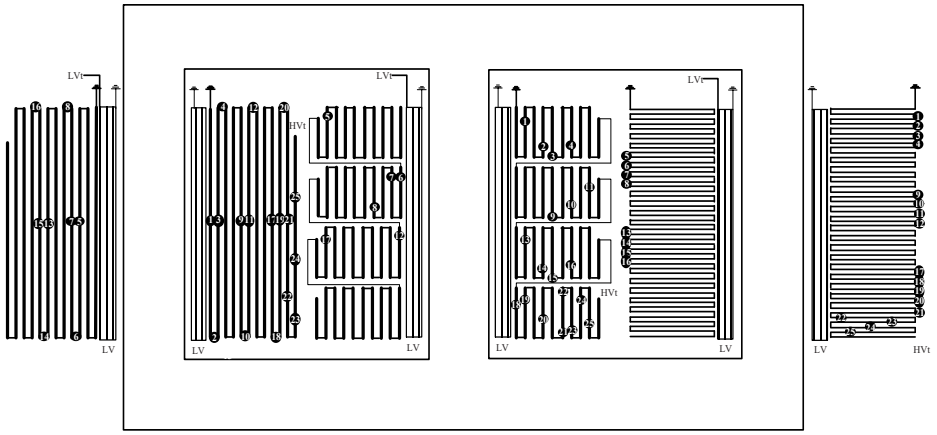

Figure. 3-2 The Layout of manufactured 500 kVA transformer.

4 Selected Publications

The scope of study in this thesis is detailed in the following five papers. In this section, summary of the papers are expressed. While, the complete papers are inserted in the Appendix.

Paper I

Resonant overvoltage assessment in offshore wind farms via a parametric black-box wind turbine transformer model

Amir Hayati Soloot, Hans Kristian Høidalen and Bjørn Gustavsen

Wind Energy, Vol. 18, issue 4, pp. 1061-1074, June 2015.

In this paper, we study how switching overvoltages at the Wind Turbine Transformer (WTT) Medium Voltage (MV) side can lead to high overvoltages on the Low Voltage (LV) side.

The effect of overvoltage protective devices is analyzed. A detailed model of an OWF row is developed in Alternative Transients Program-ElectroMagnetic Transient Program (ATP-EMTP), including interconnecting cables, WTT, surge arresters and resistive–capacitive filters. A parameterized black-box WTT model is developed based on an established model of a 300 kVA 11/0.23 kV YNyn0 transformer. The model is used to investigate the transfer of resonant overvoltages from the MV to the LV side.

The transformer model introduces frequency shift and amplitude scaling factors to enable systematic variation of its frequency response. Simulation results show that wind turbine energization in an OWF can lead to overvoltages on the LV terminals. The rate of rise of overvoltages (du/dt) is in the range of 300–500 pu/μs. It is found that resistive–capacitive filters should be installed on both MV and LV terminals of WTTs to decrease both resonant overvoltages amplitude and du/dt, which is unachievable by surge arrester alone. In addition, the selection of energization topology, i.e. WTT position in wind turbine and breaker closing sequence, is discussed in this paper.

Paper II

Investigation of Resonant Overvoltages in Offshore Wind Farms-Modeling and Protection

Amir Hayati Soloot, Himanshu J. Bahirat, Hans Kristian Høidalen, Bjørn Gustavsen and Bruce A. Mork

In proc. of the International Conference on Power Systems Transients (IPST2013), Vancouver, Canada, July 18-20, 2013.

In this paper, resonant overvoltage due to close-up earth faults is simulated in detail. High frequency black-box WTT model as in paper I is used. The power converter is modeled with two back-to-back voltage source converters. The resistive-inductive (RL) harmonic filters and snubber circuits are included. This converter model can simulate the steady state operation as well as resonant overvoltage due to earth fault in ATP-EMTP software, but a long simulation time is required. A simplified model, which has the same accuracy as the first model for resonant transients, is introduced.

Simulation results show that the transferred overvoltages to LV side due to earth fault at critical cable lengths may lead to resonant overvoltages with amplitude and rate of rise up to 30 p.u. and 400 p.u./μs, respectively. It is also shown that the installation of surge arresters at LV and HV terminal of WTTs only decreases the amplitude of overvoltages to safe margin and not the du/dt. However, the application of RC filters instead of surge arresters can protect offshore wind farm components from overvoltages.

Paper III

Internal Resonant Overvoltage in Wind Turbine Transformers-Sensitivity Analysis of Measurement Techniques

Amir Hayati Soloot, Hans Kristian Høidalen, Bjørn Gustavsen

In proc. of International Conference on Electrical Machines and Systems, Busan, Korea, Oct. 26-29, 2013.

The effect of measurement equipment on internal resonant overvoltages is analyzed in this paper. The motivation was to obtain high quality measurements specially to enable comparison with calculations of internal resonant overvoltages in the range of 10 kHz-10 MHz.
The effects of foil, voltage and current probes are surveyed. Measurement results show that foil around transformer increases the capacitance to ground, resulting in increased input admittance.
The active part was placed outside the tank for easy access to internal measurement points. This will influence its capacitive behavior. To study this effect, aluminum foil was wrapped around the active part to simulate the tank surface.
The transferred voltage measurements are sensitive to voltage probe selection. Passive voltage probes with minimum loading effect and adequate bandwidth is used to achieve stable and reproducible results. Transferred resonant and anti-resonant frequencies, the admittance or impedance magnitude and phase are highly sensitive to the location of the current probes. They should be installed at terminal not in ground side of winding.
The measured magnitude or phase of admittance or impedance is more accurate when current transformer CM-100-6L-IR50 is used compared to Tektronix P6021. On the other hand, Tektronix P6021 represents almost the same transferred resonant or anti-resonant frequencies. The current probes were compared for impedance measurement of 1 kΩ metal film resistor. The applied Tektronix P6021 requires more adjustment in the

calibration process and it is recommended to apply the current transformer CM-100-6L-IR50 for impedance measurements.

Paper IV

Influence of the winding design of wind turbine transformers for resonant overvoltage vulnerability

Amir Hayati Soloot, Hans Kristian Høidalen, Bjørn Gustavsen

IEEE transaction on Dielectric and Electrical Insulation, Vol.22, Issue 2, pp. 1250-1257, April 2015.

In this paper, internal resonant overvoltages in three winding designs; layer, disc and pancake, are measured and compared. The details of the design of the prototype 500 kVA transformer are explained.
The measurements show that a HV winding of layer type gives the highest transferred voltage to the LV terminal and this happens at 1.6 MHz which could be excited for close-up earth faults. Although disc winding seems the least vulnerable when measuring the transferred voltage to the LV terminal, it has higher potential of internal resonances in the HV winding compared to the two other types, both for voltage-to-ground and for voltage drops. Pancake and layer windings have less vulnerability in the case of internal resonances. Pancake windings have modular design characteristic. This eases the repair for offshore wind applications.

Paper V

Modeling of wind turbine transformers for the analysis of resonant overvoltages

Amir Hayati Soloot, Hans Kristian Høidalen, Bjørn Gustavsen

Electric Power Systems Research, Vol. 115, pp. 26–34, 2014.

The aim of this paper is to introduce the high frequency modeling of wind turbine transformer. This model is verified with the measurements of the three windings on the 500 kVA transformer. In this way, the findings of the 500 kVA transformer can be generalized.
This paper explains in detail the Lumped-Parameter Model (or RLC ladder model). The analytical equations for inductance, capacitance and internal resistance of conductors are explained. The necessity of core and insulation material properties is discussed. Also, the challenge to model the internal conductor resistances is explained.

5 Result & Discussion

In this chapter, the main results shown in the papers are discussed and the connection between papers is emphasized. In section 5.1, the simulation of transferred resonant overvoltages for energization transients and close-up earth faults is discussed. Section 5.2 is about internal resonant overvoltage measurement and modeling. Transformer behavior under resonance condition can be in analogy with the short-circuited transmission line. At certain frequencies a low loss, short-circuited transmission line behaves like a high-Q series-resonant circuit, with minimum input impedance (maximum input current). It exhibits a standing wave pattern of an integer number of half sine loops distributed along its length and experiences large amplitude voltage oscillations at the anti-nodes. The transformer winding behaves similarly and that type of resonance will be defined here as a "terminal resonance". In addition, at other frequencies the low loss transmission line behaves in the same manner as a high-Q parallel-resonant circuit, with maximum input impedance (minimum input current). Again a standing wave pattern exists consisting of a odd integer number of quarter sine loops. The similar anti-resonant condition in the transformer winding will be referred to as a "terminal anti-resonance"[32]. If a winding section, e.g a disc pair or a layer, located between two out-of-phase anti-nodes in the standing wave pattern at some particular frequency, a maximum voltage will appear between the two ends. This can be referred to as an "internal resonance" for the winding section. In section 5.3, the calculation results of Lumped-parameter high frequency model for the three winding types, mentioned in section 3, are presented.

5.1 Transferred resonant overvoltages

5.1.1 Parametric wide band model

A parametric wideband model of the 300 kVA 11/0.23 kV transformer, which can scale the amplitude and shift the frequency response, is introduced. This model helps to get an insight into the transferred resonant overvoltages of larger transformers with the help of black box model of 300 kVA transformer. Detailed information of the parametric model is described in paper *I*. Figure 5-1 shows the outcome of parametric model for shifting frequency response and scaling the amplitude.

Transformer models generated by the parametric model and shift factor 1-10 are employed to study the energizations leading to resonant overvoltages at LV side. The simulation circuit is shown in figure 5-2 (a). As we know, the first condition for the transferred resonance overvoltage is the equity of cable quarter wave frequency and one of resonant frequencies of transformer. The second condition is that transformer input impedance should be higher compared to cable surge impedance at resonant frequency. These conditions are also addressed in literature, e.g. [17].

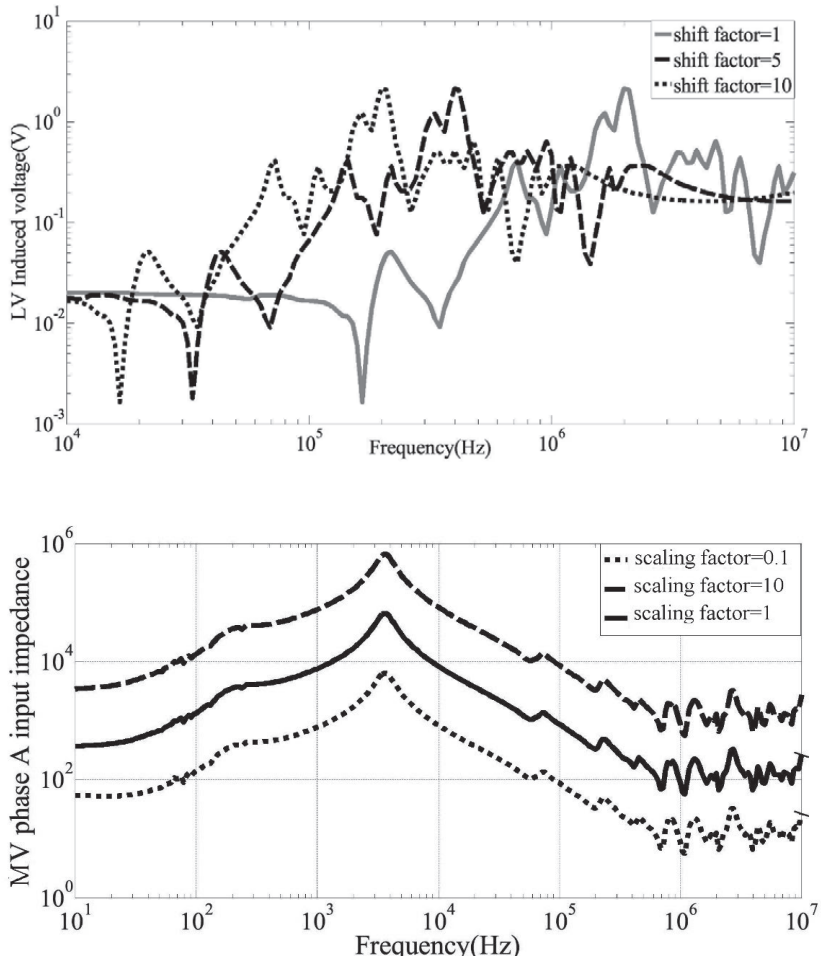

Figure 5–1. (a) Shifted frequency response of the LV induced voltage and (b) scaled frequency responses of MV phase A input impedance of the 300 kVA transformer.

As it can be seen in Figure 5-1 (a), the 300 kVA transformer (shift factor=1) has the dominant resonant frequency at 2 MHz. This frequency is equivalent to the quarter wave frequency of a 23 m cable with relative insulation permittivity of 2.67. As one can see in Figure 5-2 (b), the pattern shows that the maximum resonant overvoltage amplitude is on the diagonal zone, meaning that the most critical cable length for each shifted transformer has the quarter wave frequency equal to the dominant resonant frequency of that transformer. In the case of rate of rise (du/dt), higher values can be observed for transformers with a lower shift factor (see Figure 5-2 c).

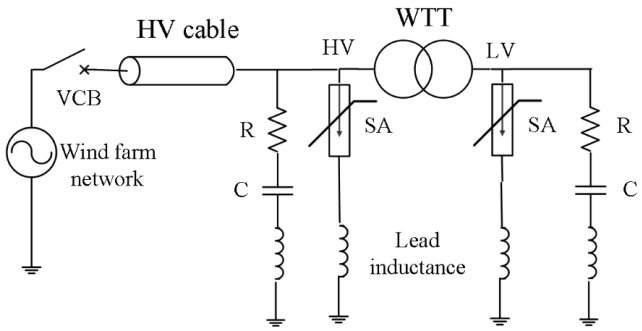

(a)

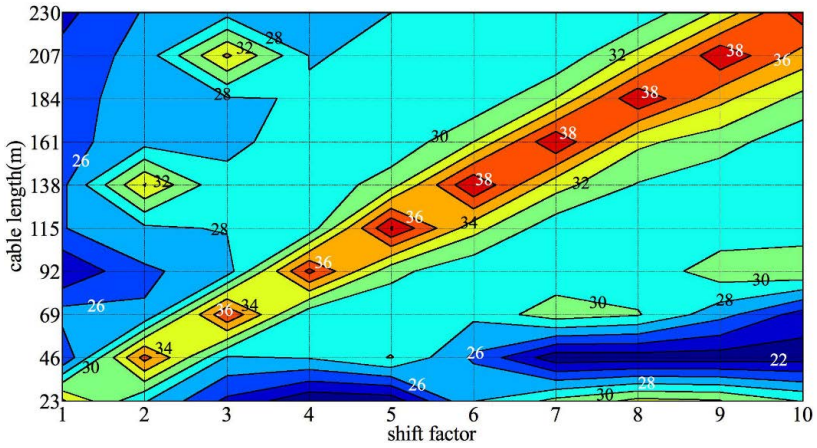

(b)

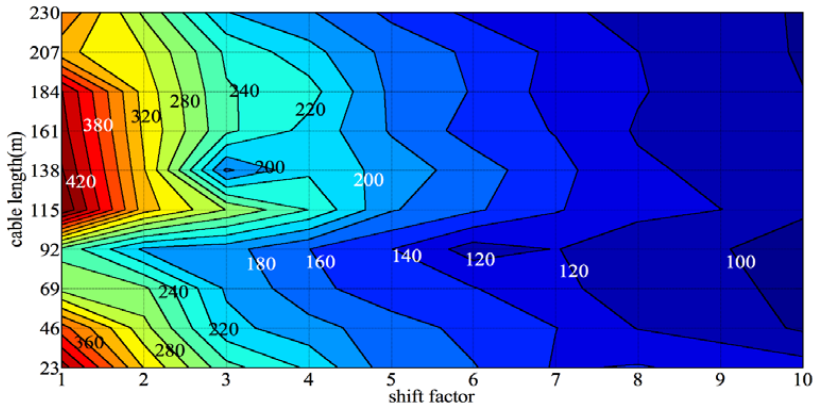

(c)

Figure 5–2. (a) Simulation circuit to study resonant overvoltages. (b) Resonant overvoltage peak at LV terminal as a function of cable length and shift factor. No protective device is applied. (c) du/dt in p.u./μs at the LV terminal as function of cable length and shift factor. No protective device is applied.

Generally speaking, transformers with larger sizes have higher inductances and capacitances. This leads to lower resonant frequencies according to equation (13). With careful consideration, the effect of transformer size can be formulated. Assuming constant current density, flux density, insulation space factor, the kVA scaling relations for transformer can be obtained. When scaling the kVA by a factor of m, the physical dimensions of transformer should be scaled by the factor $m^{0.25}$. Therefore, inductances and capacitances also scale by the factor $m^{0.25}$, and resonance frequencies are scaled by factor $m^{-0.25}$ according to:

$$f_r = \frac{1}{2\pi\sqrt{LC}} \tag{13}$$

5.1.2 Windings comparison

In paper IV, the measured frequency responses of three winding types on the studied transformer is presented (see figure 5.3). All of the three windings have a dominant resonant frequency around 800 kHz. The trend of the frequency response around 800 kHz for the pancake winding is similar to the disc winding, while the amplitude of the transferred voltage is in the range of the layer winding.

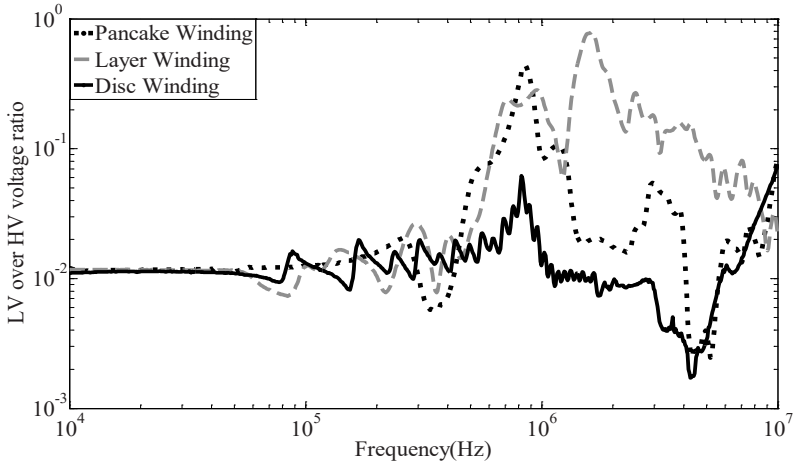

Figure 5.3 Transferred voltage to LV for Disc, layer and pancake winding in the 500 kVA study transformer.

The disc winding has comparably lower transferred voltage at 800 kHz, but there are many resonant frequencies in the range of 100 kHz-1 MHz indicating that there can be a risk of internal resonances along the HV disc winding and its associated LV winding.

Layer winding has the most dominant resonant frequency at 1.6 MHz and some resonant frequencies in higher range. This means that close-up short circuits can lead to high transferred resonant overvoltages at LV terminal.

5.1.3 Protection schemes

The protection schemes against induced resonant overvoltages are assessed via a simulation circuit of typical offshore wind farm (Fig. 5-4 a). The induced voltage on LV side phase A shows that RC filters are more effective compared to surge arresters both in the sense of amplitude and rate of rise. The reduction of overvoltage amplitude can be studied in Fig. 5-4 b. The impact on the rate of rise/fall is highlighted in table 5-1. In the case of no protection, the rate of rise is 93 p.u./µs while it drops to 25 or 9.5 p.u./µs if ideal surge arresters or RC filters are considered respectively. The base for p.u. calculations is the voltage peak at LV side. It is studied that the consideration of stray inductance of surge arresters or RC filters has a slight effect on their performance.

TABLE 5-1: RATE OF RISE/FALL OF VOLTAGE (P.U./µS) FOR VARIOUS PROTECTION SCHEMES.

Protective devices	WTT in the base	WTT on the nacelle
No protection	154	93
SA(LV) with L*	44	27
Ideal SA(LV)	36	25
RC(LV) with L*	25	11
Ideal RC(LV)	16	9.5
SA(LV) & RC(LV)*	20	11
SA(LV),RC(LV) & SA(HV)*	19	10
SA(LV),RC(LV),SA(HV) & RC(HV)*	13	4
RC(LV) & RC(HV)*	16	4.5

*In this cases, stray series inductance is included to protective devices.

Close-up earth faults can also lead to transferred resonant overvoltages if the two aforementioned conditions are valid. The simulation results in paper *II* (see figure 5-5 a) show that the induced voltage to LV for this phenomenon is higher when LV is open circuit compared to the case where the power converter is connected and wind turbine is under normal operation (see figure 5-5 b). The rate of rise of overvoltages is in the same range as critical switching transients. Seq. 1-6 are the sequences of switch ignition in Grid Side Converter (GSC).

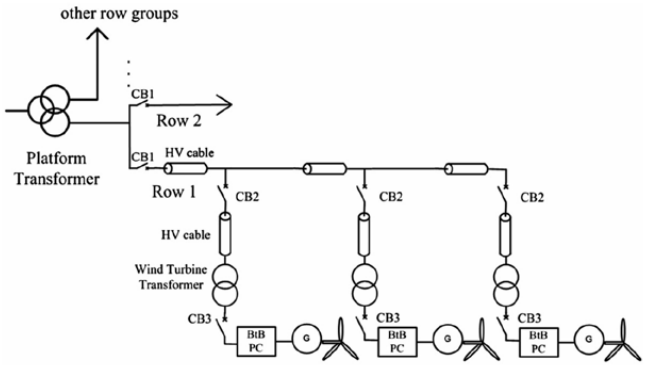

(a)

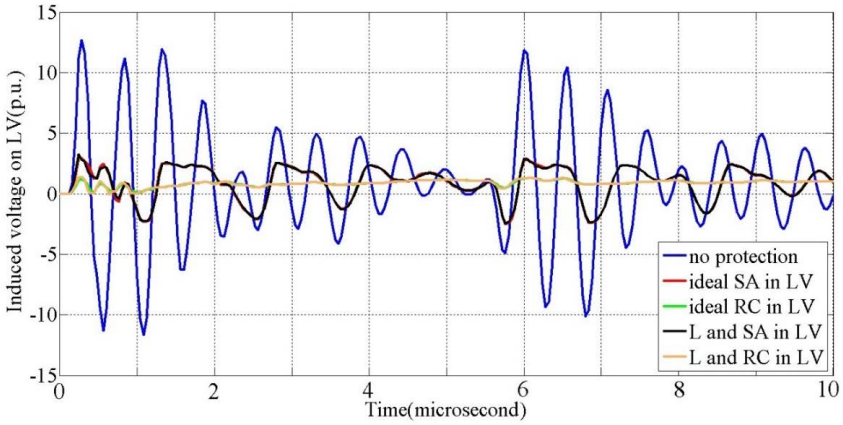

(b)

Figure 5–4. (a) Simulation circuit for resonant overvoltages in a typical offshore wind farm. (b) Induced voltage on LV-phase A for the energization of first WTT.

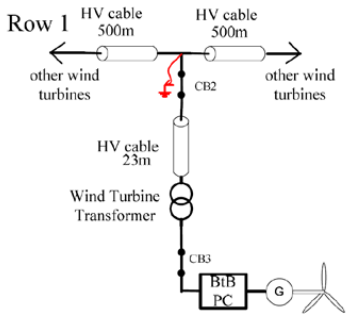

(a)

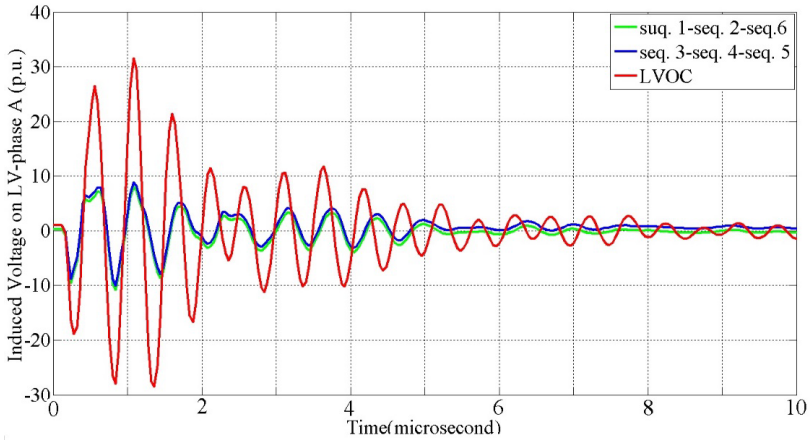

(b)

Figure 5–5. (a) Simulation circuit for resonant overvoltages due to earth fault. (b) Induced voltage on LV phase A for earth fault at peak phase A at the base of wind turbine. LVOC: Low Voltage Open Circuit. seq. 1-seq. 6: converter in various switching sequences.

5.2 Internal resonant overvoltages

Theoretically in resonance condition, the stored energy in the coils of transformer transfers to/from the available insulation capacitors. Thus, resonances typically occur at relatively high frequencies where a coil impedance in the transformer winding is in the range of an adjacent capacitor's impedance.

In this thesis, the internal resonant overvoltages are studied by means of measurement and modeling for three winding types, i.e disc, layer and pancake windings. In this way, an extended understanding can be achieved:

- The measurement technique is Sweep Frequency Response Analysis (SFRA).A 500 kVA transformer with three winding types, i.e. disc, pancake and layer, on three legs are presented and compared in paper *IV*.
- The abovementioned 500 kVA windings are modelled analytically in detail. The model is compared and verified by the measurements in paper *V*.

Along each of the windings, 25 taps are implemented to measure the transferred voltage along windings. The SFRA of the transferred voltage to the taps along 500 kVA 11kV disc winding shows that the voltage distribution is based on turn numbers along the winding up to 30 kHz (see figure 5.6). The first resonant frequency (terminal resonant frequency) at 70 kHz is in the form of one standing wave along the winding with nodes at the HV terminal and ground . The anti-node is located at the middle of winding. The amplitude of transferred voltage at the anti-node is 4 p.u. At higher resonant frequencies, there are more nodes and anti-nodes but lower transferred voltage amplitude compared to 70 kHz. It is also shown that the frequency response for taps along HV disc winding does not change significantly, if LV winding is short-circuited. The importance of voltage-to-ground measurements is to investigate the internal resonant overvoltages at winding parts close to LV winding or core yoke. For example, tap 2 ,which is close to top yoke, has high transferred voltage at resonant frequencies; 97, 161, 213, 276, 361 and 393 kHz compared to the transferred voltages at f <97 kHz.

The measurement of transferred voltage to the 25 taps along layer winding are shown in Figures 5-7 and 5-8 for open circuit and short circuited LV winding, respectively. As one sees in both figures, the trend of voltage distribution along layer winding is linear up to 680 kHz (=the first resonant frequency for tap number 1). Meanwhile, resonant frequencies for taps near to HV terminal, i.e. 23-25, can be observed with transferred voltages in the range of 1. p.u. 680 kHz is the dominant resonant frequency at tap 1 where the amplitude of transferred voltage is 1.2 p.u. which is relatively high compared to the response at lower frequencies. The energization of the transformer with short cables, e.g. wind turbine energizations, can lead to internal resonant overvoltages at this weak point, located near to LV terminal, if the quarter wave frequency of the cable matches with 680 kHz. The overvoltage can also occur during earth fault at short cable distance.

At 926 kHz, the transferred voltage pattern along taps looks like a standing wave superimposed on a decreasing linear trend. The anti-nodes of this standing wave are located at taps 24, 20 and 17 among which tap 20 is located on top of 10th layer and close to yoke or core frame and there is also high potential of internal overvoltages. For f > 926 kHz, the decreasing trend of transferred voltage vanishes and only the standing wave pattern can be observed at resonant frequencies (see Figure 5-7 top). When the LV terminal is short circuited, there is no significant change up to 680 kHz. For f > 680 kHz, the main changes in the transferred voltage pattern are

- At 926 kHz, the amplitude at anti-nodes located at taps 24, 20 and 17 slightly decrease.
- Addition of some resonant frequencies such as 823 kHz for tap 1, 1.8 MHz for tap 25, 22 and 20.

The transferred voltage pattern of pancake winding in Fig. 5-9 shows that combinational characteristics of both layer and disc windings can be observed here due

to the physical design of pancake winding. The standing wave at 40 kHz is similar to those at 70 kHz of Disc winding. The general decreasing trend up to 1.1 MHz is coming from layer nature of the bobbins of the pancake winding. The resonant frequencies at 3.27 and 7 MHz also have the decreasing trend along winding, the former one is also a resonant frequency for layer winding with low amplitude of transferred voltage at anti-nodes. The latter one is not common, though. A characteristic of the pancake winding is the dominant decreasing trend even at high frequency. This means that taps near the top yoke, which are close to ground terminal have lower transferred voltage at resonant frequencies compared to layer or disc winding.

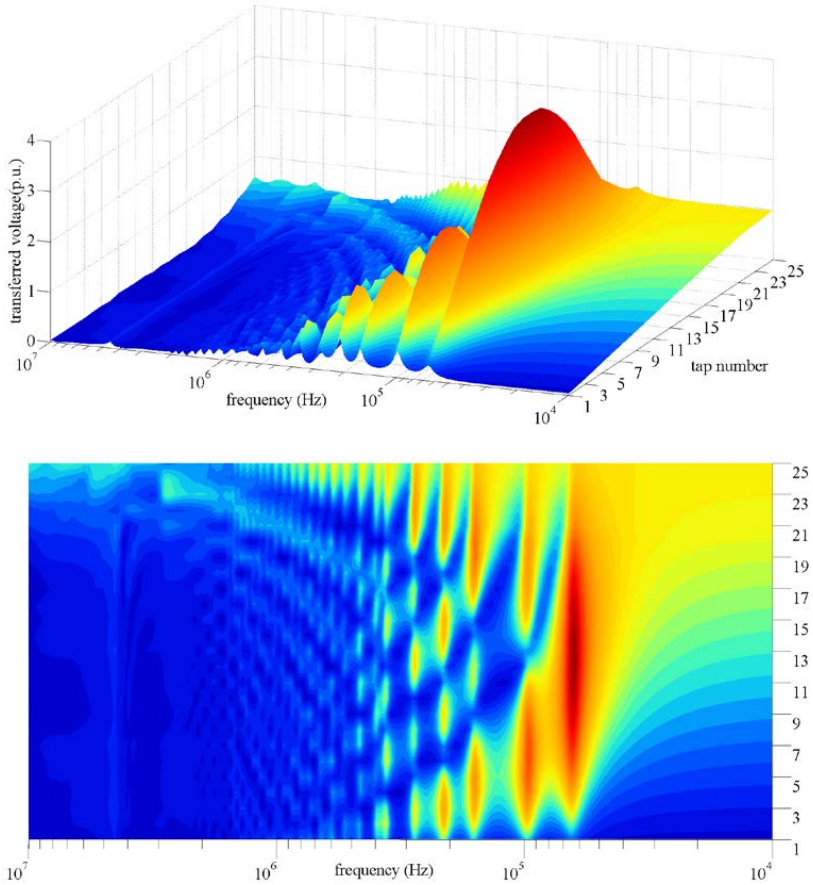

Figure 5-6. Measured transferred voltage to taps along disc winding-LV terminal is open. (Top: 3D view, bottom: 2D view.).

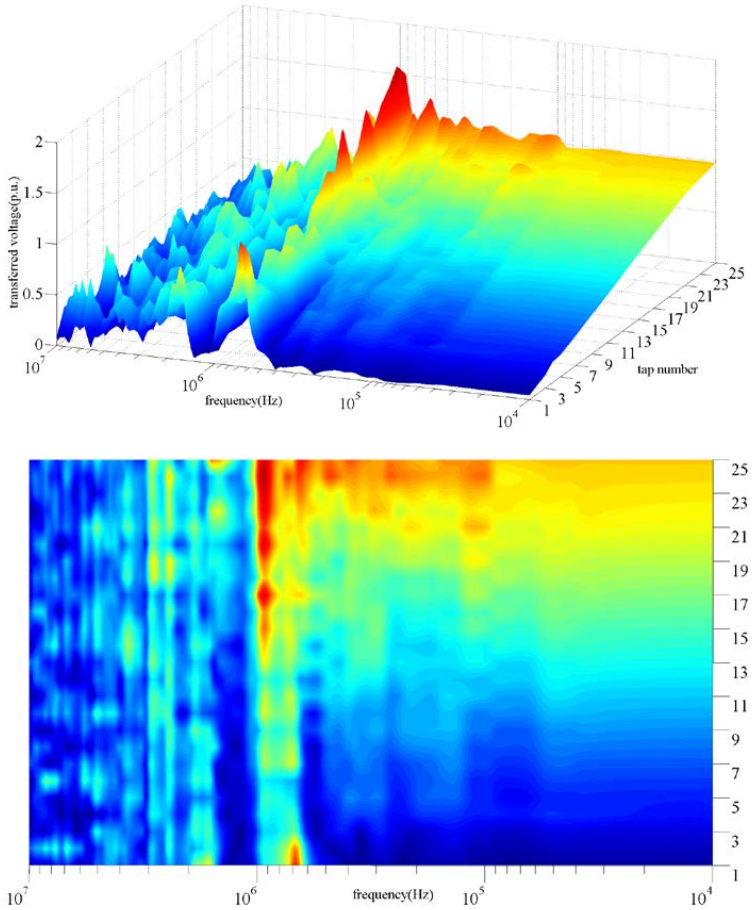

Figure 5-7. Measured transferred voltage to taps along layer winding-LV terminal is open. (Top: 3D view, bottom:2D view).

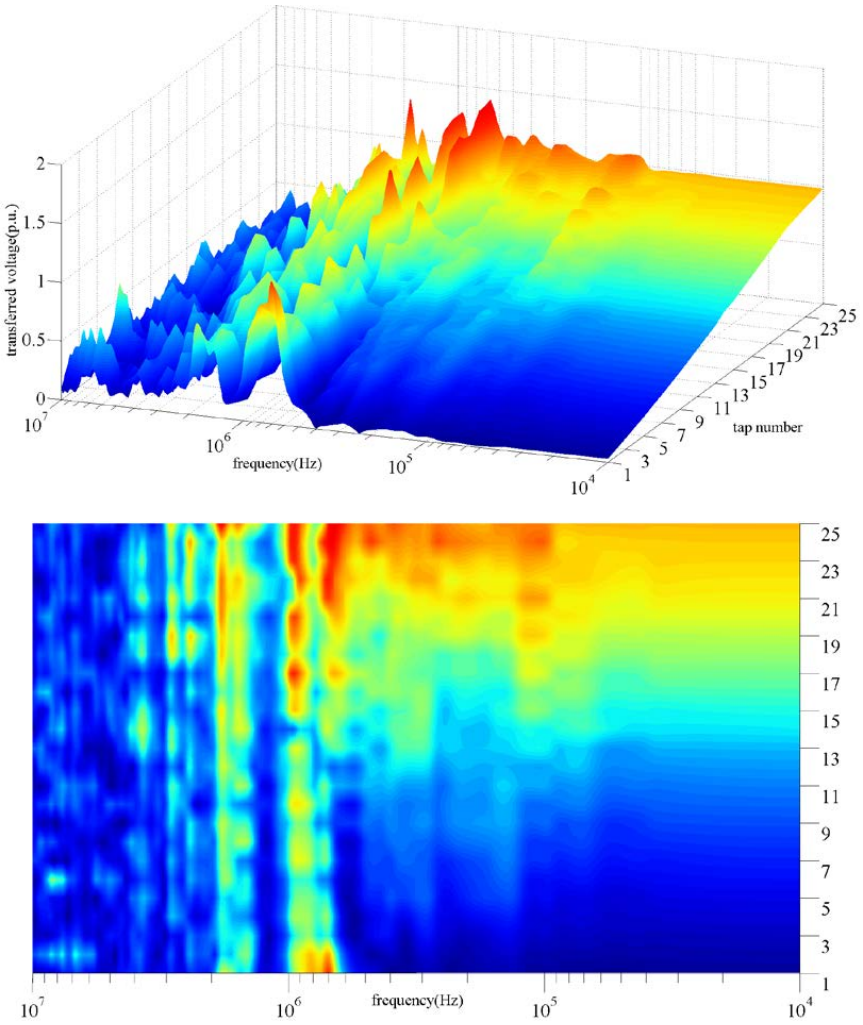

Figure 5-8. Measured transferred voltage to taps along layer winding-LV terminal is short circuited. (Top: 3D view, bottom:2D view).

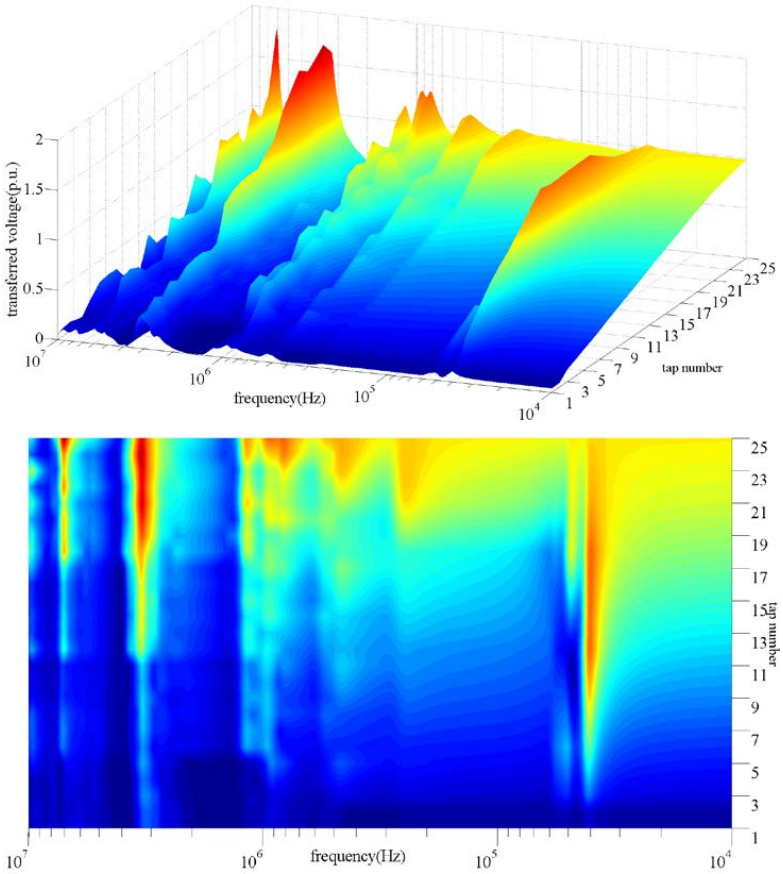

Figure 5-9. Measured transferred voltage to taps along pancake winding-LV terminal is open.(Top: 3D view, bottom:2D view).

Resonant overvoltages inside transformer can be seen as excessive voltage-to-groundor voltage drops, introduced as terminal resonance and internal resonance earlier. The first one is critical at resonant frequencies where the associated anti-nodes in HV winding are close to LV winding or yoke. The second one is critical at resonant frequencies where the associated out-of-phase anti-nodes are located closely in HV winding.

Figure 5-10 depicts the voltage drop across adjacent taps along three windings. It should be mentioned that voltage drop *i* means the voltage difference between taps *i+1* and *i*. As one can see in figure 3-2, taps 1-21 are located in the outer turn of disc pairs. Thus, the investigation of the voltage drop between taps in frequency domain is beneficial to perceive the internal resonance phenomena. It should be emphasized that the base for these voltage drop measurement is voltage-to-ground at HV terminal, which the color code for all of the measurements is according to. Regions with yellow up to red are assumed to have the high risk of internal resonances.

As one sees in Figure 5-10, the pattern of the internal resonances for disc winding is also based on standing wave theory same as voltage-to-ground in figure 5-6. The main resonant frequencies, which can result in internal resonant overvoltages, are 65, 100, 160, 200, 215, 290, 370 and 470 kHz. Comparing these frequencies with those in Fig. 5-6, we can find that they are related to the standing waves at 70, 100, 158, 210, 275, 360, 393 and 450 kHz respectively. The energization transient of transformers with short cables, i.e. 50-150m, in wind turbines has such frequency components. It is thus not recommended to use transformers with disc windings.

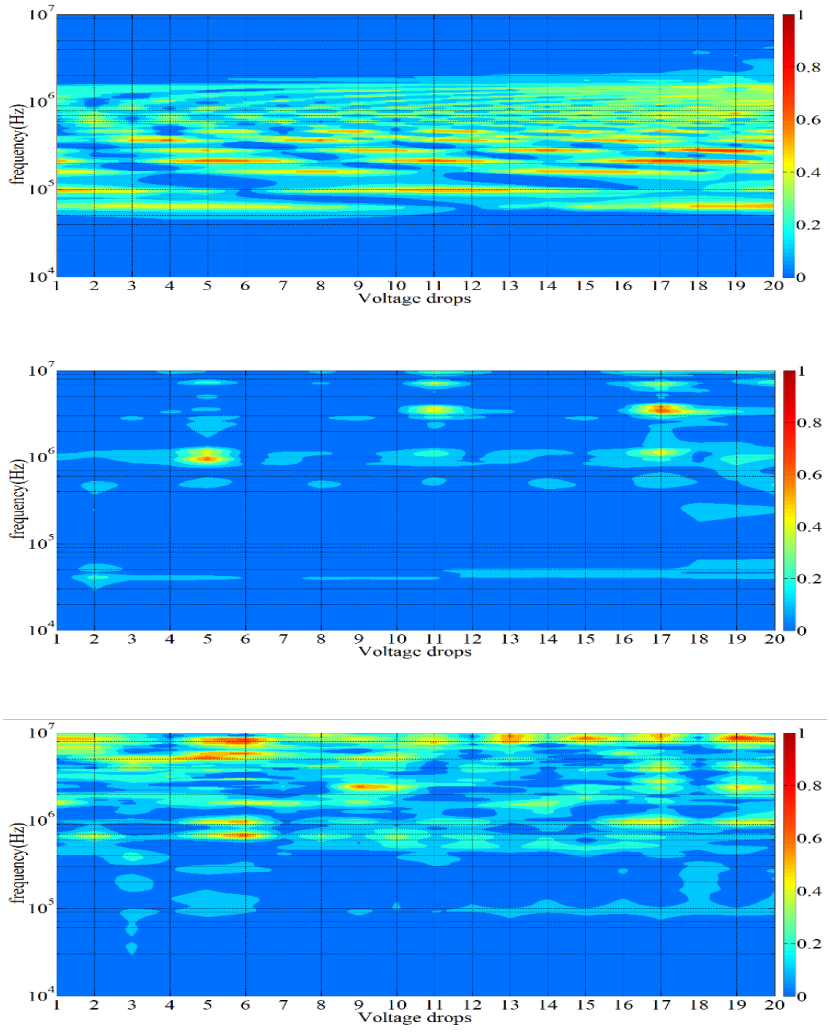

Figure 5–10. Measured voltage drops along disc (a), pancake (b) and layer (c) windings when LV terminal is open.

The pattern of voltage drops in pancake winding in Fig. 5-10 shows that this winding is not as vulnerable as disc winding. 0.950, 1.15, 3.5 and 4 MHz are the internal resonant frequencies. Not all of the taps in pancake winding are located in close distance as in disc or layer winding owing to designing the tap positions in the way that they are in the same turn numbers in three windings. It means that the adjacent points are not necessarily shown in the plot.

The voltage drop in the layer winding is shown in Figure 5-10 in the same way as disc and pancake windings. For layer winding, the adjacent taps *i+1* and *i* have a distance equal to half of winding height. Voltage drops are not cross the layers but along it. Therefore, they are not critical in the sense of insulation failure due to internal resonant overvoltages. In contrast, figures 5-11 show the voltage drop across the taps located close in adjacent layers (see Figure 3.2). Figure 5-11-(a) shows the voltage drop along odd taps which are located in the middle of the layer winding. There is high potential of internal resonance between tap 3 and 1 at 600-700 kHz. Most of the internal resonances are higher than 1 MHz and mostly between tap 17 and 19.

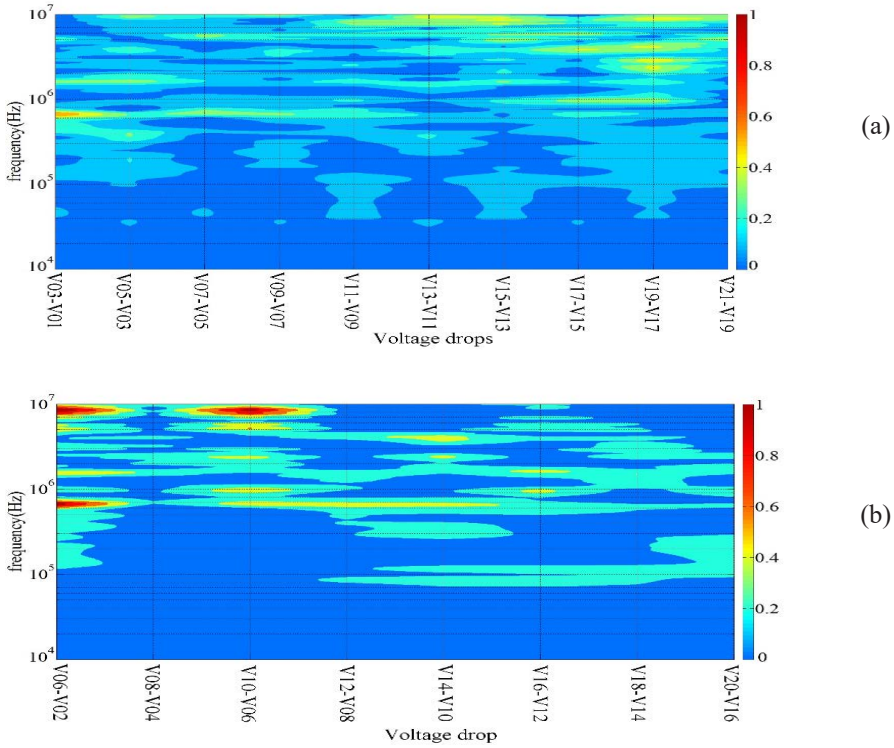

Figure 5–11. Measured voltage drops along layer windings when LV terminal is open. (a) adjacent taps in the middle of layer winding. (b) adjacent taps on top or bottom of layer winding.

Internal resonances across taps on top or bottom of adjacent layers are shown in figures 5-11-(b). The most critical ones occur for the voltage drop between tap 2 and 6 for 600-700 kHz or 9 MHz. The former can be excited with cable energization of transformer and the latter can happen due to close-up short circuits. Voltage drop across taps 6 and 10 has also high potential of internal resonance at 9 MHz

5.3 Modeling transformer windings

The proposed high frequency model, Lumped-parameter model, assists to draw general conclusions about both terminal and internal resonant overvoltages for the three aforementioned windings. The highest partitioning level for the representation of LV and HV windings has been used in the model. In this section the calculation results of this model are represented in comparison with the measurements. Then challenges and limitations are discussed. In Figure 5-12, the input impedance of HV layer, disc and pancake windings are shown. It can be observed that the calculations follow the trend of the measurement for Layer winding. The resonant frequency at 10kHz is not represented since flux linkage with other phases is not included in the model. This resonant frequency is also not represented for disc and pancake windings. The shortcoming of the model is that the resonant frequencies at 100 and 300 kHz for the measured HV winding is presented with a shift in the calculated model at 50 and 130 kHz.

Except from 10 kHz, the calculation result for HV input disc impedance is in good agreement with measurement for disc winding. The shortcoming is the shift in the resonant frequencies and slight higher amplitude of the calculated results.

For the pancake winding, the calculated results for HV impedance has the same decreasing trend and same amplitude range of the measurement results. Same as disc and layer windings, shift in the frequency response should be corrected. The double resonant frequencies at 40 and 50 kHz in the measurements is only represented with one resonant frequency at 30 kHz in the calculation results. In addition, the resonant frequency at 600 kHz is not represented in the calculation results.

The induced voltage on the LV terminal calculated by (12) in 2.4.2.2 is compared with measurements in Fig. 5-13 for three windings. The frequency range is now extended to 10 MHz, since the voltage probes are accurate also above 1MHz as mentioned in test setup section. Although quarter wave frequency of wind park feeder cables rarely can be in this range, close-up ground faults can give oscillations with such high frequencies. This also gives an opportunity to test the analytical model at higher frequencies.

As it can be seen in Figure 5-13, the model results for layer winding are in good agreement with measurements for f<1MHz. But, for f>1MHz, it only follows the decreasing trend of the measurements. The dominant resonant frequency in 1.6 MHz is not well represented. This will be discussed in detail in section 5.3.1. For disc winding, the model results follow the trend of measurement around 100 kHz. For the higher frequencies, this correspondence reduces.

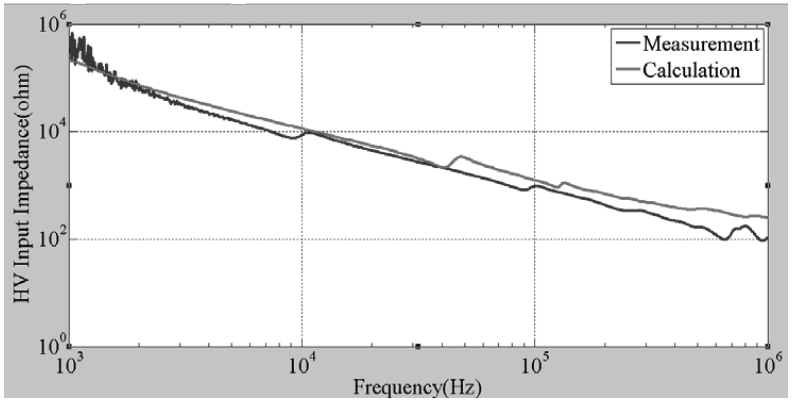

(a)

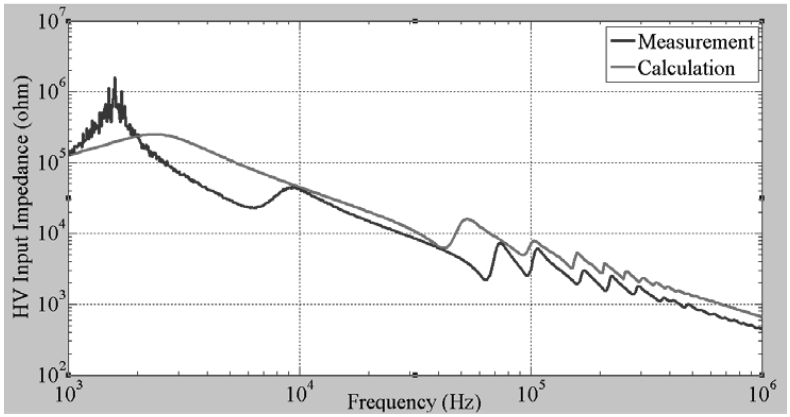

(b)

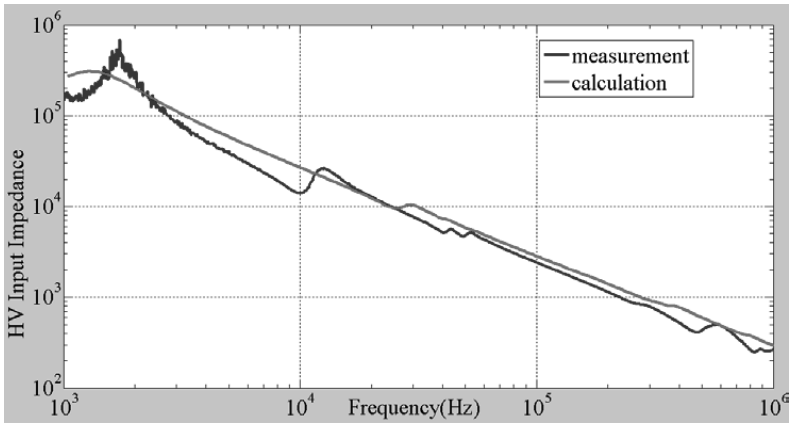

(c)

Figure. 5-12. The input HV impedance of the layer (a), disc (b) and pancake (c) winding.

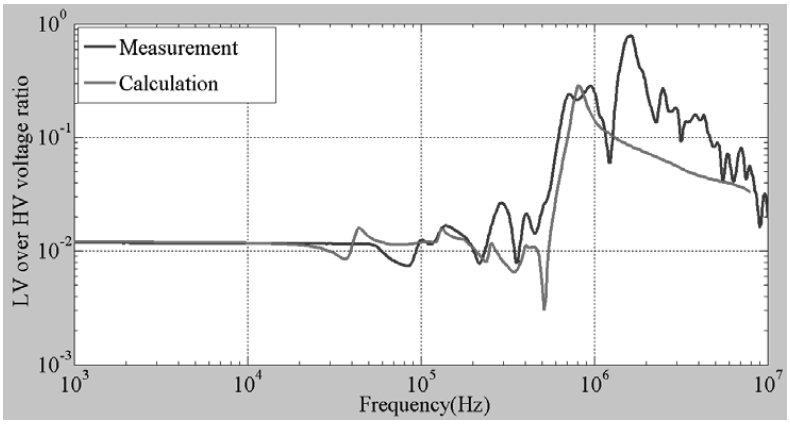

(a)

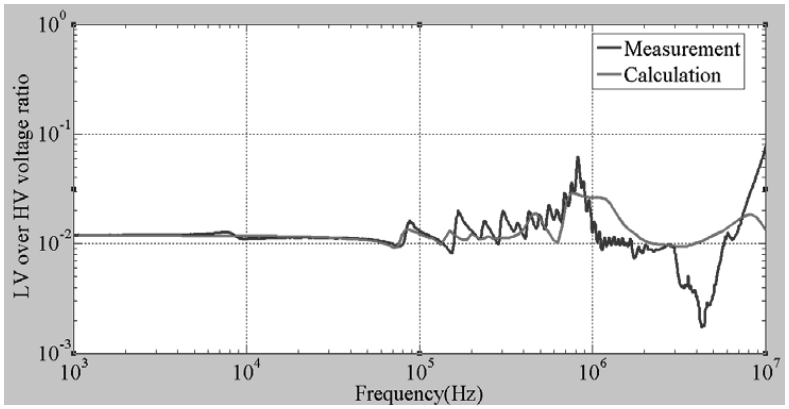

(b)

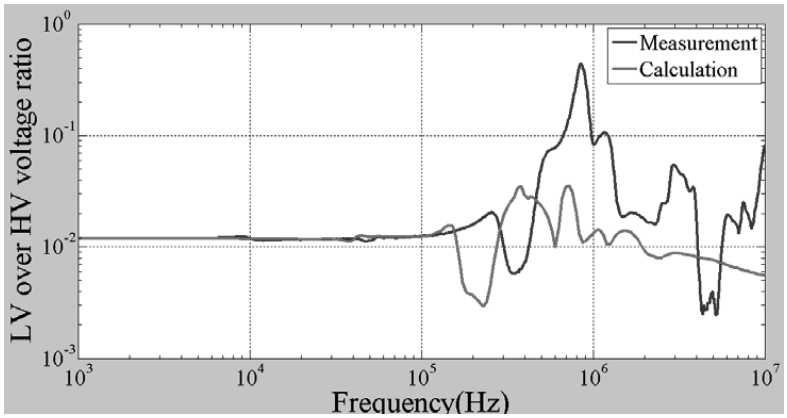

(c)

Figure. 5-13. The transferred voltage to LV for the layer (a), disc (b) and pancake (c) winding.

In the case of pancake winding, it seems that, the model results can represent the position of the resonant frequencies. However it can not represent the amplitude of the measurement near 800 kHz. According to equation (12), the calculation results for the transferred voltages to LV are sensitive to the accuracy of Z(nL,m) and Z(m,m) calculation The latter one is input HV impedance. Small, but not ignorable, deviations of calculation results from measurements can be observed in Fig. 5-12. There can be noticeable deviations in the Z(nL,m) calculations, but measurement cannot be obtained. These two deviations in numerator and denominator of (12) may lead to higher deviations for the calculation of transferred voltages.

5.3.1 Limitation of analytical RLC formula in Lumped-Parameter Model

As explained in the 2.4.2.2, the components of RLC matrices are calculated analytically. For this reason the precise geometrical data and material property of the transformer under study is required. In this work, we designed and produced this 500 kVA transformer. Therefore, detailed geometrical design data are available. The other input for modeling is conductor, core and insulation material properties, where only conductor material properties are available accurately. Core parameters mentioned in appendix of paper V, i.e. μ_z, σ_{core} and γ, are not available. Wilcox et al. proposed measurement techniques to obtain these parameters in the case of the mutual impedance between two coils [19]. However, those techniques cannot be applied to this special 500 KVA transformer. The calculation results are sensitive to core material properties. The three core parameters are estimated and optimized by the comparison of repetitive calculation results with measurements. A slight variation within the acceptable range [19] is made for one parameter in each calculation.

In the case of insulation materials, their permitivities are well-known. But, the detailed frequency dependency of the dissipation factors (tanδ) of all insulators, which is needed for accurate modeling, especially f>1 MHz is not available. One analytical equation from literature is included for all transformer insulations.

It should be mentioned that the layer winding conductor is aluminum due to design limitations. According to discussion with manufacture, it was not possible to choose any available copper wire cross section so that radial width, 50 Hz transformer impedance and turn ratio of layer winding became similar to those of disc and pancake winding. Nevertheless, Aluminum has higher skin depth compared to cupper. The conductor resistances at high frequency would be different between layer and two other windings. This will influence the amplitude of terminal impedances at resonant frequencies. But, the value of resonant frequencies is not dependent to conductor resistances, but to the capacitances and inductances.

The next issue to be discussed is the analytical calculation of the internal conductor resistance, which is one part of self-resistance. The other part is the self-resistance due to the core and is calculated by Wilcox formula. Fig. 5-14 shows the total self-resistance of the LV foil associated with disc winding according to the proposed model. The black solid line represents self-resistance due to core skin effect [57]. The dashed line shows

the internal conductor resistance based on Dowell's equation. The dashed-dotted line is the internal conductor resistance only due to skin effect [72].

It can be found that total resistance is dominantly affected by proximity effect for f>4MHz. Ignoring the proximity effect in the model and including just skin effect by the analytical formula in [72] leads to higher amplitude of the LV transferred voltage at resonant frequencies around 100 kHz in layer winding (see and compare Fig.13-a and Fig. 5-15). The reason is that the internal conductor resistance becomes two orders of magnitude lower for 10 kHz<f<1MHz by ignoring proximity (see Fig. 5-14). The calculation results for transferred voltage in this case has poor agreement with measurement for 50 kHz<f<500kHz. However, the calculations based on proximity effect formula cannot represent the trend of transferred voltage to LV in layer winding for f > 1MHz (see Fig. 5-13-a). Also, the dominant resonant frequency at 1.6 MHz is not represented. The calculations based on skin effect formula can represent the trend much better in this frequency range. But, improvements are still required for amplitude agreement. All in all, it can be concluded that based on the frequency range of study, the appropriate formula for the analytical calculation of the internal conductor resistance can be brought in the model.

In case of disc winding, the introduced Dowell formula leads to good amplitude calculation for resonant frequencies around 100 kHz (See Fig. 5-13). It however deteriorates the trend of induced LV voltage for higher frequencies. In the case of pancake winding, the amplitude of resonant frequencies around 1 MHz is considerably lower than measurements and it requires improvement.

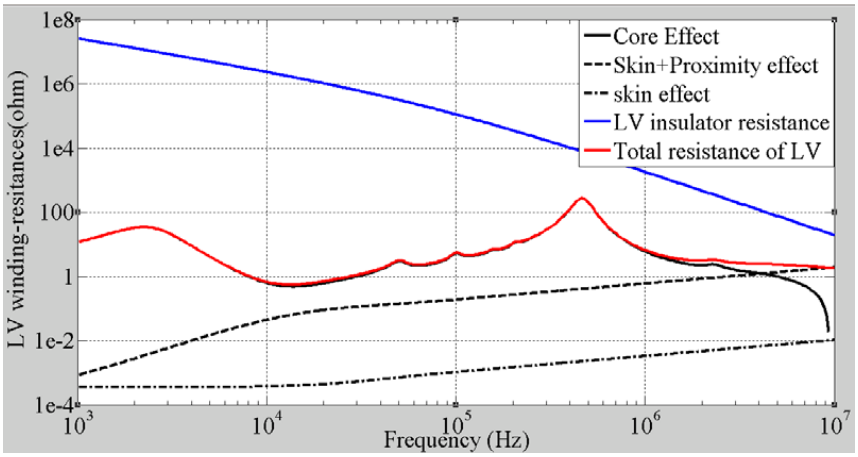

Figure. 5-14. The comparison of different resistances in LV winding with total resistance

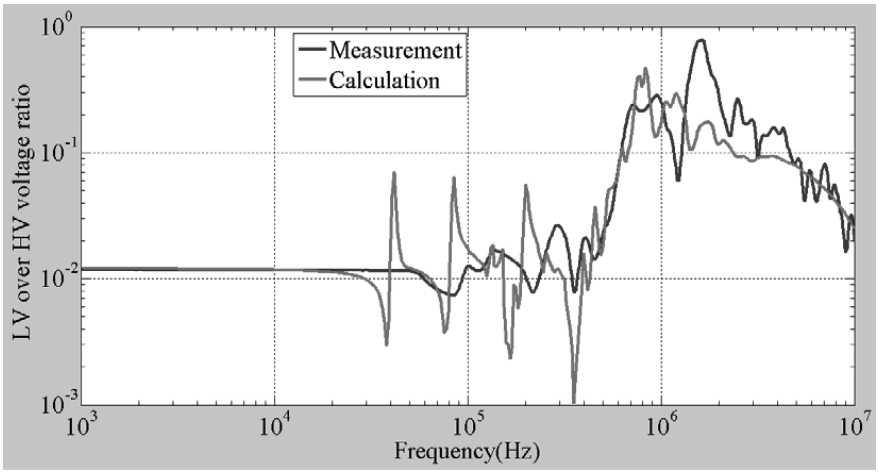

Figure. 5-15. Transferred voltage from HV to LV for layer winding. Proximity effect ignored in the calculations.

6 Conclusions and Future work

6.1 Conclusions

In this work, a comprehensive study of resonant overvoltages was carried out. The study was both system-oriented and component-oriented. The former was the simulations of resonant overvoltages in wind farm systems for the cases of energization transients and close-up earth faults. The latter dealt with wind turbine transformer as the main component between LV and MV systems. The internal resonant overvoltages are surveyed with measurements and modeling.

Referring to the energization simulation of the shifted 300 kVA transformer models with critical cable lengths in papers I the resonant overvoltages amplitude increases as the shift factor increases from 1 to 6 after that remains constant, i.e. larger transformers has slightly higher resonant overvoltage. For rate of rise/fall of overvoltage, increase in shift factor from 1 to 3 leads to abrupt reduction in du/dt from 460 to 240 p.u./μs. For shift factors more than 3 and towards 10, du/dt decreases slightly. For the base transformer model with shift factor equal to 1, the amplitude and du/dt are 30 and 400 p.u./μs, respectively for energization with 23 m cable.

In reality, during the energizations of transformers in wind farms, the LV terminal is open circuit since the power converter is not initiated while earth faults normally occur during operation of wind turbines, the power converter is connected at the LV side of transformer. To consider all of the probable situations, the earth fault at HV terminal when LV is open circuit is also studied here.

The simulation results for the 300 kVA transformer in the case of close-up earth faults at critical cable length, when power converter is connected, show a reduction of the amplitude and du/dt to one-third of the case when LV terminal is open circuit. When LV is open circuit and earth-fault occurs at 23 m distance from transformer at the peak of phase A in wind farm, the result is similar to a standalone cable-transformer energization. The amplitude and du/dt is 30 p.u and 400 p.u./ μs, respectively.

Regarding the protective and preventive measures against resonant overvoltages, surge arresters keep the amplitude of overvoltages low at LV terminal, but the du/dt cannot be decreased sufficiently. Simulation results indicate that just the implementation of RC filters alone can securely protect WTTs MV and LV terminal from resonant overvoltages. The selection of RC values should be carried out on the basis of both transient and steady state situations.

A white-box model for wind turbine transformer is introduced in this research for investigation of internal resonances. A 500 kVA transformer with three winding types, i.e. disc, layer and pancake, is designed and produced for this purpose. The validation of

the model is achieved by comparison of measurement on the test object and calculation results for the input HV impedance, input LV impedance and transferred voltages to LV in the frequency range 10 kHz-1 MHz:

- The model can represent i) the decreasing trend of the HV input impedance, ii) the increasing trend of the LV input impedance.
- The calculated resonant frequencies of the HV and LV input impedances are in good agreement with measurements.
- The dominant resonant frequency of the transferred voltage to LV for disc and pancake winding (800 kHz) is represented. This frequency is also critical for layer winding.

The shortcomings of the model can be listed as:

- There is slight frequency shift between measurement of impedance and the model.
- The Dowell's equation, which is applied to represent conductor resistance of windings, leads to overdamping of transferred voltage amplitudes at resonant frequency in the case of disc and pancake winding. But, the result for layer winding is quite good.

It is concluded that the simultaneous agreement between these calculation results, achieved by analytical model, and measurements is quite challenging. However, improved agreement can be achieved if:

1- All the dimension data, core parameters, the frequency dependent dissipation factors of LV, HV and LV-HV insulations are available.
2- The highest partitioning level for LV and HV winding is selected for the modeling.

The recommendation of this thesis is to compare winding types in the sense of internal resonances. In this way, the most vulnerable ones for wind farm applications can be identified and avoided. Winding types with moderate frequency response in these frequencies can be protective and preventive measures. Disc winding with many internal resonant frequencies in the range of 0.1-1 MHz is the most critical winding type while it is the least vulnerable in the case of transferred voltage to LV. The pancake winding with the modular winding design and repair easiness can be considered as an interesting alternative winding type for offshore wind farm.

6.2 Future work

The focus of this thesis work is on the transferred voltages inside HV windings when applying reference voltage and LV terminal is open circuited or earthed.

The following research works are proposed as future work:

- Since the proposed model aims to assist wind transformer designers and operators to improve windings design against very fast transients, especially resonant

overvoltages, the model should have this feature to draw general conclusions. In future work, the sensitivity of calculation results on core and insulation material properties is going to be investigated in more detail to improve agreements with calculations, particularly the transferred voltages to LV in pancake windings.

- The frequency characteristic of the internal winding resistance can not be represented properly with Dowell's equation for disc winding in the range of 100 kHz- 1 MHz. The improvement of internal resistance matrix can be assessed with numerical FEM methods.

- Internal resonant in LV windings associated with the three HV windings, disc, layer and pancake can be calculated via the analytical model. In this way, the effect of HV winding type on the vulnerability of the LV windings can be understood.
- The effect of power converters on overvoltages can be analyzed during de-energization or switching off at MV grid.
- Resistive-Capacitive filters at both HV and LV terminals are effective protective measures for transferred resonant overvoltages. Their effect on moderating internal resonance can be investigated both analytically and by measurement on the 500 kVA transformer.
- The internal resonances in HV winding can be studied when the LV terminal is energized and HV winding is open circuit, earthed or loaded. In this way, the transfer of high frequency spikes from power converters to HV side can be investigated.

References

[1] T. Ackermann, *Wind power in power system*, Chichester: Wiley, p. 54-55.,2005.

[2] "Key World Energy Statistics", ed. Online: International Energy Agency, 2014.

[3] "Wind in Power, 2014 European statistics", ed Online: European Wind Energy Associasion, 2015.

[4] M. J. Pasqualetti, "Opposing wind energy landscapes: A search for common cause", *Annals of the Association of American Geographers,* vol. 101, no. 4, pp. 907-917, 2011.

[5] H. R. Zamot, E. O'Neill-Carrillo, and A. Irizarry-Rivera, "Analysis of wind projects considering public perception and environmental impact", in proceeding of *37th Annual North American Power Symposium, 2005*, Piscataway, NJ, USA, 2005, pp. 591-6.

[6] A. R. Henderson, C. Morgan, B. Smith, H. C. Sørensen, R. J. Barthelmie, and B. Boesmans, "Offshore wind energy in Europe - A review of the state-of-the-art", *Wind Energy,* vol. 6, no. 1, pp. 35-52, 2003.

[7] S. Gordon, "Supergrid to the rescue", *Power Engineer,* vol. 20, no. 5, pp. 30-33, 2006.

[8] P. W. Carlin, A. S. Laxson and E. B. Muljadi, "The History and State of the Art of Variable-Speed wind Turbine Technology", Technical report, National Renewable Energy Laboratory/National Wind Technology Center, 1617 Cole Boulevard, Golden, CO 80401, USA, Feb. 2001.

[9] J. Larsen, H. C. Soerensen, E. Christiansen, S. Naef, P. Vølund, "Experiences from Middelgrunden 40 MW Offshore Wind Farm", in proceeding of Copenhagen Offshore Wind, 26-28 October 2005.

[10] E. Ayers, M. Dickinson, "Wind Farm Transformer Design Considerations, Unique requirements call for thoughtful analysis and re-evaluation", available online: http://www.power-eng.com/articles/print/volume-115/issue-11/features/wind-farm-transformer-design-considerations.html

[11] T. Steeber, "Why do wind turbine transformers fail so often?" , available online: http://www.windpowerengineering.com/featured/business-news-projects/why-do-wind-turbine-transformers-fail-so-often/

[12] Solomon Corporation, "Custom Design Transformers For Wind Farms", available online: http://www.solomoncorp.com/wind-farm-design.html

[13] J. O'Brien, M. Lashbrook, M. Martin, "Synthetic Ester Transformer Fluid A Total Solution to Offshore Transformer technology", in proceeding of European Offshore Wind Conference 2009, Stockholm, Sweden.

[14] R. Walling "Power Transformer Application for Wind Plant Substations", IEEE PES Wind Plant Collector System Design Working Group, 2010.

[15] Torgny Moller, “Major Transformer Failure at Nysted, Denmark”, Windpower Monthly, 2007, available online: http://www.windaction.org/posts/10341-major-transformer-failure-at-nysted-denmark

[16] Mortenson Construction, “Design Considerations for Wind Turbine Generator Padmount Transformers,” available online: http://www.mortenson.com/ResourcePage_Article_art_REGNews_2013_winter_design_considerations_padmount_transformers.aspx

[17] B. Gustavsen, “Study of transformer resonant overvoltages caused by cable-transformer high frequency interaction,” IEEE transaction on Power Delivery, Vol. 25, No. 2, pp. 770-779, April 2010.

[18] M. R. Meshkatodini, A. Shahmohammadi, M. Majidi and M. Karami,"Comparative Study of the Effect of Various Shields on Lightning Electric Field in Power Transformer Windings," in proc. of IEEE Trondheim PowerTech, 2011.

[19] A. Shahsiah, R.C. Degeneff and J.K. Nelson, "A Study of the Temperature-Based Dynamic Nature of Characteristic Gases in Oil-cellulose Insulation Systems", IEEE Transactions on Dielectrics and Electrical Insulation, vol. 14, no. 2, April 2007.

[20] D. E. Ayers and M. Dickinso, "Wind Farm Transformer Design Characterstics", Power engineering, volume 115, issue 11, online: http://www.power-eng.com/articles/print/volume-115/issue-11/features/wind-farm-transformer-design-considerations.html

[21] R. Piwko, N. Miller, R. Girad, J. MacDowell, and K. Clark, “Generator fault tolerance and grid codes,” IEEE Power Energy Mag., vol. 8, no. 2, pp. 18–26, Mar./Apr. 2010.

[22] J. I. Marvik, H.G. Svendsen, "Analysis of Grid Faults in Offshore Wind Farm with HVDC Connection", In proc. DeepWind 2013, Energy Procedia, Volume 35; 2013

[23] C. Feltes, R. van de Sandt, F. Koch, F. Shewarega, I. Erlich, "Neutral Grounding in Wind Farm Medium Voltage Collector Grids", in proc. of Power Systems Conference and Exposition (PSCE), 2011 IEEE/PES, Phoenix, AZ, USA, 2011.

[24] C. Han , D. E. Martin, M. R. Lezama, "Transient Over-Voltage (TOV) and its suppression for a large wind farm utility interconnection", in Proceedings of International Conference on Sustainable Power Generation and Supply, 2009.

[25] L. Liljestrand, A. Sannino , H. Breder, and S. Thorburn, “Transients in collection grids of large offshore wind parks,” Wiley Inter science, vol. 11, Issue 1, Pages 45 – 61, 2008.

[26] I. Arana: Switching overvoltages in off-shore wind power grids. PhD thesis, Lyngby: Technical University of Denmark, 2011.

[27] A. Holdyk: Interaction between main components in wind farms. PhD thesis, Kgs. Lyngby: Technical University of Denmark, 2013.

[28] B. Badrzadeh, M. Høgdahr, N. Singh, H. Breder, K. Srivastava, M. Reza, ” Transient in wind power plants- part II: case studies”, in proc of IEEE Industry Applications Society Annual Meeting (IAS), October 2011.

[29] M. Reza, H. Breder, L. Liljestrand. A. Saninno, T. Abdulahovic, T. Thiringer, “An experimental investigation of switching transients in a wind-collector grid scale model in a cable system laboratory”, in proc. of 20th International Conference and Exhibition on Electricity Distribution (CIRED), Czech Republic, 2009

[30] B. Badrzadeh, B. Gustavsen, “High frequency modeling and simulation of wind turbine transformer with doubly fed asynchronous generator”, IEEE transaction on Power Delivery, Vol. 27, No. 2, pp. 746-756, 2012.

[31] T. Adielson, A. Carlson, H. B. Margolis, and J. A. Halladay, “Resonant overvoltages in EHV transformers-Modeling and application,” IEEE Trans. Power App. Syst., Vol. 100, pp. 3563–3572, 1981.

[32] W. J. McNutt, T. J. Blalock and R. A. Hinton, “Response of transformer windings to system transient voltages”, IEEE Trans. Power Syst. Apparatus and Systems, Vol. 93, pp. 457-467, 1974.

[33] N. Ito, “Local Resonance in a Main Transformer Winding,” ThermalNucl. Power, Vol. 47, pp. 651–654, 1996.

[34] G. Paap, A. Alkema, and L. van der Sluis, “Overvoltages in power transformers caused by no-load switching,” IEEE Trans. Power Delivery, vol. 10, pp. 301–307, Jan. 1995.

[35] B. Gustavsen, A. P. Brede, and J. O. Tande, “Multivariate analysis of transformer resonance overvoltages in power stations,” IEEE trans. on power del., vol. 26, no. 4, pp. 2563–2572, 2011.

[36] A. H. Soloot, H. J. Bahirat, H. K. Høidalen, B. Gustavsen, B. A. Mork, ” Investigation of resonant overvoltages in offshore wind farms-modeling and protection”, in proc. International Conference on Power Systems Transients (IPST), 2013.

[37] M. Kaufhold, G. Borner, M. Eberhardt and J. Speck, “Failure mechanism of the Interturn insulation of low voltage electric machines fed by pulse-controlled inverters”, IEEE Electr. Insul. Mag., Vol. 12, No. 5, pp. 9-16, 1996.

[38] K. Nakanishi. S. Fujita, H. Kurita. A Kishi and Y. Shibuyn. “High frequency voltage oscillation in transformer winding and electrical breakdown properties of lntertum Insulation Immersed in oil at VFT Voltage”, IEEE Conf. Electr. Insul. Dielectr. Phenomena (CEIDP), Minneapolis, USA, pp. 490-493, 1997.

[39] Tarek Abdulahovic: Analysis of high-frequency electrical transients in offshore wind parks. PhD. Thesis, Göteborg: Chalmers University of Technology. 2011.

[40] B. Gustavsen, ”Wide band modeling of power transformers”, IEEE Transactions on Power Delivery, Vol.19, No. 1, pp. 414–422, January 2004.

[41] B. Gustavsen, ”Computer code for rational approximation of frequency dependent admittance matrices, IEEE Transactions on Power Delivery, Vol. 17, No. 4, pp. 1093–1098, October 2002.

[42] J. A. Martinez-Velasco, Power System Transients Parameter Determination, London, U.K.: CRC Press, 2010.

[43] K.J. Cornick, B. Filliat, C. Kieny, and W. Muller, ”Distribution of very fast transient overvoltages in transformer windings”, CIGRE Session, Report 12–204, 1992.

[44] Y. Shibuya, S. Fujita, and N. Hosokawa, ”Analysis of very fast transient overvoltage in transformer winding”, IEE Proceedings C, Generation, Transmission and Distribution, Vol.144, No. 5, pp. 461–468, September 1997.

[45] Y. Shibuya, S. Fujita, and E. Tamaki, Analysis of very fast transients in transformer, IEE Proceedings C, Generation, Transmission and Distribution, Vol. 148, No. 5, pp. 377–383, September 2001.

[46] M. Popov, L.V. Sluis, and G.C. Paap, ”Computation of very fast transient overvoltages in transformer windings”, IEEE Transactions on Power Delivery, Vol. 18, No. 4, pp. 1268–1274, October 2003.

[47] G. Liang, H. Sun, X. Zhang, and X. Cui, ”Modeling of transformer windings under very fast transient overvoltages”, IEEE Transactions on Electromagnetic Compatibility, Vol. 48, No. 4, pp. 621-627, November 2006.

[48] M. Popov, L. van der Sluis, R.P.P. Smeets, and J. Lopez Roldan, “Analysis of very fast transients in layer-type transformer windings”, IEEE Transactions on Power Delivery, Vol. 22, No. 1, 238–247, January 2007.

[49] L. Bergeron, Water Hammer in Hydraulics and Wave Surges in Electricity, Wiley, New York, 1961.

[50] J.L. Naredo, A.C. Soudack, and J.R. Marti, “Simulation of transients on transmission lines with corona via the method of characteristics”, IEE Proceedings C, Generation, Transmission and Distribution, Vol. 142, No. 1, pp. 81–87, 1995.

[51] C.R. Paul, “Incorporation of terminal constraints in the FDTD analysis of transmission lines”, IEEE Transactions on Electromagnetic Compatibility, Vol. 36, No. 2, pp. 85–91, May 1994.

[52] J. Wilcox, “Numerical Laplace transformation and inversion”, International Journal of Electrical Engineering Education, Issue. 15, pp. 247–265, 1978.

[53] P. Moreno and A. Ramirez, “Implementation of the numerical Laplace transform: A review”, IEEE Transactions on Power Delivery, Vol. 23, No. 4, pp. 2599–2609, October 2008.

[54] L. Rabins, “Transformer Reactance Calculations with Digital Computers”, Transactions on AIEE, July 1956, Vol.75, pp. 261-267.

[55] P.I. Fergestad and T. Henriksen, “Transient Oscillations in Multiwinding Transformers”, IEEE Transactions on Power Apparatus and Systems, January/June 1974, Vol.PAS-93, pp. 500-509.

[56] D.J. Wilcox, W.G. Hurley and M. Conlon, “Calculation of Self and Mutual Impedances between Sections of Transformer Windings”, IEE Proceedings, Part C, September 1989, Vol.136, No.5, pp. 308-314.

[57] L.F. Blume, A. Boyajian, G. Camilli, T.C. Lennox, S. Minneci and V.M. Montsinger, “Transformer Engineering”, John Wiley & Sons Publications, New York, London, 1951

[58] J.H. McWhirter, C.D. Fahrnkopf and J.H. Steele “Determination of Impulse Stresses within Transformer Windings by Computers”, Transactions on AIEE, February 1957, Vol.75, pp. 1267-1274.

[59] R.B. Shipley, D. Coleman and C.F. Watts, „Transformer Circuits for Digital Studies”, Transactions on AIEE, February 1963, Vol.81, pp. 1028-1031.

[60] E.C. Cherry, “The Duality between Interlinked Electric and Magnetic Circuits and the Formation of Transformer Equivalent Circuits”, Proceedings of the Physical Society, February 1949, Section B, Vol.62, pp. 101-111.

[61] H. Edelmann, “Anschauliche Ermittlung von Transformator-Ersatzschaltbildern”, Archiv für elktrische Übertragung, 1959, Band 13, Heft 6, S. 253-261.

[62] N. A. Demerdash, F.A. Fouad, T.W. Nehl and O.A. Mohammed, “Three Dimensional Finite Element Vector Potential Formulation of Magnetic Fields in Electrical Apparatus”, IEEE Transactions on Power Apparatus and Systems, August 1981, Vol.PAS-100, No.8, pp. 4104-4111.

[63] F. De León and A. Semlyen, “Efficient Calculation of Elementary Parameters of Transformers”, IEEE Transactions on Power Delivery, January 1992, Vol.7, No.1,pp. 376-383.

[64] R.S. Girgis, D.A. Yannucci and J.B. Templeton, “Performance Parameters of Power Transformers using 3D Magnetic Field Calculations”, IEEE Transactions on Power Apparatus and Systems, September 1984, Vol.PAS-103, No.9, pp. 2708-2713.

[65] G. Lian, Y. Ruoping and C. Pizhang, “An Equivalent Magnetization Surface Current Approach of Calculation 3-Dimentional Leakage Fields of a Transformer”, IEEE Transactions on Power Delivery, July 1987, Vol.2, No.3, pp. 817-822.

[66] A. Holdyk: Critical Voltage Distributions in the dry type transformers of large wind turbines when exposed to transients . PhD thesis, Kgs. Lyngby: Technical University of Denmark, 2007.

[67] H. B. Margolis, J. D. Phelps, A. A. Carlomagno, and A. J. McElroy, “Experience with part-winding resonance in EHV auto-transformers: Diagnosis and corrective measures,” IEEE Trans. Power App. Syst., vol. PAS-94, no. 4, pp. 1294–1300, Jul./Aug. 1975.

[68] T. Teranishi, Y. Ebisawa, T. Yanai, and M. Honda, “An approach to suppressing resonance voltage in transformer tap windings,” IEEE Trans. PAS-102, no. 8, pp. 2552–2558, Aug. 1983.

[69] T. Teranishi, T. Yanari, M. Honda, and T. Inoue, “Dielectric strength of transformer insulation models against oscillatory impulse voltages,” Trans. Inst. Elect. Eng. Jpn. B, vol. 104, no. 1, pp. 57–63, 1984.

[70] K. Nakanishi, S. Fujita, H. Kurita, A. Kishi, T. Hasegawa, and Y. Shibuya, “High frequency voltage oscillation in transformer windings and electrical breakdown properties of interturn insulation immersed in oil at VFT voltage,” Trans. Inst. Elect. Eng. Jpn. B, vol. 118, no. 11, pp. 1228–1234, 1998.

[71] H. Nakao, Y. Nakagoshi, M. Hatano, S. Nogawa, K. Kajimura, and M. Kuwata, “Insulation design of AC filter reactor tap winding for HVDC converter station,” Trans. Inst. Elect. Eng. Jpn. B, vol. 119, no. 12, pp.1536–1541, 1999.

[72] J.Lammeraner, M. Stafl, *Eddy Current*, Iliffe books Ltd., London, 1966, pp.21.

Appendix

The complete five papers are inserted in the chapter.

Paper I

Wind Energy

WIND ENERGY
Wind Energ. 2015; **18**:1061–1074
Published online 10 April 2014 in Wiley Online Library (wileyonlinelibrary.com). DOI: 10.1002/we.1748

RESEARCH ARTICLE

Resonant overvoltage assessment in offshore wind farms via a parametric black-box wind turbine transformer model

Amir Hayati Soloot[1], Hans Kristian Høidalen[1] and Bjørn Gustavsen[2]

[1] Department of Electrical Power Engineering, Norwegian University of Science and Technology, Trondheim N-7491, Norway
[2] SINTEF Energy Research, Trondheim N-7465, Norway

ABSTRACT

The protection of offshore wind farms (OWFs) against overvoltages, especially resonant overvoltage, is of paramount importance because of poor accessibility and high repair costs. In this paper, we study how switching overvoltages at the wind turbine transformer (WTT) medium voltage (MV) side can lead to high overvoltages on the low voltage (LV) side. The effect of overvoltage protective devices is analyzed. A detailed model of an OWF row is developed in electromagnetic transients program–alternative transients program (EMTP-ATP), including interconnecting cables, WTT, surge arresters and resistive–capacitive filters. A parameterized black-box WTT model is obtained from measurements and is used for investigating the transfer of resonant overvoltages from the MV to the LV side. The model is capable of shifting systematically the frequencies and adjusting the transformer input impedance. Simulation results show that wind turbine energization in an OWF can lead to overvoltages on the LV terminals. The rate of rise of overvoltages (du/dt) is in the range of 300–500 pu/μs. It is found that resistive–capacitive filters should be installed on both MV and LV terminals of WTTs to decrease both resonant overvoltages and du/dt, which is unachievable by surge arrester alone. Copyright © 2014 John Wiley & Sons, Ltd.

KEYWORDS

offshore wind farms; wind turbine transformers; resonant overvoltages; surge arresters; energization topologies

Correspondence

A. H. Soloot, Department of Electrical Power Engineering, Norwegian University of Science and Technology, Trondheim N-7491, Norway.
E-mail: amir.h.soloot@ntnu.no

Received 29 August 2013; Revised 27 January 2014; Accepted 18 March 2014

NOMENCLATURE

OWF	Offshore wind farm
WTT	Wind turbine transformers
SA	Surge arrester
VCB	Vacuum circuit breaker
RC	Resistive–capacitive filter
HV, MV, LV	High voltage, medium voltage, low voltage
du/dt	Maximum rate of rise (or fall) of overvoltages
f_{dr}	Dominant resonant frequency in voltage transfer function
Z_t	Transformer MV input impedance
Z_c	Surge impedance of feeding cable
f_s	Cable quarter-wave resonant frequency
f_r	Transformer resonant frequency
α	Shifting factor
β	Scaling factor
s	Laplace variable

m	The kVA scaling factor
v_{cable}	The surge velocity in lossless feeder cable
l	Feeder cable length
τ	Traveling time in cable
c	Speed of light in vacuum
ε_r	Relative permittivity of cable insulation

1. INTRODUCTION

Because of the increased distance of OWFs from shores and adverse weather conditions in oceans, the main criteria in their design and operation are high reliability and little maintenance requirement. To achieve this, the protection of electrical components against various overvoltages should be improved compared with land-based installations. In the work by King *et al*.,[1] the overvoltages were categorized, and the upcoming destructive events in OWFs were reviewed according to the IEC60071-1 classification: continuous operating voltage, temporary overvoltages, slow front (switching), fast front (lightning) and very fast front transients. Besides, attention must be paid to the voltage level, i.e. HV, MV or LV, in which these overvoltages occur, since the effective protective measures depend on both the overvoltage type and the voltage level in wind farm. For example, an OWF can be connected to a power network with 132 kV (HV level) subsea cables. The platform transformer has the collection grid in the secondary side at 33 kV, MV level. The WTTs are connected in cable rows to platform transformer at this MV level. Each WTT has the generator at its secondary side at 230 V, LV level.

The analysis of temporary overvoltages in long HV cables initiated by disconnection of wind power plants is presented in the work by Akhmatov *et al*.[2] It is concluded that the converter-controlled wind turbine generators should be supported by having fault-ride-through requirements to mitigate such temporary overvoltages. Transient overvoltages are analyzed in the work by Han *et al*.[3] during inadvertent cable feeder deenergization and fault clearing scenarios on the collection grid of a large wind farm (300 MW). The impact of WTT configuration, Δ/Yn or Yn/Yn, is evaluated, and solutions to suppress the overvoltage, i.e. grounding transformer and fast grounding switch, are proposed. The energization (switching) overvoltages of cable feeders are simulated while other feeders are not connected and compared with the case where other feeders are connected.[4] Arana *et al*. compared the simulation results for energization overvoltages with measurements in Nysted OWF.[5] They compared the modeling and simulation results in Power System Computer Aided Design (PSCAD) and Power Factory.

The switching overvoltages at MV collection grid can also be studied with the consideration of the impact of restrikes and reignitions of VCBs on wind transformer terminals.[6,7] The propagation of the overvoltages along WTTs winding connected to MV collection grid is also prominent to investigate.[8] The high-frequency properties of a 3.14 MVA 35/1.0/0.4 kV WTT, commonly used for the doubly fed asynchronous generator, are investigated, and it is shown that the voltage transfer from the 35 kV side to either of the two LV taps is strongly dependent on the loading of the other tap.[9] It is also shown that the use of a simplified transformer model based on lumped capacitances gives unrealistic results.

There have been few studies on the transferred resonant overvoltage to LV side. Therefore, the motivation of this paper is investigating these overvoltages, which are harmful for both transformer and power converters. The resonant overvoltages can occur both due to energization transients[10] and close-up short circuits,[11,12] when the frequency of a sustained voltage oscillation at the transformer MV terminals matches with a resonant frequency in the WTT voltage transfer function. The frequency of such oscillations is closely linked to the topology and lengths of the cables. The conditions of resonant overvoltage in cable-transformer interaction is discussed in detail in the work by Gustavsen,[13] showing overvoltages as a function of cable lengths. Furthermore, the transformer transfer characteristics are prominent in resonant overvoltages.

Resonant overvoltages can also occur inside transformer winding[14] and is dominantly dependent on winding type, i.e. disk, layer or pancake.[15,16] In the work by Soloot *et al*.,[17] it is shown that the measurement of resonant frequencies and the amplitude of transferred voltages at LV or internal HV winding are quite sensitive to the voltage and current measurement techniques.

The novelty of this paper is introducing a parametric wideband WTT model to comprehensively calculate resonant overvoltages for various transformer designs and power ratings. This model is based on a black-box model[18] obtained from measurements where we introduce shifting and scaling factors for the model's poles, residues as well as the input impedance.

The other aim of this paper is systematic investigation of overvoltages resulting from the energization of a row. The impact of the feeding cable length and wind turbine connection topologies on resonant overvoltages are assessed. The impact of SAs and RC filters on overvoltage mitigation is also highlighted. Finally, the induced overvoltages due to energization of the other rows in OWFs are surveyed.

Wind Energ. 2015; **18**:1061–1074 © 2014 John Wiley & Sons, Ltd.
DOI: 10.1002/we

In this paper, the parametric model of WTT is explained and justified in Section 2. The appropriate modeling of the cables, the protective devices and energization topologies are introduced in Section 3. Simulation results are analyzed in Section 4. In Section 5, the strengths and limitations of the proposed modeling and the achieved simulation results are briefly discussed.

2. WTT BLACK-BOX PARAMETRIC MODEL

2.1. Black box model

For representing the WTTs in electromagnetic transients program–alternative transients program, we used a wideband model of a 300 kVA 11/0.230 kV transformer developed in the work by Gustavsen.[13] Here, the following steps were taken.

1. The 6×6 admittance matrix of the transformer was established by measurements as a function of frequency from 10 Hz to 10 MHz. The coaxial measurement cables were compensated.
2. A six-terminal black-box model of the transformer on pole-residue form [equation (1)] was obtained on the basis of vector fitting[18,19] followed by passivity enforcement via residue perturbation.
3. An equivalent resistor, inductor, and capacitor (RLC) lumped network was generated from the rational model and implemented in alternative transients program.

$$Y(s) = \sum_{m=1}^{N} \frac{\boldsymbol{R}_m}{s - a_m} + \boldsymbol{D} + s\boldsymbol{E} \tag{1}$$

2.2. Shifting the frequency response

To study the effect of shift in frequency response on the resonant overvoltages, the black box model of the transformer is modified by multiplying the frequencies (s) in equation (1) by a factor α. This gives the following shifted model,

$$Y(\alpha s, a_m, R_m D, E) = Y\left(s, \frac{a_m}{\alpha}, \frac{R_m}{\alpha}, D, \alpha E\right). \tag{2}$$

The effect of the shifting is demonstrated for the computed voltage transfer from MV terminal phase A to LV terminals with terminal conditions shown in Figure 1 (left). Figure 1 (right) shows the terminal connection for the computation of input impedance of MV terminal phase A. The resistance values connected to MV terminals phase B and C represent the surge impedance of cables connected to them.

Figure 2 shows the frequency sweep of the transferred voltage to LV terminal phase A when the MV phase A is 1 pu, with alternative shift factors, $\alpha = 1$, 5 and 10. As observed in Figure 2, the dominant resonant frequency (f_{dr}) moves down from 2 to 0.4 MHz and 0.2 MHz for shift factors 5 and 10. Because of shifting, higher input impedances of MV phase A for lower frequencies can be observed in Figure 3.

Since the measurements on the 300 kVA transformer are carried out until 10 MHz, shifting of the frequency responses to lower range leads to undefined values for MV input impedance and transferred voltage to LV in high frequencies in the range of megahertz. As an instance, shifting by factor 10 leads to undefined values for impedances and transferred voltages for $f > 1$ MHz. Considering this limitation, the simulation cases (cable lengths and shift factors) in Section 3 are selected such that the transformer frequency responses are defined for.

2.3. Scaling the frequency response

To study the effect of scaling in the admittance matrix on the resonant overvoltages, the black-box model of the transformer is modified by multiplying R_m, D and E in equation (1) by a factor β. This gives the following scaled model,

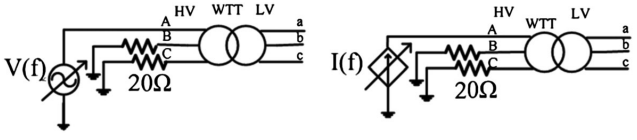

Figure 1. Circuits for extracting the frequency response of voltage ratio (left) and input impedance (right).

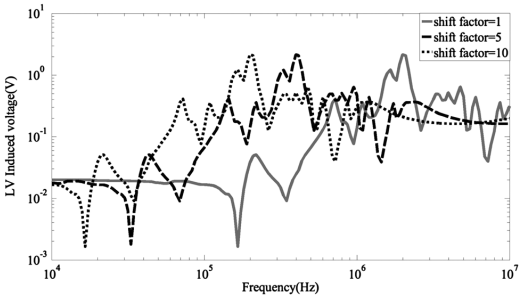

Figure 2. Frequency sweep of the transferred voltage to LV terminal phase A for 300 kVA transformer (solid trace), with alternative shift factors.

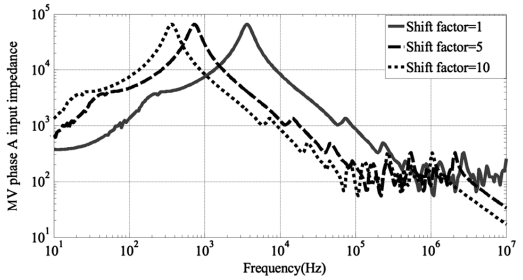

Figure 3. MV input impedance of phase A for 300 kVA transformer (solid trace), with alternative shift factors.

$$\beta Y(s, a_m, R_m, D, E) = Y(s, a_m, \beta R_m, \beta D, \beta E). \tag{3}$$

The dashed and dotted traces in Figure 4 show the scaled input impedances by factors 10 and 0.1, respectively. In Section 4.1, the effect of scaling is simulated in no load transformer energization without the protective devices in order to observe how they increase or impede resonance initiation.

2.4. Justification of shifting and scaling approach by design considerations

The shifting and scaling of the WTT frequency response is treated conceptually in this paper. But it can also, within moderate limits, be justified physically from the following considerations:

1. The kVA scaling of transformer: generally speaking, transformers with larger sizes have higher inductances and capacitances. This leads to lower resonant frequencies according to equation (4). With careful consideration, the

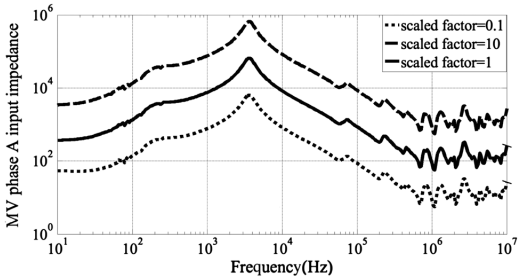

Figure 4. MV phase A input impedance for 300 kVA transformer (solid trace) with alternative scale factors.

Wind Energ. 2015; **18**:1061–1074 © 2014 John Wiley & Sons, Ltd.
DOI: 10.1002/we

effect of transformer size can be formulated. Assuming constant current density, flux density, insulation space factor and frequency, the kVA scaling relations for transformer can be obtained.[20] When scaling the kVA by a factor of *m,* the physical dimensions of transformer should be scaled by the factor $m^{0.25}$. Therefore, inductances and capacitances also scale by the factor $m^{0.25}$, and resonance frequencies are scaled by factor $m^{-0.25}$ according to

$$f_r = \frac{1}{2\pi\sqrt{LC}}. \tag{4}$$

2. Transformers with various insulating material: the application of various insulating materials in transformers such as mineral oil, ester based oils as well as cast resin dry insulator leads to different series and shunt capacitors for a constant winding frame. Therefore, according to equation (4), the resonance frequencies will be scaled inversely by the variation of the square root of ε_r since the transformer capacitances are directly related to ε_r.
3. Winding type (layer, disk etc.): assuming a fixed core window, i.e. fixed axial winding height and radial radius, the series capacitance (C_s) of a layer winding is typically smaller compared with a disk winding leading to a lower value of resonance frequencies for disk winding.

The actual frequency response of input impedance and voltage transfer to LV is strongly dependent on the transformer design (e.g. winding type) and the vector group. Therefore, the applied approach of shifting and scaling the admittance matrix of the given 300 kVA transformer cannot represent an arbitrary transformer very well. In this work, the shifting/scaling is simply used for gaining insight in the phenomenon of high-frequency cable-transformer resonance in OWFs.

The approach of shifting/scaling can however be very useful also in practical studies. There is always some uncertainty in the accuracy of wideband transformer black-box models because of inaccuracies in the measurements and model extraction procedure. A sensitivity study based on small shifting/scaling of the frequency domain behavior will therefore give more faith in the conclusions derived from simulation results.

3. MODELING OF CABLE, PROTECTIVE DEVICES AND ENERGIZATION TOPOLOGIES

3.1. System overview and modeling considerations

The OWF considered for simulations is illustrated in Figure 5. It consists of several WTTs which are connected in a row with the MV cables. There are VCBs to switch each transformer and one VCB for switching the entire row. The main components in OWFs for the switching transient investigations are WTTs, cables, SAs and RC filters. In the LV side of WTTs, depending on the wind turbine configuration,[21] soft start or full-scale frequency converters are installed. The soft start or the frequency converter is initiated after the energization of transformers. Therefore, they are off and can be disregarded in the simulation.

The modeling of the components should be performed on the basis of the frequency range of the phenomena and time interval of study. The transformers for the initial time interval after energization are adequately modeled on the basis of the high frequency behavior, which is taken into account by the parameterized model in Section 2. VCBs have multiple prestrike and multiple reignitions in energization and de-energization, respectively, which can mainly affect the amplitude

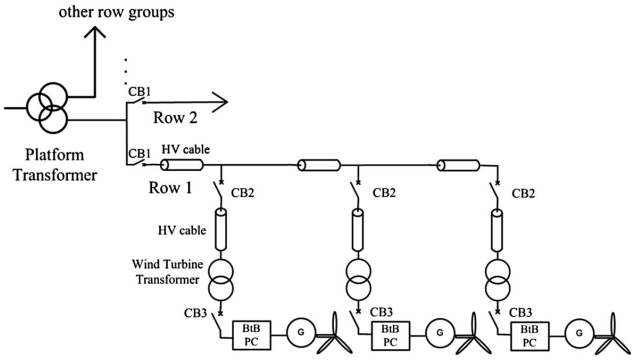

Figure 5. Single phase diagram of OWF system

and waveform of overvoltages at HV terminal.[4] However, since the focus of this paper is on resonant overvoltages at the LV terminal, VCBs are simply modeled as ideal switches.

3.2. Cable modeling

For cable modeling, the JMarti model[22] is used. This model considers the modal transformation matrix as real and constant, which is computed at a user-defined frequency that can be chosen equal to a dominant frequency component in the simulation. Such modeling is valid for single-core cables at high frequencies since all waves propagate essentially as coaxial waves. In the case of a single cable that is subjected to a step voltage on one end, the open-end voltage response has a dominant frequency equal to the cable quarter-wave resonant frequency,

$$f_s = \frac{1}{4\tau} = \frac{v_{cable}}{4l} = \frac{c}{4l\sqrt{\varepsilon_r}}. \tag{5}$$

The v_{cable} for high frequencies is defined inversely proportional to the square root of relative permittivity (ε_r) of the cable insulation. The single-core cable parameters used in this paper is shown in Table I. The cable and 300 kVA transformer model is verified with the simulation of experimental energization circuit in the work by Gustavsen[13] (Figure 6), and the LV resonant overvoltages were reproduced in good agreement (Figure 7).

3.3. RC filters

Resistive–capacitive filters can be applied at both LV and MV terminals of a transformer for controlling overvoltages; especially du/dt. In the work by Piasecki *et al.*,[23] the resistance and capacitance value used for protecting the arc furnace transformer from restrikes due to VCB disconnection is 50 Ω and 30–200 nF, respectively. The selection of RC values should be carried out on the basis of both transient and steady state situations. R = 10 Ω and C = 500 nF are used for MV and LV filters in this paper. The active and reactive power of these RC filters are $P_{3phase} = 13$ mW and $Q_{3phase} = 8$ VAr, which are well ignorable values for steady state situations.

3.4. SA

Generally, arresters are installed at WTT MV and LV terminals to protect them from lightning surges which strike the wind turbine blades or nacelle.[24] In this paper, the non-linear and frequency-dependent model introduced by IEEE working group[25] is applied. The characteristics of arresters applied at LV and MV terminals of the 300 kVA transformer are based on the ABB surge arrester POLIM-R-2N datasheet[26] and ABB surge arrester POLIM-C-N datasheet,[27] respectively. Series stray inductances of 0.5 and 0.25 μH are introduced for representing the ground lead in MV and LV arresters, respectively.

Table I. MV cable parameters.

Speed of light in vacuum (m s^{-1})	3×10^8
Core outer radius (m)	0.02
Core resistivity (ohm × m)	1.72×10^{-8}
Relative core-sheath insulation permittivity	2.671
Sheath inner radius (m)	0.035
Sheath outer radius (m)	0.038
Sheath resistivity (ohm × m)	2.2×10^{-7}
Relative sheath insulation permittivity	2.3

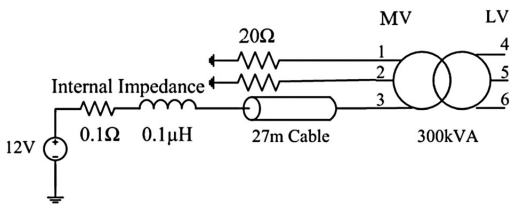

Figure 6. One phase energization with 23 m cable—in good accordance with Figure 14 in the work by Gustavsen.[13]

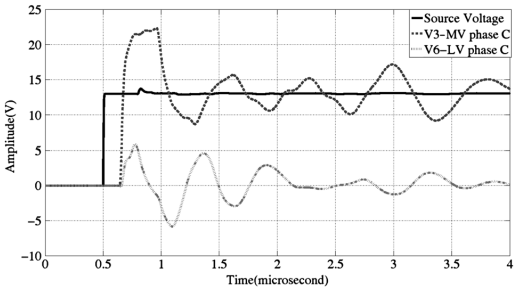

Figure 7. Verification of cable modeling according to Figure 6. Source voltage (solid line), voltage on phase C MV terminal (dashed line) and voltage on phase C LV terminal (dotted line).

3.5. Energization topologies

Considering the alternative locations of transformers inside wind turbines, and CB2 status (VCB for each transformer energization), the possible energization topologies become as listed in Table II. A decrease in cross section of the cables along rows could also be considered for energization topologies. However, it does not affect overvoltage amplitudes significantly, and it is not considered among the energization topologies.

3.6. Resonant overvoltage withstand capability

The overvoltage withstand capability of the apparatuses in the MV and LV sides of WTT is crucial, and they should be selected on the basis of thorough transient study of wind farms. According to table 5 in IEC_60076-3, the minimum clearance at MV terminal bushing of 11 kV transformers should be selected to withstand 75 kV impulse voltages. The standard impulse voltage test for 11 kV XLPE cable is also 75 kV.[28]

For LV equipment, the accepted 1.2/50 μs impulse overvoltages with peak voltage <300 V is 4 kV according to table B.1 in IEC 60664-1. This means that impulse overvoltages up to 21 pu and du/dt up to $21/1.2 = 17.5$ pu/μs should be tolerated by equipment at LV side of WTTs including LV bushing. These maximum allowed values are assumed as a general but not sufficient criterion for safety margins against resonant overvoltages in this paper. In the discussion section, the limitations of using this criterion are explained.

4. SIMULATION RESULTS

4.1. Resonant overvoltage for single transformer energization

A resonant overvoltage between a transformer and a feeding cable can occur during the energization of the cable if f_s, obtained by equation (5), is approximately equal to the f_{dr} of transformer. The circuit in Figure 8 is used for investigating the overvoltage calculation at the transformer LV terminals with alternative frequency shift factors, $\alpha = 1$–10. RC filters and arresters are applied to protect the transformers from overvoltages. The critical cable length for the 300 kVA transformer is 23 m[29] with $\alpha = 1$, corresponding to $f_s = f_{dr} = 2$ MHz.

It is found that the amplitude of resonant overvoltages at LV terminal phase A is highest when the energization occurs at the peak of MV terminal phase A. In this way, the upcoming results are presented for this case. The impact of scaling the transformer impedance is shown in Figure 9.

The dotted trace is the energization of transformer, which has one order of magnitude lower impedance, compared with the 300 kVA one. With such scaling, the transformer input impedance at the MV side is no longer much higher than cable impedance at 2 MHz, and the resonant overvoltage buildup does not occur as the transformer damps the impinging voltage

Table II. Energization topologies.

	CB2 open	CB2 closed
WTT at base	*a*1	*a*2
WTT at nacelle	*b*1	*b*2

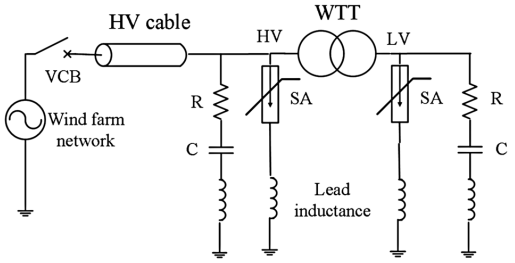

Figure 8. Simulation circuit for calculating resonant overvoltages and effect of MV, LV protection by RC filters and SAs. Source represents the steady state 50 Hz voltage of the OWF row.

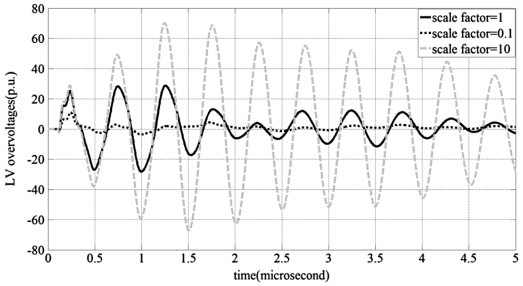

Figure 9. The impact of scaled transformer impedances on LV resonant overvoltages.

oscillation. Although this approach significantly presents the effect of MV input impedance on resonant overvoltages, there is some limitation. Transformer impedances in reality are linked to their size and power. Larger transformers have higher impedances and lower resonant frequencies. Therefore, the effect of scaled transformer impedances is better to be carried out with shifting. Feeding cable lengths should also be adjusted accordingly. However, this requires detailed transformer modeling based on white-box models and analytical investigation of the transformer size effect on shifting of resonant frequencies and scaling of impedances. This approach is interesting but is out of scope of this paper.

The effect of SA and RC filter on LV-induced resonant overvoltage is shown in Figures 10 and 11. Without protective devices, the overvoltage approaches about 30 pu with du/dt equal to about 400 pu/μs. The calculation method of du/dt is shown in the lower right part of Figure 10. The application of arresters at both LV and MV sides decreases the overvoltage amplitude noticeably. Nevertheless, the rate of rise is still high. The effect of stray lead inductances of arresters on LV overvoltages is assessed by comparing gray trace and black dashed one in Figure 11. The presence of stray inductance reduces the arrester effectiveness and doubles the overvoltage compared with an ideal one. Nevertheless, the overvoltage is still lower than 21 pu.

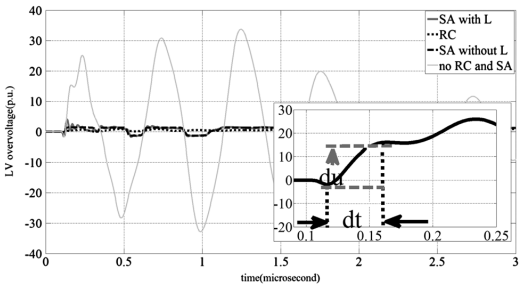

Figure 10. Resonant overvoltage when energizing 300 kVA transformer with 23 m cable. Lower right inset: the definition of du/dt.

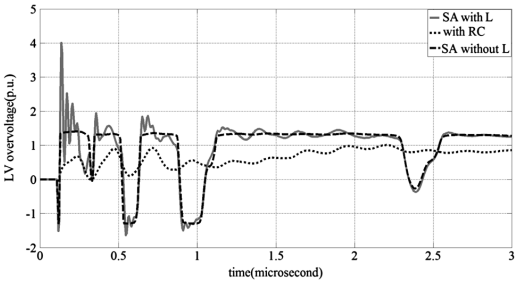

Figure 11. The effect of protective devices (zoomed-in waveforms in Figure 10).

The usage of RC filters on both MV and LV terminals results in lowered overvoltages including both amplitude and du/dt (see the dotted trace in Figures 10 and 11). Even in the case of application of both arrester and RC filters, the impact of the RC filters dominates the arrester, and the waveform is similar to the dotted trace in Figures 10 and 11. It can be concluded that just RC filters can be implemented to protect transformers.

Energization of transformers with shifting factors 1–10 and variable cable lengths is performed, and the calculation results are depicted in Figure 12. It shows that there are energizations which cause LV resonant overvoltages up to 40 pu. It should be mentioned that the selection of the shifting factors and cable lengths is such that only for one calculation case out of 100, the transformer frequency response has undefined value. The case is $\alpha = 10$ and the cable length is equal to 23 m. For $\alpha = 10$, the shifted frequency response is defined until 1 MHz (Figures 2 and 3), and when cable length equals to 23 m, $f_s = 2$ MHz, the simulation of this energization may lead to unrealistic results. Meanwhile, this case is not in the region of critical overvoltage amplitudes, as seen in Figure 12.

Surge arresters reduce the voltage peaks to below 7 pu, as shown in Figure 13. The application of only RC filters further diminishes the overvoltage peaks to 1.3–1.6 pu. Since the latter values are low and moderate in entire space, the results are

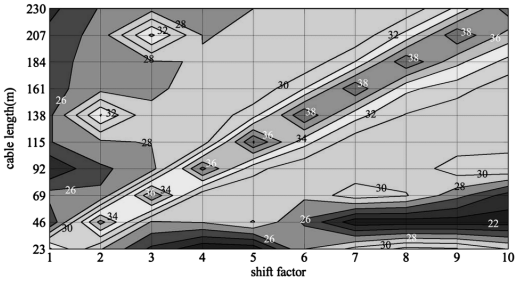

Figure 12. Resonant overvoltage peak at LV terminal as a function of cable length and shift factor. No protective device is applied.

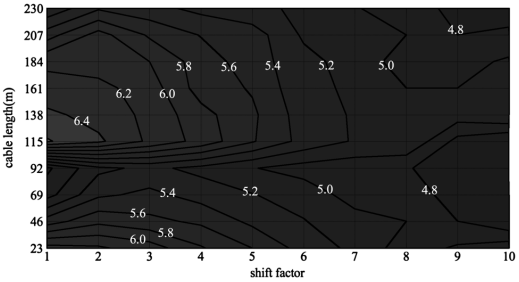

Figure 13. Resonant overvoltage peak on LV terminal as function of cable length and shift factor. SAs applied on both LV and MV terminals.

not shown here. The du/dt in these energizations is illustrated in Figures 14, 15 and 16, respectively, for the energizations without protective devices, with SA and with RC filter. It can be concluded that

1. du/dt is lower for transformers with higher shift factors (Figure 14). This means that resonant overvoltages have more destructive effect on smaller transformer with lower kVA.
2. Although arresters can reduce the overvoltages to 6 pu, which is far below 21 pu, du/dt is decreased ineffectively (Figure 15).
3. The selected RC filter can reduce both the overvoltage peak and the rate of rise of overvoltages effectively (Figure 16)

It should be mentioned that the installation of RC filters just at LV terminal plus arresters at both LV and MV terminals can be the sufficient protective scheme for some resonance-leading energizations as described in table IV in the work by Soloot *et al.*[11] But it cannot be generalized since there are cases leading to 20 pu/μs even with RC filters at both LV and MV terminals as shown in Figure 16.

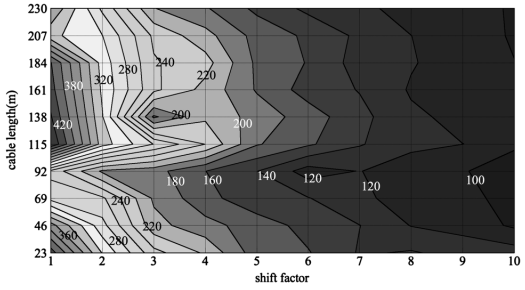

Figure 14. du/dt in p.u./μs at the LV terminal as function of cable length and shift factor. No protective device is applied.

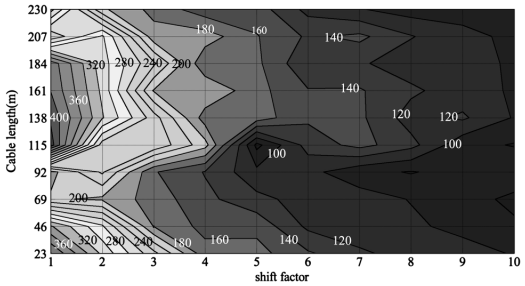

Figure 15. du/dt in p.u./μs at the LV terminal as function of cable length and shift factor. SAs applied at both MV and LV terminals.

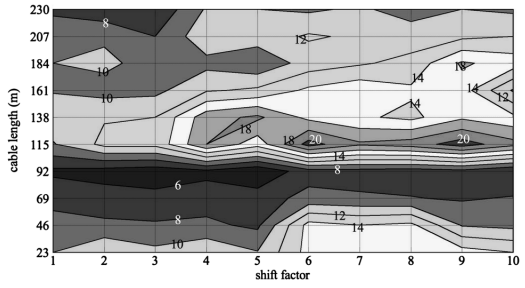

Figure 16. du/dt in p.u./μs at LV terminal as function of cable length and shift factor. RCs applied at both MV and LV terminals.

DOI: 10.1002/we

It is also found that the du/dt of overvoltages at LV terminal is more sensitive to the resistance of RC filter compared with its capacitance, e. g. the increasing of the resistance from 10 to 20 Ω, which equals to surge impedance of cable, increases the du/dt to three times higher, whereas increasing the capacitance from 0.5 to 1 μF does not change the du/dt so much.

Surge impedance of transformers is actually input MV terminal impedance at the frequency of resonance. The value of this impedance at resonant frequency controls the value of resonant overvoltage. By inserting low RC parallel filter at MV terminal, the effective input impedance of transformer and the overvoltage amplitude can be decreased at resonance condition.

4.2. Resonant overvoltage versus OWF energization topologies

In this section, overvoltages due to the energization topologies in Table II are surveyed for the row 1 in Figure 5. Similar to the previous subsection, energizations are performed at the time of voltage peak of MV phase A. In topologies *b*1 and *b*2, it is assumed that the 300 kVA transformer is connected with 23 m cable to CB2. The simulation results are depicted in Figures 17 and 18. It can be found that

1. The induced overvoltages at LV terminal can be up to 18 pu (Figure 17, case b1), which is within safety margins in accordance with the standard for unipolar impulse tests. But the du/dt are far above the safety margins and in the range of 300–500 pu/μs. Thus, RC filters should be installed at both MV and LV terminals to decrease both resonant overvoltage amplitudes and du/dt.
2. The first peak of resonant overvoltage in case b1 is lower than the 25 pu, obtained in Figure 10 because the transient surge entering to MV wind turbine cable has amplitude reduced from 1 to 2/3 pu for the first transformer with $Z_c << Z_t$. The second and third peaks are quite lower than those in Figure 10. That is due to the damping effect of the row cable.
3. If topologies *a*1 and *b*1 are applied for the last transformer in the row, the transferred overvoltages at LV become lower than those for the first transformers, especially for *b*1. Since the surge impedance of the row cable and the wind

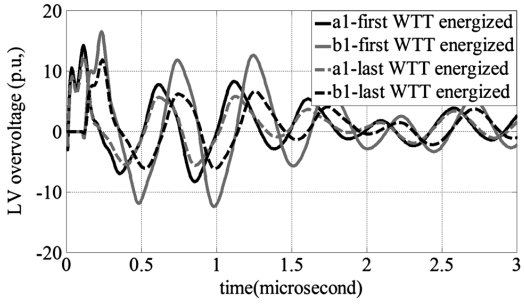

Figure 17. Overvoltages at LV terminal phase A of first and last WTT due to energization topologies *a*1 and *b*1.

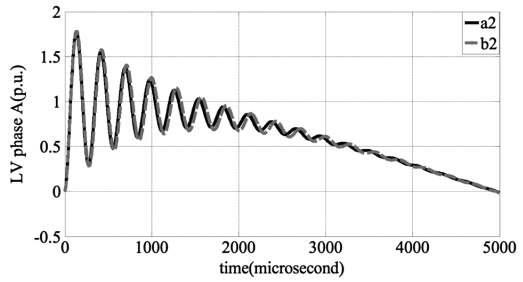

Figure 18. Overvoltages at LV terminal phase A of first WTT due to energization topologies *a2* and *b2*.

turbine cable are equal in *b*1, the incoming surge to WTT will be 0.5 pu compared with 2/3 pu in the first WTT energization.
4. In topologies a2 and b2, CB2 is already closed, and the energization is carried out via CB1, which results in lower overvoltages with low du/dt. Thus, they are not critical (Figure 18), but the platform transformer experiences the sum of inrush currents of transformers.

4.3. Resonant overvoltage versus energization in the second row

The energization of the second row, while the first row is already energized, was investigated in the previous work[30], and here, the main findings are summarized:

1. The second row cable experiences lower overvoltages during row energization compared with the first row since the initial surge is reduced to 0.5 pu.
2. The induced overvoltage at LV terminal of each transformer is similar to the ones in the first row; the maximum peak is 18 pu, which occurs in case *b*1.

The first and last energization leads to the same overvoltages as in the first row. However, the energization of transformers in the second row leads to resonant overvoltages at the LV side of the transformers in the first row, which is investigated here. The induced overvoltage at LV terminal of the first transformer in the first row is shown in Figure 19. The energization topology is assumed *b*1.The amplitude is not critical, but the du/dt reaches 40 pu/μs. It reveals that the RC filters are not just helpful for direct energization of transformers but for the overvoltage transients of other transformers even in the other rows.

5. DISCUSSION

As it is mentioned in the work by Abdulahovic,[8] critical impulse voltage for distribution transformer is not defined in standards for rise times lower than 1.2 μs. In the work by Abdulahovic,[8] the measured critical voltage for a 34.5 and 200 kVA transformer decreased by shorter rise times. For 50 ns rise time, the critical voltage reduces to 1 pu, meaning that 1/0.05 = 20 pu/μs is the critical du/dt for that transformer, which is slightly different from, but in the range of, what derived in Section 3.6.

Besides, the waveform of resonant overvoltages is different from unipolar 1.2/50 μs lightning impulse voltage, and there is no standard defined for it as well. Therefore, only the peak value and du/dt of standard 1.2/50 μs lightning impulse can be used as a general but not sufficient criterion for safety margins as mentioned in Section 3.6. Although further discussion on standard definition for resonant overvoltage is out of scope of this paper, it is necessary to be highlighted.

Although detailed model of circuit breakers could result in slightly higher resonant overvoltages, the general pattern of overvoltage peaks and du/dt in Figures 12–16 would be more or less similar. This means that the selected RC filter is sufficient protective measure for transformer terminals.

The effect of RC filters resonant overvoltage can be investigated for internal overvoltages as well. How severe internal overvoltages are and how deep inside winding can be protected by RC filters on terminal should be assessed by detailed resistor, inductor, and capacitor modeling of transformer.

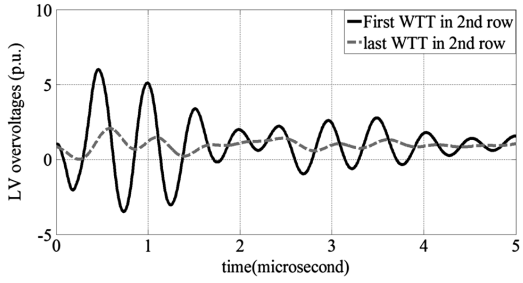

Figure 19. Overvoltage at the LV terminal phase A of the first transformer in the first row due to the energization of the first or the last transformers in the second row.

6. CONCLUSION

In this paper, a comprehensive study of energization transients in OWF was carried out with focus on transferred resonant overvoltages to the LV side of WTTs. The study introduces the novel idea of parametric black-box model of a WTT, which includes scaling and shifting factors for impedance and frequency, respectively. By scaling/shifting the 300 kVA transformer frequency response, it was found that two conditions are necessary for resonant overvoltage initiation: (i) the transformer MV input impedance at resonant frequency should be much higher than the cable surge impedance and (ii) the quarter-wave resonant frequency of the cable should be equal to the transformer dominant resonant frequency. By shifting the WTT frequency response, dominant resonant frequencies resulted in the range 0.2–2 MHz. These transformer models were exposed to no-load energization with corresponding critical cable lengths. This gave the following results:

a. Without application of SA and resistive-capacitor filter, the maximum resonant overvoltages can reach up to such a high value as 40 pu.
b. Shifting the transformer frequency response toward higher frequencies gives a higher frequency for the resonant overvoltage. Therefore, the resonant overvoltage gets a higher du/dt. Only well-designed RC filters can decrease this critical du/dt to safety margins.
c. The scaling of the WTT impedance response shows that low input impedance of a transformer MV terminal can prevent the initiation of resonant overvoltages.
d. The inclusion of SA keeps the amplitude of overvoltages at LV terminal low, but the du/dt cannot be decreased sufficiently. The stray inductance of SA ground lead should be considered in the simulations as this increases both overvoltage and du/dt.
e. RC filters have a considerable effect on both overvoltage amplitudes and du/dt. Simulation results indicate that just the implementation of RC filters alone can securely protect WTTs MV and LV terminal from resonant overvoltages. The selection of RC values should be carried out on the basis of both transient and steady state situations.

The selection of energization topology, i.e. WTT position in wind turbine and breaker closing sequence, should be carried out after comprehensive simulations and calculations. The model should include the platform transformer and protection equipment.

ACKNOWLEDGEMENT

The authors greatly appreciate funding support from the Norwegian Research Center for Offshore Wind Technology (NOWITECH),Work Package 4.

REFERENCES

1. King R, Moore F, Jenkins N, Haddad A, Griffiths H, Osborne M. Switching transients in offshore wind farms—impact on the offshore and onshore networks. *Proceedings of International Conference on Power Systems Transients (IPST)*, 2011.
2. Akhmatov V, Gellert BC, McDermott TE, Wiechowski W. Risk of temporary over-voltage and high-voltage fault-ride-through of large wind power plant. *Proceedings of 9th Int. Workshop on Large-Scale Integration of Wind Power into Power Systems*, 2010.
3. Han C, Martin DE, Lezama MR. Transient over-voltage (TOV) and its suppression for a large wind farm utility interconnection. *Proceedings of International Conference on Sustainable Power Generation and Supply*, 2009.
4. Liljestrand L, Sannino A, Breder H, Thorburn S. Transients in collection grids of large offshore wind parks. *Wind Energy* 2008; **11**: 45–61. DOI: 10.1002/we.233
5. Arana I, Holbøll J, Sørensen T, Nielsen AH, Sørensen P, Holmstrøm O. Comparison of measured transient overvoltages in the collection grid of Nysted offshore wind farm with EMT Simulations. *Proceedings of International Conference on Power Systems Transients (IPST)*, 2009.
6. Badrzadeh B, Høgdahr M, Singh N, Breder H, Srivastava K, Reza M. Transient in wind power plants—part II: case studies. *Proceedings of IEEE Industry Applications Society Annual Meeting (IAS),* 2011.
7. Reza M, Breder H, Liljestrand L, Saninno A, Abdulahovic T, Thiringer T. An experimental investigation of switching transients in a wind-collector grid scale model in a cable system laboratory. *Proceedings of 20th International Conference and Exhibition on Electricity Distribution (CIRED)*, 2009.

8. Abdulahovic T. Analysis of High-Frequency Electrical Transients in Offshore Wind Parks. Chalmers University of Technology: Göteborg, 2011.
9. Badrzadeh B, Gustavsen B. High frequency modeling and simulation of wind turbine transformer with doubly fed asynchronous generator. *IEEE Transaction on Power Delivery* 2012; **27**: 746–756. DOI: 10.1109/TPWRD.2011.2181429.
10. Soloot AH, Hoidalen HK, Gustavsen B. The assessment of overvoltage protection within energization of offshore wind farms. *Energy Procedia* 2012; **24**, DOI: 151-158. DOI: 10.1016/j.egypro.2012.06.096
11. Soloot AH, Bahirat HJ, Hoidalen HK, Gustavsen B., Mork BA. Investigation of resonant overvoltages in offshore wind farms-modeling and protection. *Proceedings of International Conference on Power Systems Transients (IPST)*, 2013.
12. Soloot AH, Hoidalen HK. High frequency modeling of transformers in ATP for investigation of resonances in offshore wind park. *Proceedings of the EEUG Meeting, European EMTP-ATP Conference*, 2010.
13. Gustavsen B. Study of transformer resonant overvoltages caused by cable-transformer high frequency interaction. *IEEE Transaction on Power Delivery* 2010; **25**: 770–779. DOI: 10.1109/TPWRD.2010.2040292.
14. Soloot AH, Hoidalen HK, Gustavsen B. Upon the improvement of the winding design of wind turbine transformers for safer performance within resonant overvoltages. *Proceedings of Cigré Joint Colloquium – SC A2/C4*, 2013.
15. Soloot AH, Hoidalen HK, Gustavsen B. Modeling of wind turbine transformers for the analysis of resonant overvoltages. *Electric Power System Research*, 2014, DOI: 10.1016/j.epsr.2014.03.004.
16. Soloot AH, Hoidalen HK, Gustavsen B. The effect of winding design on transformer frequency response with application on offshore wind farm energization. *Proceedings of International Conference on Renewable Energy Research and Applications (ICRERA)*, 2012.
17. Soloot AH, Hoidalen HK, Gustavsen B. Modeling of wind turbine transformers for resonant overvoltage—sensitivity analysis. *Proceedings of International Conference on Electrical Machines and Systems (ICEMS)*, 2013.
18. Gustavsen B. Wide band modelling of power transformers. *IEEE Transaction on Power Delivery* 2004; **19**: 414–429. DOI: 10.1109/TPWRD.2003.820197
19. Gustavsen B, Semlyen A. Rational approximation of frequency domain responses by vector fitting. *IEEE Transaction on Power Delivery* 1999; **14**: 1052–1061. DOI: 10.1109/61.772353
20. Scaling relations for transformers, Available at: http://www1.eere.energy.gov/buildings/appliance_standards/commercial/pdfs/transformer_draft_tsd_appendix5b_version080105.pdf
21. Ackermann T. Wind Power in Power Systems. Wiley: Chichester, 2005; 54–55.
22. Marti JR. Accurate modeling of frequency-dependent transmission lines in electromagnetic transient simulations. *IEEE Transaction on PAS* 1982; **101**: 147–157. DOI: 10.1109/MPER.1982.5519686.
23. Piasecki W, Ostrogorska M, Fulczyk M, Florkowski M, Kouzmine O, Werle P. Modeling and simulation of VCB related transients in industrial installation. Case study: Arc furnace transformer. *Proceedings of XVII International Symposium on High Voltage Engineering*, 2011.
24. Yasuda Y, Uno N, Kobayashi H, Funabashi T. Surge analysis on wind farm when winter lightning strikes. *IEEE Transaction on Energy Conversion* 2008; **23**: 257–262. DOI: 10.1109/TEC.2007.905361
25. IEEE Working Group on Surge Arrester Modeling. Modeling of metal oxide surge arresters. *IEEE Transaction on Power Delivery* 1992; **7**: 302–309. DOI: 10.1109/61.108922.
26. ABB surge arrester POLIM-R-2N datasheet, Available at: http://www.abb.com/search.aspx?q=POLIM-R 2N&abbcontext=products.
27. ABB surge arrester POLIM-C-N datasheet, Available at: http://www.abb.com/product/db0003db004279/c125739900636470c125708c003fd77a.aspx
28. UGVCL-specifications, 11 kV XLPE power cable, Available at: http://www.ugvcl.com/tender/corporate/ugvcl-sp-246/5%20%2011kV%20XLPE%20CABLE.pdf
29. Soloot AH, Hoidalen HK, Gustavsen B. Frequency domain investigation of switching transients in offshore wind farms. *Proceedings of IEEE Powertech conference*, 2011.
30. Soloot AH, Hoidalen HK, Gustavsen B. A Study of switching overvoltages in offshore wind farm. *Proceedings of XVII Inter. Symp. on High Voltage Engineering,* 2011.

Paper II

Investigation of Resonant Overvoltages in Offshore Wind Farms- Modeling and Protection

Amir Hayati Soloot, Himanshu J. Bahirat, Hans Kristian Høidalen, Bjørn Gustavsen and Bruce A. Mork

***Abstract*-- Earth fault and switching operation may lead to resonant overvoltages in Offshore Wind Farms (OWF) with higher amplitude and rate of rise (du/dt) compared to other overvoltages. Overvoltages appear on High Voltage (HV) cables and Low Voltage (LV) side of wind turbines, and can result in insulation failure of the Wind Turbine Transformers (WTTs), interconnecting cables and Power Converters (PC). This paper aims to study the circumstance of the occurrence of these overvoltages and suggests proper protection methods.**

This paper uses high frequency black box model for WTT. The power converter is modeled with two back to back voltage source converters. The RL harmonic filters and snubber circuits are included. This model can simulate the steady state operation as well as resonant overvoltage due to earth fault in ATP-EMTP software. But, it requires long simulation time. A simplified model which has the same accuracy as the first model for resonant transient is introduced.

Simulation results show that the transferred overvoltages to LV side due to earth fault at critical cable lengths may lead to resonant overvoltages with amplitude and rate of rise up to 30 p.u. and 400 p.u./µs, respectively. It is also shown that the installation of surge arresters at LV and HV terminal of WTTs only decreases the amplitude of overvoltages to safe margin and not the du/dt. However, the application of RC filters instead of surge arresters can protect offshore wind farm components from overvoltages.

***Keywords*: offshore wind farm, wind farm energization, earth fault, power converter, wind turbine transformers, RC filters.**

I. Introduction

DUE to the recent focus of power operating and Transmission & Distribution (T&D) companies on offshore wind farm installations as a renewable energy solution, the maintenance and protection of the wind power components have become of great importance. The challenges of accessibility and repair require more effective protective devices compared to land-based wind farms. In literature, switching transients in land-based wind farms and OWFs [1]-[8] have been studied and analyzed, mainly concentrated on transients in the HV interconnecting grid. Different aspects are discussed such as the inrush current [1,2], the energization overvoltages on HV terminal of WTTs and inside winding [2,3,6,7,8] and earth fault interruption challenges in the adjacent network [2,4,5,6,7]. However, there have been few studies on the transferred resonant overvoltage to LV side [8]. Thus, the motivation of this paper is to study the transient overvoltages, mainly resonant overvoltage, transferred to LV terminal of WTT. Besides, the effect of protective devices, such as surge arrester and RC filters are analyzed.

The energization of each wind turbine may result in cable-transformer resonant transients. The length of cables in wind turbines typically are such that their quarter wave frequency can match resonance frequencies of WTTs. The resonant overvoltages may lead to internal insulation failures in transformers. Resonant overvoltages can also occur due to earth fault in cables or joints. In this case, they can be harmful for the connected power converters at LV terminal as well.

Typical components in offshore wind farms are modeled in this paper considering the high frequency content of the involved transients. In this paper, the model of a typical OWF is explained in section II. The simulation results for energization and earth fault transients are analyzed in section III.

II. Offshore Wind Farm Modeling

The OWF considered for simulations is illustrated in Fig. 1. Several wind farm rows are connected to each winding of platform transformer. Each row consists of several WTTs connected with the HV cables. There are Vacuum Circuit Breakers (VCBs) to switch each WTTs and one VCB for switching the entire row. In the LV side, full-scale frequency converters are installed. The power converters are initiated after the energization of WTTs. Therefore, they are off and can be disregarded. However, during earth fault, the wind turbines are producing power and power converters are connected to the system. Thus, they should be modeled in the earth fault simulations.

The modeling of the OWF components should be performed based on the frequency range of the phenomena and time interval of study. The WTTs, for the initial time interval after energization or ground fault, are modeled based on the high frequency behavior. VCBs have multiple prestrike and multiple reignitions in energization and de-energization respectively, which can significantly affect the amplitude and waveform of overvoltages in OWF [2]. However, since the

This work was supported by the Norwegian Research Center for Offshore Wind Farm (NOWITECH)-Work package (4).

A. H. Soloot and H. K. Høidalen are with the Department of Electrical Power Engineering, Norwegian University of Science and Technology (NTNU), Trondheim N-7491,Norway (e-mail: amir.h.soloot@elkraft.ntnu.no, hans.hoidalen@elkraft.ntnu.no).

H. J. Bahirat and B. A. Mork are with the Department of Electrical and Computer Engineering, Michigan Technological University, Houghton, MI 49931 USA (e-mail: hjbahira@mtu.edu, bamork@mtu.edu).

B. Gustavsen is with SINTEF Energy Research, Trondheim N-7465, Norway (e-mail: bjorn.gustavsen@sintef.no).

Paper submitted to the International Conference on Power Systems Transients (IPST2013) in Vancouver, Canada July 18-20, 2013.

focus of this paper is on resonant overvoltages at the LV terminal, VCBs are simply modeled as ideal switches. The platform transformer is modeled with the typical saturable 50 Hz transformer model. In sub-sections A-E, the component models are described in detail.

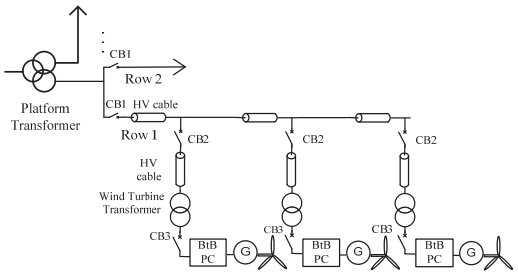

Fig. 1. The layout of typical offshore wind farms

A. Wind turbine transformer

For representing the 300 kVA transformer in ATP-EMTP, we used a wide-band model of the transformer developed in [9]. Here, the following steps were taken.

1. The 6×6 admittance matrix of 11.4/0.23 kV, 300 kVA transformer was established by measurements as a function of frequency from 10 Hz to 10 MHz. The coaxial measurement cables were compensated for.
2. A six-terminal black box model of the transformer on pole-residue form was obtained based on vector fitting [10]-[11] followed by passivity enforcement by residue perturbation.
3. An equivalent RLC lumped network was generated from the rational model and implemented in ATP-EMTP.

Fig. 2 shows the transferred voltage to LV for the transformer model. The transferred voltage is maximum at 2 MHz and this is denoted the dominant resonance frequency (f_{dr}).

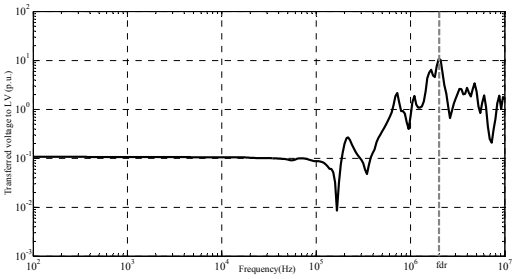

Fig. 2. The transferred voltage to LV for 300 kVA transformer in p.u. HV

B. Power Converter model with both GSC and MSC

In this model, the wind turbine has two Voltage Source Converters (VSC) connected in back to back configuration (see Fig. 3). The control and the operation of the converters are based on the modeling and control design discussed in [12].

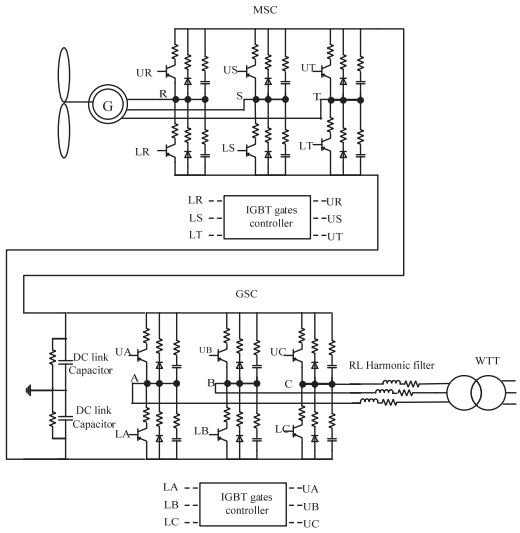

Fig.3. Wind turbine with back to back full-scale converter and transformer

The VSC connected to the generator is referred to as the Machine Side Converter (MSC) and the second converter connected to the WTT through RL harmonic filters is referred to as the grid side converter (GSC). In order to study the transient behavior in this paper, the generator is modeled as an ideal source behind impedance. Switched converters along with detailed control systems are model for both the MSC and the GSC. A set of three phase Pulse Width Modulated (PWM) switching signals is obtained from the converter control system and applied to the switches in the converter. In the present work, the MSC controls the DC bus voltage. The GSC controls the reactive and the active power fed into the collection system. Fig. 4 shows the controller block diagram for decoupled active and reactive power control of the converter. In the transient simulation, a 0.03μs time step is used. The converter control system is implemented as a MODELS code for the studies reported in this paper. To speed up the simulation, the MODELS code is executed with an increased (down sampled) time step of 10 microseconds, reasonably adapted to the time constants of its input signals.

As the simulations is still time consuming, a model valid and adequate only for the short time interval (<10μs) during resonant transients is introduced in next subsection. The simulation time with same computing machine drops from couple of minutes to seconds.

IGBTs in both MSC and GSC have 6 different switching positions (sequences). For the GSC, they are listed in table I. For instance in seq. 1, LA,UB and LC are on and phase A and C are connected together and via DC link capacitor connected to phase B. RC snubber circuits parallel to each IGBT in Fig. 3 are protecting them from high voltage variations. RL harmonic filters are used to smooth the output of GSC during

steady state and decrease harmonics [13]. The typical values of these four elements and DC link capacitor and its parallel resistance are listed in table II.

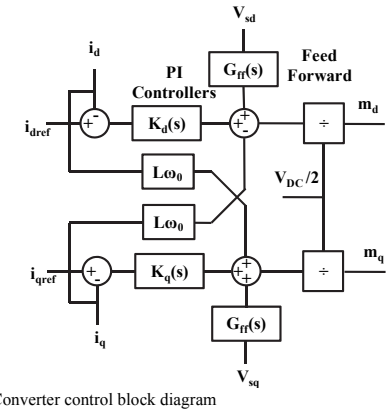

Fig.4. Converter control block diagram

TABLE I
SPECIFICATION OF IGNITED SWITCHES IN GSC IN EACH SEQUENCE

Seq. 1	LA	UB	LC
Seq. 2	UA	UB	LC
Seq. 3	UA	LB	LC
Seq. 4	UA	LB	UC
Seq. 5	LA	LB	UC
Seq. 6	LA	UB	UC

*L and U are abbreviation of Lower switch and Upper switch.
* A,B and C are phases.

TABLE II
TYPICAL VALUES OF RC SNUBBER AND RL FILTER

parameters	value
RC snubber in GSC	100Ω, 2μF
RC snubber in MSC	1000Ω, 0.2μF
RL harmonic filter	0.4mΩ, 2.3μH
DC link RC	10kΩ,16 mF

C. Power Converter model with GSC and DC link capacitor

When an single phase earth fault occurs at the peak of phase A and GSC is in operation, the IGBTs would be in one of the 6 different switching positions (sequences) listed in table I. since the duration of resonant overvoltages is typically 5-10 μs. It should be mentioned that in this model, the DC link capacitor is considered passive and charged. During this time interval, the power production does not change and DC link capacitor functions only as filter for resonant transients. Meanwhile, MSC and generator are not considered. This model is only valid for resonant transient studies.

D. Cable Modeling

The JMarti model [14] is used to model interconnecting cables in OWF. This model considers the modal transformation matrix as real and fixed. It can be computed at a user-defined frequency. In this paper, it is considered to be equal to the cable quarter-wave resonance frequency (1). Such modeling is valid for single core cables at high frequencies since all waves propagate essentially as coaxial waves. In the case of a single cable that is subjected to a step voltage on one end, the open-end voltage response has a dominant frequency at the cable quarter-wave resonance frequency,

$$f_s = \frac{1}{4\tau} = \frac{v_{cable}}{4l} = \frac{c}{4l\sqrt{\varepsilon_r}} \quad (1)$$

v_{cable} for high frequencies is defined inversely proportional to the square root of relative permittivity (ε_r) of the cable insulation. The speed of light in vacuum is denoted with c. The single core cable parameters used in this paper is shown in table III. In order to verify the cable and WTT model, the experimental energization circuit in [9] was simulated (see Fig. 5) and the LV resonant overvoltages were reproduced in good agreement (see Fig. 6).

TABLE III
HV CABLE PARAMETERS

core outer radius (m)	0.02
core resistivity (ohm×m)	1.72×10^{-8}
Relative core-sheath insulation permittivity	2.671
sheath inner radius (m)	0.035
sheath outer radius (m)	0.038
sheath resistivity (ohm×m)	2.2×10^{-7}
Relative sheath insulation permittivity	2.3

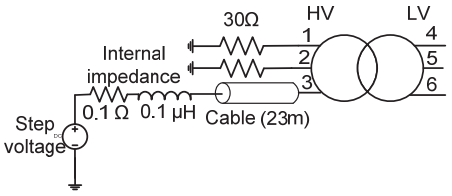

Fig.5. one phase energization with 23 m cable in accordance with Fig. 14 in [9].

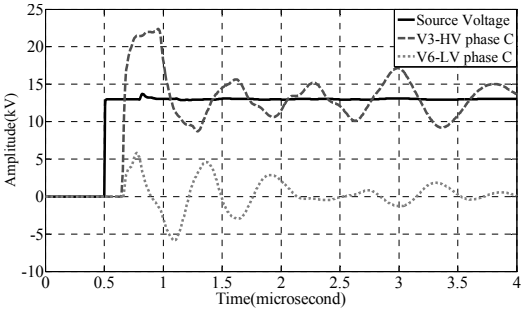

Fig.6. Verification of cable modeling according to Fig. 5. Source voltage (solid line), voltage on phase C HV terminal (dashed line), voltage on phase C LV terminal (dotted line).

E. RC Filters

RC filters can be applied at both LV and HV terminals of a WTT for controlling overvoltages; especially du/dt. The selection of RC values should be done based on both transient and steady state situations. R=10Ω and C=500 nF are used for HV and LV filters in this paper, leading to P_{3phase}=13mW and Q_{3phase}=8VAr which are well ignorable values for steady state situation. Series stray inductances of 0.25 µH are introduced for representing the ground lead in HV and LV RC filters. This inductance decreases the efficiency of RC filter and should be minimized. In next section, the effect of them will be analyzed.

F. Surge Arrester

Generally, Surge Arresters (SA) are installed at HV and LV terminals of transformers to protect them from lightning surges which strike the wind turbine blades or nacelle [15]. In this paper, the non-linear and frequency dependent model introduced by IEEE working group in [16] is applied. The characteristics of SA applied at LV and HV terminals of the WTT are based on [17] and [18], respectively. Series stray inductances of 0.5 µH and 0.25 µH are introduced for representing the ground lead in HV and LV SAs, respectively.

III. Simulation Results

In this section, simulation results for both wind turbine energization and single phase earth fault are reported. Since protective devices and their design are going to be analyzed and compared in this section, there should be criteria for the selection of adequate protection.

For LV equipment, the accepted 1.2/50µs impulse overvoltages with Vpeak <300V is 4 kV according to Table B. 1 in IEC 60664-1. This permits impulse overvoltages up to 21 p.u. and du/dt up to 21/1.2=17.5 p.u./µs to be acceptable for LV terminal of WTTs. Meanwhile, depending on dominant resonance frequency, f_{dr}, and the availability of critical voltage vs. rise time, the typical value of rise time can be assumed as $1/(4f_{dr})$ and the critical voltage for that rise time can be considered for more accuracy. In [7], the measured critical voltage envelope vs. rise time for a 34.5 kV, 200 kVA transformer decreases by shorter rise times such as for 50 ns rise time, the critical voltage reduces to 1 p.u. Thus, 1/0.05=20 p.u./ µs is the critical du/dt which is in good agreement with the aforementioned standard value. Fig. 7 shows the layout of possible protective devices installed at WTT terminals.

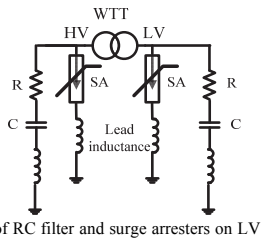

Fig.7. Installation of RC filter and surge arresters on LV and HV terminal of WTT.

A. Wind turbine energization

Fig 1. shows the layout of OWF when WTT is on top of nacelle. In fact, it can also be installed in the base. Thus, the energization can directly be done on the HV terminal. In this paper, energizations occur at the peak voltage of phase A. Figs 8 and 9 show the induced voltage on the LV terminal for various protection schemes when the transformer is in the base or on top of nacelle, respectively. Having no protection, the amplitude of the overvoltages (blue waveforms in Figs 8 and 9) are 12 p.u., which is well within safe margin. The quarter wave frequency of the HV cable (length=23 m) is equal to dominant resonance frequency of WTT (2MHz) and leads to resonant overvoltages in Fig. 9 which persist for longer time (in this case double duration) compared to energization at HV terminal. On the other hand, the energization of the transformer in the base has slightly higher du/dt compared to resonant overvoltages (see table. IV).

According to Figs 8 and 9 and table IV, the existence of stray series inductances results in less affectivity of protective devices. For example, inductance-free (ideal) RC filters at LV terminal can diminish both overvoltage amplitude and du/dt to safe levels (acceptable du/dt=17.5 p.u./µs). Comparing the protection options in table IV, RC filters at both HV and LV terminal, which have low series impedance (in this case 0.25µH) can compensate the negative effect of series inductance and decrease the du/dt to safe margin. In [19], it is shown that even during energization of the second WTT in a row, there is a potential of resonant overvoltage induction on LV terminal of the first WTT. In that case, the RC filters also are adequate protective devices.

B. Earth Fault in the wind farm

As analyzed in previous sub-section, for this 300 kVA WTT, the switching at the peak of phase A with 23 m cable length leads to resonant overvoltages at LV terminal. That is also valid for earth fault since it can be interpreted as switching at the peak of phase A to ground potential. WTT can be on the top of nacelle or at the base. Therefore, earth fault scenarios which can lead to resonant overvoltage are different (see Fig.10).

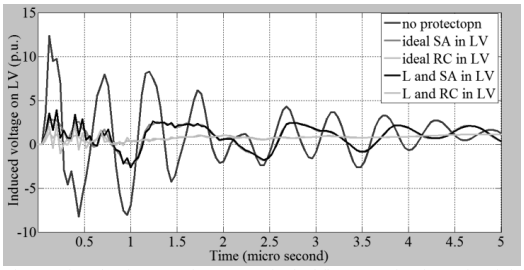

Fig.8. Induced voltage on the LV terminal of first WTT in Fig.1 when it is in the base with various protection devices at LV side (L and SA means surge arrester with inductive lead.).

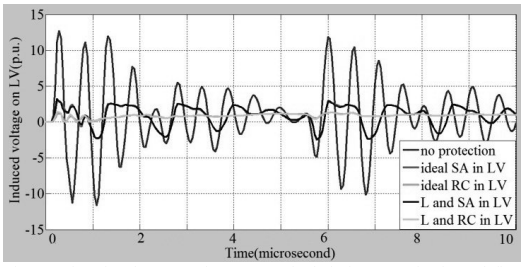

Fig.9. Induced voltage on the LV terminal during energization of first WTT in Fig.1 when it is on top of nacelle.

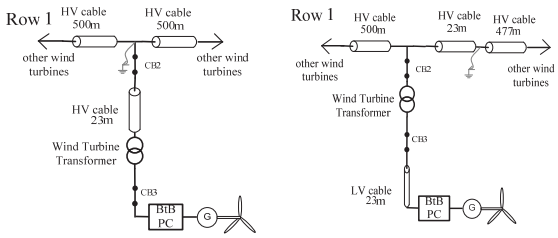

Fig.10. resonant overvoltage due to earth fault. left: WTT on top of nacelle, right: WTT in the base.

TABLE IV
RATE OF RISE/FALL OF VOLTAGE (P.U./μS) FOR VARIOUS PROTECTION SCHEMES INCLUDING RESULTS IN FIGS. 8 AND 9.

Protective devices	WTT in the base	WTT on the nacelle
No protection	154	93
SA(LV) with L*	44	27
Ideal SA(LV)	36	25
RC(LV) with L*	25	11
Ideal RC(LV)	16	9.5
SA(LV) & RC(LV)*	20	11
SA(LV),RC(LV) & SA(HV)*	19	10
SA(LV),RC(LV),SA(HV) & RC(HV)*	13	4
RC(LV) & RC(HV)*	16	4.5

*In this cases, stray series inductance is included to protective devices.

Fig. 11 shows the comparison between the two models for induced overvoltages to LV phase A due to single phase earth fault in the base (Fig. 10-left). The simulation results for both models are in good agreement. It can be concluded that the PC model with GSC and DC link capacitor is adequately accurate for resonant transient studies. It should be mentioned that all IGBT sequences in the latter model results in the same transient result. The simulation results of both models had dc biases due to fixed voltage at DC link capacitor, which are subtracted for easier comparison. When the middle point of DC link capacitor is not grounded, the resonant transient is more persistent. The peak-to-peak of overvoltages in GSCs with grounded and ungrounded DC link middle points are 12 and 18 p.u., respectively. The maximum value of du/dt equals to 70 for both cases.

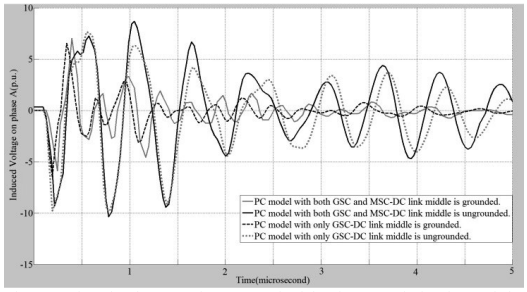

Fig.11. Induced voltage on the LV terminal for the scenario in Fig. 10-left

Since ungrounded DC link leads to more severe resonant transients, it is further analyzed in this paper. Besides, the model with GSC and DC link capacitor is applied. Fig. 12 shows the induced voltage on the LV terminal during earth fault for the two scenarios in Fig. 10. When WTT is in the nacelle and earth fault occurs in the base (cable length=wind turbine height=23m), the first transient surge arriving at the transformer is double compared to when WTT is in the base and earth fault occurs in 23 m distance in row cable. In the former case, the first surge meets the HV input impedance of WTT, which is high. While in the latter case, it meets the equivalent impedance of the transformer and other HV cables, which approximately equals to the surge impedance of the HV cable.

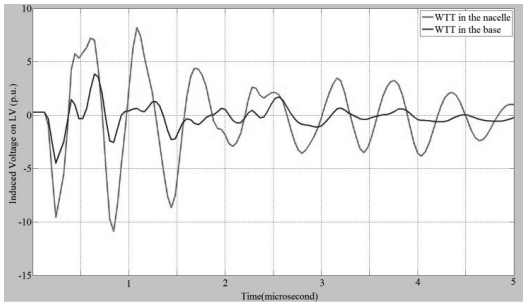

Fig.12. Induced voltage on the LV terminal for two earth fault scenarios in Fig. 10 when the DC link middle point is ungrounded and GSC has seq.1.

Earth faults for WTT on the top of nacelle are now further investigated. Since, it is more critical than other scenario. If earth fault in resonance condition occurs when GSC is not connected, the highest overvoltage will be induced at the LV terminal of WTT (30 p.u. and 400 p.u./μs). Earth fault at th e peak of phase A in critical cable length (in this case 23 m) with low earth fault impedance results in persistent resonance oscillations at the LV terminal. The red waveforms in Figs 13-15 show the induced voltage on phases A, B and C for this situation. According to the simulation results in Figs 13-15, the voltages of each phase are almost the same regardless to the IGBT switching sequences. Thus, we analyze the effect of components in GSC, RL harmonic filter and RC filters at LV and HV terminal only for one sequence, e.g. seq. 1.

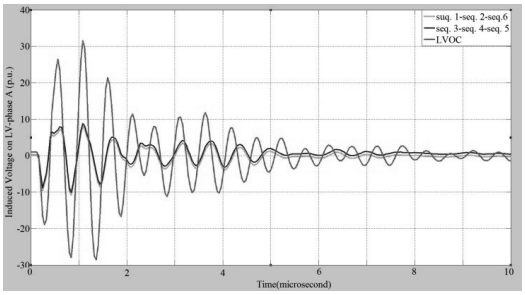

Fig.13. Induced voltage on LV-phase A for earth fault at peak phase A for the scenario in Fig. 10-left with converter in various sequences according to table I or LV open circuit.

As shown in Fig. 13, the amplitude and du/dt of the induced voltage are decreased to one-third on LV when the GSC is connected. The reason can be explained in this way: seq. 1 can be interpreted with good approximation as a short circuit between phase A and C and other sequences has other kind of two phase short circuits. This short circuit effects the transformer terminal connection and consequently the transients.

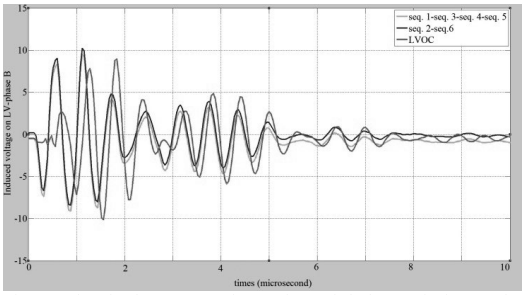

Fig.14. Induced voltage on LV-phase B for earth fault at peak phase A for the scenario in Fig. 10-left in various sequences in table I and LV open circuit.

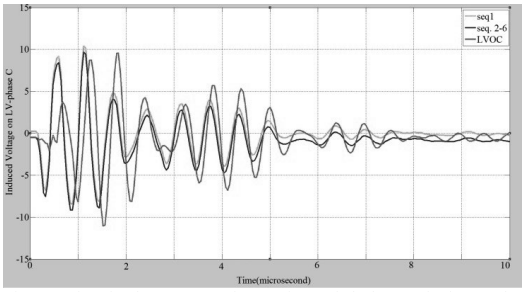

Fig.15. Induced voltage on LV-phase C for earth fault at peak phase A for the scenario in Fig. 10-left in various sequences in table I and LV open circuit.

The main component with dominant effect on overvoltage transients at the LV terminal is the RL harmonic filter. Fig. 16 shows that the increase of the inductance leads to the increase of the overvoltage amplitude and du/dt. However, four times increase of the DC link capacitor or the capacitors in RC snubber circuits do not change the transients effectively.

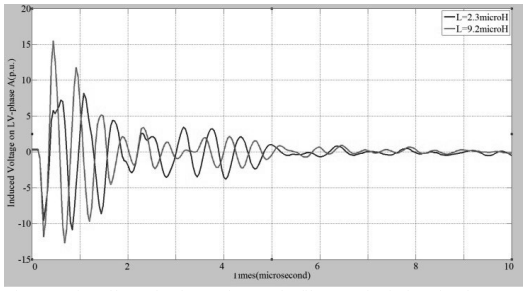

Fig. 16, The effect of L in RL harmonic filter on the induced voltage on LV-phase A.

Installing RC filter (R=10Ω and C=500 nF) at LV and HV with low stray inductance (0.25 μH) results in similar induced voltage on LV as in Fig. 9. The amplitudes decrease to 1 and 0.5 p.u. for uninitiated and initiated GSC, respectively. Besides, du/dt decrease to 10 and 5 p.u./μs, respectively. This means that the application of just RC filter protects the LV terminal of WTT and GSC components effectively.

IV. Conclusions

In this paper, the resonant overvoltages at LV terminal of wind turbine transformers due to energization or single phase earth fault in feeder cables are analyzed. Both energization and earth fault are considered to occur at the peak of phase A. It was found that if the lengths of energizing cable or cable distance of earth fault are such that their quarter wave frequencies are equal to one of resonance frequencies of the transformer, resonant overvoltages occur. In this paper, the highest resonant overvoltages occurs (30 p.u.) for earth fault in 23 m cable distance from the wind turbine transformer if grid side converter is not connected. Since single phase earth fault at peak of phase A can be interpreted as energization of negative voltage source with very low internal impedance (short circuit impedance). This creates more sustained oscillations and large induced voltage on LV side.

If earth fault occurs at the peak of phase A during power production by generator, the inductance in the series RL harmonic filter dominantly affect the resonant transients. The amplitude of resonant overvoltages and du/dt increases with higher inductances.

Simulation results also show that installation of wind turbine transformers in the base leads to relatively less vulnerable resonant overvoltages compared to transformer in the nacelle. It was found that installation of RC filters at both HV and LV terminal, which are inductance-free or has adequately low stray inductance, protects the LV terminal of WTT from resonant overvoltages due to both energization and earth fault.

V. Acknowledgment

Authors greatly appreciate Norwegian Research Center for Offshore Wind Technology (NOWITECH) which is sources of funding.

VI. REFERENCES

[1] I. Arana, A. Hernandez, G. Thumm, and J. Holboell, "Energization of wind turbine transformers with an auxiliary generator in a large offshore wind farm during islanded operation", *IEEE Trans. Power Delivery*, vol. 26, no. 4, pp. 2792-2800, Oct. 2011.

[2] L. Liljestrand, A. Sannino , H. Breder, and S. Thorburn, "Transients in collection grids of large offshore wind parks," *Wiley Inter science*, vol. 11 Issue 1, Pages 45 – 61, 2008.

[3] I. Arana, J. Holbøll, T. Sørensen, A. H. Nielsen, P. Sørensen, and O. Holmstrøm, "Comparison of measured transient overvoltages in the collection grid of Nysted offshore wind farm with EMT Simulations", in proc. 2009 *International Conference on Power Systems Transients (IPST)*, paper 38.

[4] C.D. Tsirekis, G.J. Tsekouras, N.D. Hatziargyriou, B.C. Papadias, "Investigation of switching transient effects on power systems including wind farms", *in proc. 2001 IEEE Powertech conference,* vol 4.

[5] V. Akhmatov, B. C. Gellert, T. E.McDermott, W. Wiechowski, "Risk of temporary over-voltage and high-voltage fault-ride-through of large wind power plant", *in Proc. 2010 9th Int. Workshop on Large-Scale Integration of Wind Power into Power Systems*.

[6] B. Badrzadeh, M. Høgdahr, N. Singh, H. Breder, K. Srivastava, M. Reza, " Transient in wind power plants- part II: case studies", IEEE Trans. Industry Applications, vol. 48, no. 5, Sep.-Oct. 2012.

[7] T. Abdulahovic, "Analysis of High-Frequency Electrical Transients in Offshore Wind Parks." Ph.D. dissertation, Dept. Energy and Environment, division of electric power eng.,.Göteborg : Chalmers University of Technology, 2011..

[8] B. Badrzadeh, B. Gustavsen, "High frequency modeling and simulation of wind turbine transformer with doubly fed asynchronous generator", *IEEE transaction on Power Delivery*, vol. 27, no. 2, pp. 746-756, 2012.

[9] B. Gustavsen, "Study of transformer resonant overvoltages caused by cable-transformer high frequency interaction," *IEEE trans. Power Delivery*, vol. 25, oo. 2, pp. 770-779, Apr. 2010.

[10] B. Gustavsen, "Wide band modelling of power transformers," *IEEE transaction on Power Delivery*, vol. 19, No. 1, pp. 414–429, 2004.

[11] B. Gustavsen and A. Semlyen, "Rational approximation of frequency domain responses by vector fitting," *IEEE trans. . Power Delivery*, vol. 14, no. 3, pp. 1052–1061, 1999.

[12] A. Yazdani and R. Iravani, *Voltage-Sourced Converters in Power Systems*. New York: IEEE/ Wiley, Feb 2010.

[13] N. Mohan, T. M. Undeland, W. P. Robbins, Electronics Converters, Applications and Design, New York: Wiley, 1995.

[14] J.R. Marti,"Accurate modeling of frequency-dependent transmission lines in electromagnetic transient simulations", *IEEE Trans. PAS*, vol. 101, no. 1, pp. 147-157, Jan. 1982.

[15] Y. Yasuda, N. Uno, H. Kobayashi, and T. Funabashi," Surge analysis on wind farm when winter lightning strikes", *IEEE Trans. Energy Conversion*, vol. 23, no. 1, pp. 257-262, 2008.

[16] IEEE Working Group on Surge Arrester Modeling, "Modeling of metal oxide surge arresters," *IEEE trans. power delivery*, vol. 7, no. 1, pp. 302–309, Jan. 1992.

[17] ABB surge arrester POLIM-R-2N datasheet[online]. Available: http://www.abb.com/search.aspx?q=POLIM-R-2N&abbcontext=products.

[18] ABB surge arrester POLIM-C-N datasheet, [online].Available:http://www.abb.com/product/db0003db004279/c125739900636470c125708c003fd77a.aspx.

[19] A. H. Soloot, H. Kr. Hoidalen, B. Gustavsen, " The Assessment of Overvoltage Protection Within Energization of Offshore Wind Farms," *Energy Procedia*, vol. 24, pp. 151-158, 2012.

Paper III

Is not included due to copyright

Paper IV

Is not included due to copyright

Paper V

Electric Power Systems Research 115 (2014) 26–34

Contents lists available at ScienceDirect

Electric Power Systems Research

journal homepage: www.elsevier.com/locate/epsr

Modeling of wind turbine transformers for the analysis of resonant overvoltages

A.H. Soloot [a,*], H.K. Høidalen [a], B. Gustavsen [b]

[a] Department of Electric Power Engineering, Norwegian University of Science and Technology, Norway
[b] SINTEF Energy Research, Norway

ARTICLE INFO

Article history:
Received 11 November 2013
Received in revised form 15 January 2014
Accepted 4 March 2014
Available online 24 March 2014

Keywords:
Wind turbine transformer
Resonant overvoltages
Winding design
Analytical modeling
RLC ladder model
Frequency response analysis

ABSTRACT

Switching transients and earth fault in a wind farm collection grid are two transient phenomena which can lead to resonant overvoltages at the LV terminal of the wind turbine transformers as well as inside HV and LV windings. The aim of this paper is to analyze the potential of the resonant overvoltage for various winding designs; disc, layer and pancake. In this way, the least vulnerable winding design can be recommended. For this aim, a 500 kVA transformer test object with the three aforementioned winding types has been designed and manufactured. Similar geometrical characteristics are used for all the three windings. By measuring the frequency response, the resonant frequencies can be found and the amplitude of the transferred voltage at these frequencies can be compared. The windings are also modeled in this paper in detail based on analytical functions. This RLC ladder model is verified by the measurements.

The measurements and modeling results show that all winding designs have a resonant frequency around 800 kHz for the transferred voltage to LV terminal. Disc winding shows the lowest amplitude of the transferred overvoltages (6 p.u.). The layer winding, also has a resonance at 1.6 MHz with an even higher transferred overvoltage (80 p.u.). The frequency response of the pancake winding has characteristics of both disc and layer windings. In spite of having the lowest transferred overvoltage peak, the disc winding has many additional resonant frequencies in the range of 100 kHz–1 MHz. This could excite resonances in other parts of the winding. Consequently, pancake winding designs might be the most promising to minimize resonance situations.

1. Introduction

Medium voltage transformers with ratings in the range of 300 kVA–8 MVA have been installed in both onshore and offshore wind farms. The energization of each wind turbine may result in cable-transformer resonant transients. This phenomenon has been studied in traditional medium voltage transmission and distribution networks [1–6]. The similar resonance condition can also happen in wind farms [7,8]. The length of the cables in wind turbines is in the range of 100–200 m. The quarter wave frequency of such cables can be in the vicinity of resonant frequencies of wind turbine transformers. Therefore, the energization may lead to resonant overvoltages on LV terminal of transformers and inside HV windings [9]. These overvoltages have higher amplitude and rate of rise (du/dt) compared to other overvoltages. They can lead to insulation failures in transformers. In [10], the voltage distribution due to energization of a 10 kV–200 kVA reactor with disc winding is analyzed. It was observed that energizations with short rise time (<100 ns) lead to the excitation of internal resonances. Resonant overvoltages can also occur due to earth fault in cables [11]. In this case, they can be harmful for the power converters as well. Thus, the investigation of them is necessary and appropriate protection devices such as resistive–capacitive (RC) filters are required [12].

The selection of less vulnerable winding design is a measure to prevent resonant overvoltages during wind turbine energizations. This means that knowing the cable lengths and their quarter wave frequency, a winding type can be chosen that does not have a resonant frequency in that vicinity. The aim of this paper is to compare the frequency responses of three winding types; disc, layer and pancake. A 500 kVA transformer with the three aforementioned winding types has been designed and manufactured. The transferred voltages to LV and HV input impedance of windings are measured based on frequency response analysis (FRA) technique [13–16].

An analytical model is also developed and introduced in this paper. The model assists us to draw general conclusions about

* Corresponding author. Tel.: +47 45123757.
E-mail addresses: amir.h.soloot@ntnu.no, amir.hayati@gmail.com (A.H. Soloot).

http://dx.doi.org/10.1016/j.epsr.2014.03.004
0378-7796/

the various characteristics of the three winding designs and their potential for resonant overvoltages. In literature, two main high frequency transformer modeling techniques are introduced as multi-transmission line (MTL) model and ladder RLC [17]. In [18], results from MTL and RLC ladder models of windings are compared with frequency domain measurements. It is concluded that the RLC model can give accurate results for fast transients (up to 1 MHz). However, for very fast transients (above 1 MHz) MTL model provides better results. In this paper, RLC ladder model is developed, since the maximum range of the quarter wave frequency of wind turbine cables are about 1 MHz.

In Section 2, the transformer test object and the setup for frequency response analysis are outlined. Section 3 describes the transformer model. In Section 4, the results of the analytical model for the different windings are compared. The characteristics of the three windings are also discussed. Section 5 discusses the challenges of transformer modeling.

2. Test setup

Fig. 1 shows the layout of the special 11/0.24 kV 500 kVA transformer which is designed and produced to enable comparison of the frequency response of the three different winding designs. The core and the windings are fully paper insulated and out of tank during the measurements. The LV and HV neutrals are grounded together and connected to the core with 2 cm wide braided aluminum wire.

As shown in Fig. 1, the transformer consists of a layer winding on the left limb, a pancake winding on the middle and a disc winding on the right limb. To compare the frequency response of the windings, design parameters are kept as identical as possible:

- The number of turns in HV and LV windings and rated voltage ratio are the same for the winding designs.
- The winding frame, i.e. axial winding height and radial width, is almost the same for the windings.
- The layer winding has aluminum wire and the others have copper wires. The conductors' cross-section is such that the DC resistance of the windings becomes similar.
- LV windings are all aluminum foil with the same geometrical designs and insulation materials.

In this way, the three windings have equal impedances at 50 Hz and similar steady state condition. The frequency response of the transferred voltages to LV terminals is measured from 1 kHz to 10 MHz with Agilent network analyzer E5061B and Tektronix P2220 probes. The voltage probes are used with *x10* attenuation which is appropriate for voltage measurement up to 200 MHz. Attenuation *X1* is appropriate up to 6 MHz and it may seem adequately accurate for our measurements. But, the input resistance/capacitance of attenuation *X1* is 1 MΩ/95 pF which may have loading effect on high frequency measurements compared to *X10* attenuation (10 MΩ/16 pF). Thus, *X10* attenuation is selected which has acceptable error (<5%). For measuring the input impedance of HV and LV windings, the current probe FLUKE PM6306 is used, which has low and acceptable error (<10%) in frequency range 1 kHz–1 MHz. Therefore, the results for input impedance will be shown in this frequency range in the next section.

3. Transformer model

The three winding types; disc, pancake and layer windings and the LV foil winding are represented by RLC ladder model in this paper in which windings are divided into units as shown in Fig. 2. Each unit has resistance and self inductance as well as series capacitance and insulation resistances. There are capacitances and conductances between units in adjacent layers. Mutual impedances between units of HV, LV and LV–HV are not shown in Fig. 2, but are considered. The capacitances between last layer LV and first layer in HV is not shown in Fig. 2. They are considered, though. The accuracy of the model mainly depends on the level of the discretization chosen for the windings. High discretization increases the calculation time. The procedure for the calculation of RLC parameters is explained here for layer winding. It is generally similar for the other windings with only topological adjustments. After that, input impedances of HV and LV windings and the transferred voltages to LV winding are calculated.

Let us consider nu number of units in each layer of HV layer winding. nH is the number of HV layers and therefore $nu \times nH$ is the total number of units. Besides, the LV foil winding has nL layers, and we take each layer as one unit. The total order of R, L, C and G matrices becomes $m = nL + nu \times nH$.

Performing the Kirchhoff's Voltage Law (KVL) and Kirchhoff's Current Law (KCL) for all units results in (1) and (2), respectively. In Appendix A.1, KCL and KVL for an arbitrary unit, i, is performed.

$$[A]_{m\times m}[V]_{m\times 1} = ([R]_{m\times m} + j2\pi f[L]_{m\times m})[I_b]_{m\times 1} \quad (1)$$

$$[I]_{m\times 1}[A]^t_{m\times m}[I_b]_{m\times 1} = ([G]_{m\times m} + j2\pi f[C]_{m\times m})[V]_{m\times 1} \quad (2)$$

Matrices V, I and I_b representing nodal voltages, injected nodal currents, the currents of inductive branches, respectively. A is a connectivity matrix describing the topology and linking branches and nodal quantities. The diagonal elements in A matrix are equal to 1 and sub-diagonal elements are equal to −1 and the rest is zero. Exceptionally, the first row and the row number $nL + 1$, which are for first units in LV and HV winding respectively, have only the diagonal element, since the other nodes of these units are grounded.

The nodal admittance matrix Y can be calculated by reforming (1) to obtain I_b based on V and inserting this in (2). This gives (3).

$$[I] = [Y][V], \qquad [Y] = [G] + j2\pi f[C] + [A]^t([R] + j2\pi f[L])^{-1}[A] \quad (3)$$

Since all of the R, L, C and G matrices are symmetrical, the admittance matrix also becomes symmetrical. To obtain the equation for the transferred voltage to LV, impedance matrix, Z, should be calculated from (3) by inverting Y. Since only the last element of I vector is none-zero due to the connection of last unit to the HV terminal, the last column of Z multiplies with the terminal current, I_m, and gives the nodal voltage in (4). Therefore, the transferred voltage to LV terminal is according to (5).

$$[Z(:, m)]I_m = [V] \quad (4)$$

$$\frac{V_{LV}}{V_{HV}} = \frac{Z(nL, m)}{z(m, m)} \quad (5)$$

In the following subsections, the process for the calculation of the R, L, C and G matrices are explained. It should be mentioned that these four matrices, Z matrix and equation (5) are coded and calculated in MATLAB. Inputs of this code are: (1) core and winding physical dimensions, (2) material properties of winding conductors, insulation and core. The main output of the code is input impedances of LV and HV windings as well as transferred voltage to LV.

3.1. Calculation of R and L matrices

The analytical method [19,20] for computing the self and mutual impedance is based on Eqs. (A-3)–(A-6) in Appendix A.2. In addition, the internal conductor resistance is added to the diagonal elements of R matrix, since Wilcox formulas only consider the core effect on the resistance matrix. In this paper, an analytical equation for the consideration of skin and proximity effects is applied for the calculation of the internal conductor resistances [21] in both LV

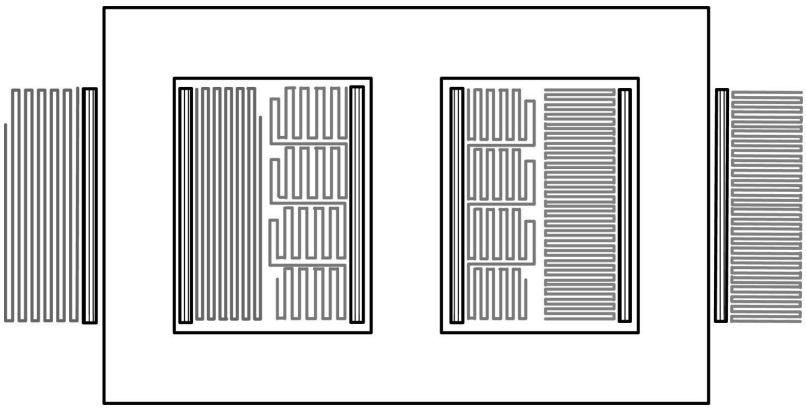

Fig. 1. The layout of the manufactured 500 kVA transformer.

and HV winding:

$$R_{LV}(n) = \mathrm{Re}\left\{\frac{\pi D(n)\gamma}{2\sigma h}[\coth(\gamma w)(2n^2-2n+1)] - \frac{2n(n-1)}{\sinh(\gamma w)}\right\},$$

$$\gamma = \frac{1+i}{\delta}\sqrt{\eta} = (1+i)(\sqrt{\pi\mu_0\sigma f})\sqrt{\frac{h}{p}} \tag{6}$$

In (6), the layer number is symbolized with n. The diameter of nth layer is $D(n)$. The conductor height and width are h and w, respectively. The skin depth in each conductor is shown with δ and is related to its conductivity, σ, frequency, f, and its permeability, $\mu = \mu_0$. The conductor height plus its insulation height is p. The ratio of h to p is called porosity factor, η. For LV foil winding, η equals to one. Since, discretized units of LV layers in the proposed model should be assumed without insulation. Thus, p equals to h and η equals to one. For HV pancake and layer winding, $0.9 < \eta < 1$. While for disk winding, it is $0.7 < \eta < 0.9$. Since, the inter disc insulations increase the effective insulation height.

3.2. Calculation of C matrix

The diagonal elements of C matrix are the sum of the capacitances connected to each unit. While the off diagonal elements are all negative and equal to the capacitance between the unit which has the row number and other units. It is obvious that there are many zero elements in C matrix, since each unit has just capacitive coupling with four other units, e.g. in layer winding the two adjacent units in the same layer, one unit in layer before and one unit in layer after. The capacitance between adjacent units is calculated based on (7),

$$C_{ij} = \varepsilon_0\varepsilon_r\frac{2\pi R(T+t)}{t} \tag{7}$$

The permittivity of vacuum and the relative permittivity of the insulation between units are shown with ε_0 and ε_r, respectively. R, T and t are shown in Fig. 3 for both cases where two units are in the same layer or adjacent layers. Units in the same layer have same radius, R, which can directly be used for inter-turn capacitance (Fig. 3, left). While, units in adjacent layers have slightly different radius. Thus, the average of these radii (R) is considered for capacitance calculation (Fig. 3, right).

T is unit height if units are in adjacent layers. For units in one layer, T is the unit thickness. The insulation thickness is shown with t. The fringing effect, which is the increment of the capacitances due to curvature of electric field lines in the edge of conductor, is considered by adding t to T [22].

3.3. Calculation of G matrix

The conductivity matrix, G, is calculated based on the conductance of the insulations between units. The insulation conductance is related to its capacitance and dissipation factor ($\tan\delta$).

$$G_{ij} = 2\pi f\tan\delta C_{ij} \tag{8}$$

Similar to C matrix, the diagonal elements of G matrix are the sum of the conductances connected to each unit. While the off diagonal elements are all negative and equal to the conductance between the unit which has the row number and other units. It should be mentioned that $\tan\delta$ in (8) is also frequency, moisture and temperature dependent and has important effect for high frequency transformer model above 100 kHz [23]. Therefore, accurate modeling necessitates obtaining the frequency dependency of all insulations; the ones between LV foils, HV units, between LV and HV, LV to ground and HV to ground. In this paper, we used an approximated equation, (9), for all the insulation dissipation factors [24],

$$\tan(\delta) = (1.082\times10^{-8})\cdot 2\pi f + 5.0\times10^{-3} \tag{9}$$

4. Model verification and winding comparison

The results of modeling the three windings are brought in this section and compared with measurements. Besides, considerations for the energization of wind farms are given.

4.1. Layer winding

In Figs. 4 and 5, the input impedance of HV layer winding and the associated LV foil winding are shown. It can be observed that the calculations follow the trend of the measurement for Layer winding in both HV and LV windings. The shortcoming of the model is that the second resonant frequency (10 kHz) is not represented due to flux linkage with other phases, as is discussed in [25]. Besides, the amplitude of the calculation results for LV winding (Fig. 5) at $f = 1$ MHz is higher than measurement.

The induced voltage on the LV terminal calculated by (5) is compared with measurements in Fig. 6. The frequency range is now extended to 10 MHz, since the voltage probes are accurate also above 1 MHz as mentioned in Section 2. Although quarter wave frequency of wind park feeder cables rarely can be in this range,

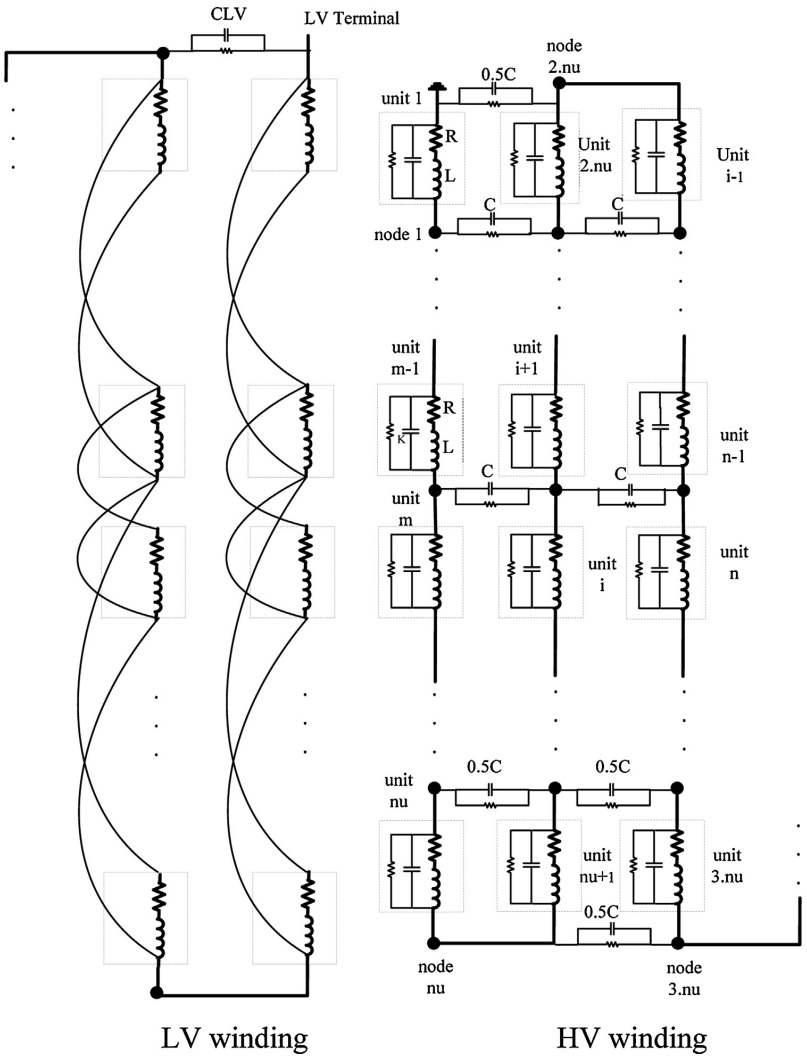

Fig. 2. RLC latter model of LV foil and HV layer winding.

close-up ground faults can give oscillations with such high frequencies. This also gives an opportunity to test the analytical model at higher frequencies.

As it can be seen in Fig. 6, the model results are in good agreement with measurements for $f < 1$ MHz. But, for $f > 1$ MHz, it only follows the decreasing trend of the measurements. The dominant resonant frequency in 1.6 MHz is not well represented. This will be discussed in detail in Section 5.

4.2. Disc winding

In Figs. 7 and 8, the input impedance of HV disc winding and its LV foil winding are shown. The calculation result for HV input impedances is in good agreement with measurement. One weakness for the calculations of the disc winding is the shift in the LV input impedance for $f > 20$ kHz. The induced voltage to LV terminal is compared with measurements in Fig. 9 for the disc winding. The model response follows the trend of measurement and represents some of the resonant frequencies and especially the dominant one. Comparing Figs. 6 and 9, it can be seen that the amplitude of the transferred voltage to LV at 800 kHz, which is the common resonant frequency, is much lower for the disc compared to layer winding. If the amount of the transferred voltage to LV at 1 kHz is considered as base value for per unit comparison, the transferred voltages to LV at 800 kHz for layer and disc windings are 21.6 and 5.4 per unit. It can be concluded that the very fast transients induce critical overvoltages at LV terminal for layer, but not for disc winding. Meanwhile, disc winding has many resonant frequencies around 100 kHz, while the layer winding has most of its resonant frequencies above 1 MHz. The resonant frequencies of disc winding are in the range of quarter wave frequency of typical wind turbines. They can be amplified inside HV or LV windings. Therefore, there can be high potential of the internal resonant overvoltages [26,27].

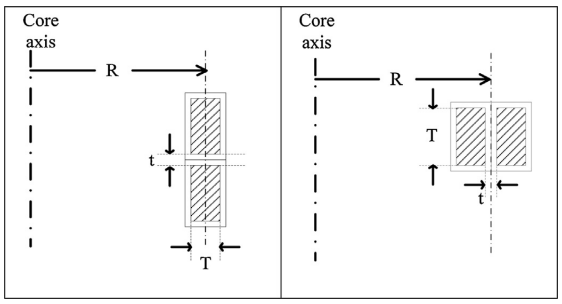

Fig. 3. Definition of *R*, *T* and *t* for capacitance calculation of units in same layer (left) or adjacent layer (right).

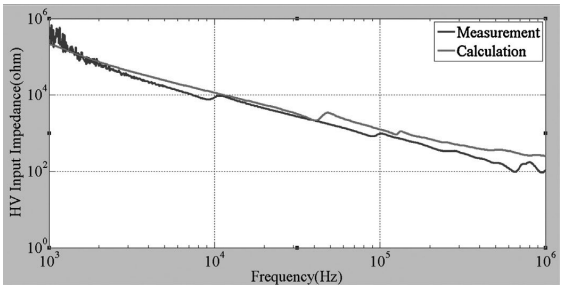

Fig. 4. HV input impedance for layer winding.

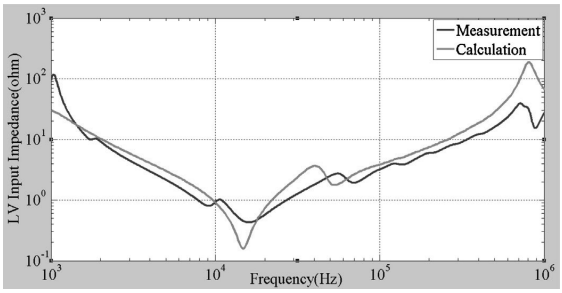

Fig. 5. LV input impedance for layer winding.

4.3. Pancake winding

In Figs. 10 and 11, the input impedance of HV pancake winding and its LV foil winding are illustrated. Compared to disc winding, the frequency shift in the LV model response is smaller but still present. The induced voltage to the LV terminal is compared with measurements in Fig. 12. It seems that, the model results cannot represent the amplitude of the measurement near 800 kHz. According to Eq. (5), the calculation results for the transferred voltages to LV are sensitive to the accuracy of $Z(nL, m)$ and $Z(m, m)$ calculation The latter one is input HV impedance. Small, but not ignorable, deviations of calculation results from measurements can be observed in Fig. 10. There can be noticeable deviations for $Z(nL, m)$ calculations, which measurement cannot be available for it. These two deviations in numerator and denominator of (5) may lead to higher deviations for the calculation of transferred voltages. Since the proposed model aims to assist wind transformer designers and operators to improve windings design against very fast transients, especially resonant

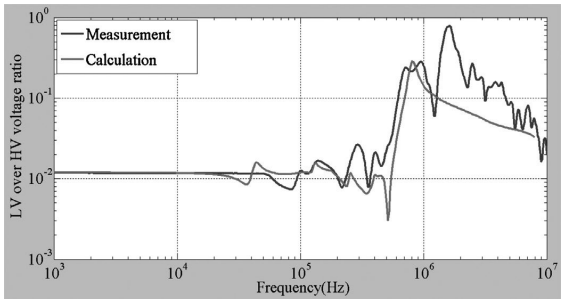

Fig. 6. Transferred voltage from HV to LV for layer winding.

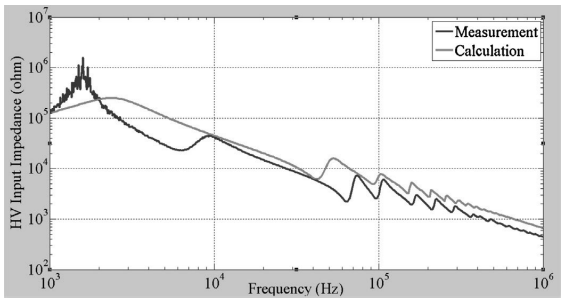

Fig. 7. HV input impedance for disc winding.

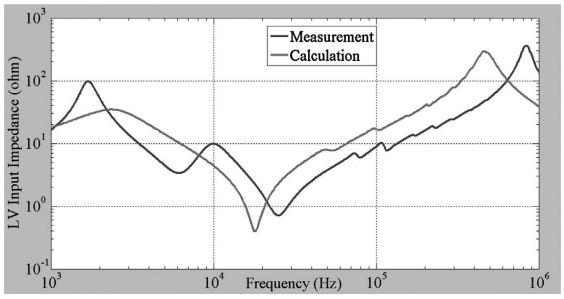

Fig. 8. LV input impedance for disc winding.

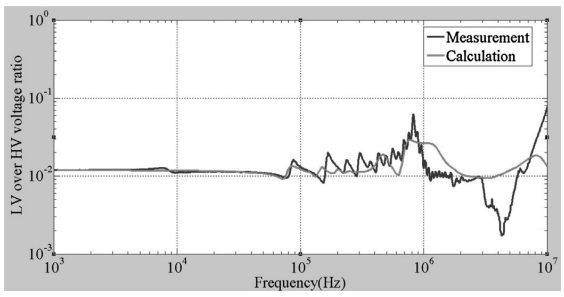

Fig. 9. Transferred voltage from HV to LV for disc winding.

overvoltages, the model should have this feature to draw general conclusions. In future work, the sensitivity of calculation results on core and insulation material properties is going to be investigated in more detail to improve agreements with calculations,

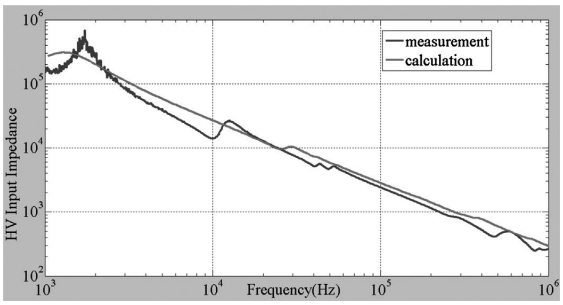

Fig. 10. HV input impedance for pancake winding.

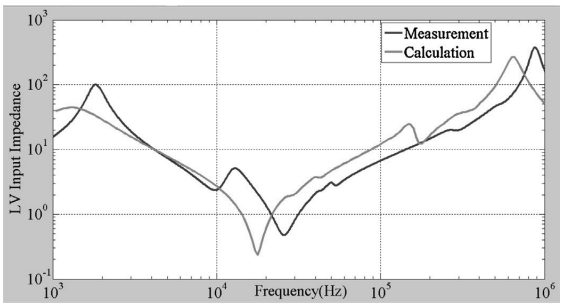

Fig. 11. LV input impedance for pancake winding.

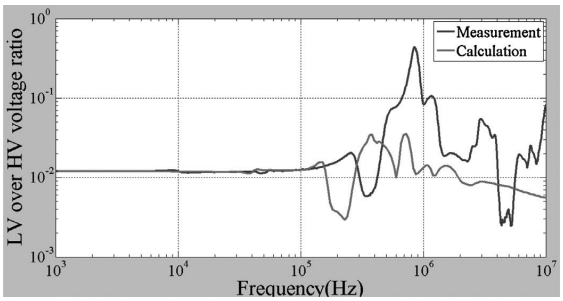

Fig. 12. Transferred voltage from HV to LV for pancake winding.

particularly the transferred voltages to LV in pancake windings.

Comparing measurement results for the transferred voltage to LV for the three windings in Fig. 13, the trend of the frequency response around 800 kHz for the pancake winding is similar to the disc winding, while the amplitude of the transferred voltage is in the range of the layer winding.

It can be concluded that if the quarter wave frequency of feeder cables is lower than 800 kHz, pancake and layer windings may be the less vulnerable winding for internal resonant overvoltages. Meanwhile, the pancake winding has the advantage of repair easiness. For example, the pancake winding here has four coils. If any internal insulation failure happens in any coils, it can be easily replaced. This feature is prominent for offshore wind farms, where long distance from shore and accessibility challenges requires maintenance-free or easy repairing components.

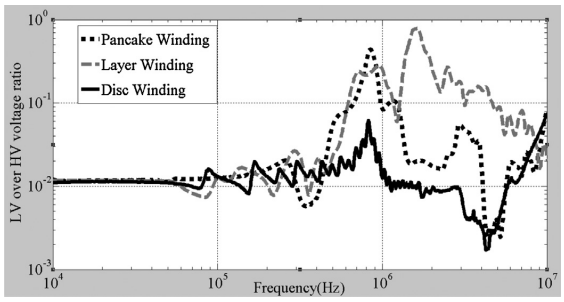

Fig. 13. Measured transferred voltage from HV to LV for the three windings.

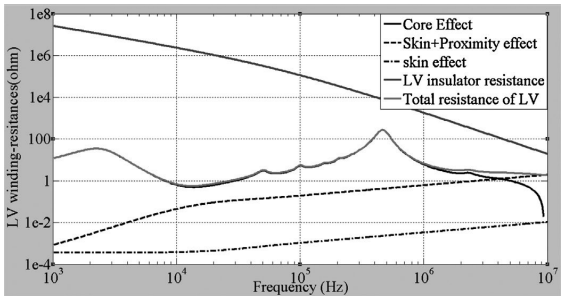

Fig. 14. The comparison of different resistances in LV winding with total resistance.

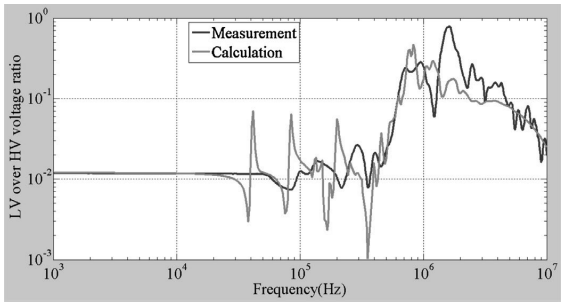

Fig. 15. Transferred voltage from HV to LV for layer winding. Proximity effect ignored in the calculations.

5. Discussion

The white box models; RLC ladder model and MTL model require precise geometrical data and material property of the transformer under study. In this work, we designed and produced this 500 kVA transformer. Therefore, detailed geometrical design data are available. The other input for modeling is conductor, core and insulation material properties, where only conductor material properties are available accurately. Core parameters, i.e. μ_z, σ_{core} and γ, are not available. Wilcox et al. proposed measurement techniques to obtain these parameters in the case of the mutual impedance between two coils [19]. However, those techniques cannot be applied to this special 500 kVA transformer. The calculation results are sensitive to core material properties. The three core parameters are estimated and optimized by the comparison of repetitive calculation results with measurements. A slight variation in the acceptable range [19] is done for one parameter in each calculation.

In the case of insulation materials, their permitivities are well-known. But, the detailed frequency dependency of the dissipation factors ($\tan\delta$) of all insulators, which is needed for accurate modeling, especially $f > 1$ MHz is not available. Eq. (9) from literature is just included for all transformer insulations. The sensitivity of LV input impedances to core and insulation parameters are higher that HV input impedances. That is why the calculation results for LV layer and LV disc (Figs. 5 and 8) still can be improved to have better agreement with measurements.

It should be mentioned that the layer winding conductor is aluminum due to design limitations. According to discussion with manufacture, it was not possible to choose any available copper wire cross section so that radial width, 50 Hz transformer impedance and turn ratio of layer winding became similar to those of disc and pancake winding. Nevertheless, aluminum has higher skin depth compared to cupper. The conductor resistances at high frequency would be different between layer and two other windings. This will influence the amplitude of terminal impedances at resonant frequencies. But, the value of resonant frequencies is not dependent to conductor resistances, but to the capacitances and inductances.

The next issue to be discussed is the analytical calculation of the internal conductor resistance, which is one part of self-resistance. The other part is the self-resistance due to the core and is calculated by Wilcox formula. Fig. 14 shows the total self-resistance of the LV foil associated with disc winding according to the proposed model. The black solid line represents self-resistance due to core skin effect. The dashed line shows the internal conductor resistance based on (6). The dashed–dotted line is the internal conductor resistance only due to skin effect [28].

It can be found that total resistance is dominantly affected by proximity effect for $f > 4$ MHz. Ignoring the proximity effect in the model and including just skin effect by the analytical formula in [28] leads to resonant frequencies, around 100 kHz, with quite high amplitudes for the transferred voltage to LV in layer winding (see Fig. 15). The internal conductor resistance becomes two orders of magnitude lower for 10 kHz $< f <$ 1 MHz by ignoring proximity and the calculation results for transferred voltage in this case has poor agreement with measurement for 50 kHz $< f <$ 500 kHz. However, the calculations based on proximity effect formula cannot represent the trend of transferred voltage to LV in layer winding for $f > 1$ MHz (see Fig. 6). Also, the dominant resonant frequency at 1.6 MHz is not represented. The calculations based on skin effect formula can represent the trend much better in this frequency range. But, improvements are still required for amplitude agreement. All in all, it can be concluded that based on the frequency range of study, the appropriate formula for the analytical calculation of the internal conductor resistance can be brought in the model.

6. Conclusions

This paper aims to propose an analytical high frequency model to study resonant overvoltages in wind turbine transformers. The outputs of this model contribute wind transformer designers and operators to improve windings design against resonant overvoltages or select the least vulnerable winding type. The verification of the proposed model is carried out by comparing the calculation results with measurements on three winding type, i.e. disc, layer and pancake. A special 500 kVA transformer with these winding designs is produced and used as test object. The frequency responses of the input HV impedance, input LV impedance and transferred voltage to LV are measured. The calculation results show that the following characteristics of the windings are represented in good qualitative agreement with measurements:

1. The general trend of the frequency response for the windings, i.e. the range of amplitude for input impedance and voltage ratio.
2. The decreasing trend of the HV input impedance.
3. The resonant frequencies of the HV and LV input impedances in the range of 10 kHz–1 MHz.
4. The dominant resonant frequency of the transferred voltage to LV for disc and pancake winding (800 kHz). This frequency is also critical for layer winding.

The shortcomings of the model can also be listed as:

1. The second resonant frequency (≈10 kHz) of the input impedance of the HV and LV windings is not represented. It can be due to flux linkage of other windings via core.
2. There is a frequency shift between impedance measurements and calculations.
3. The model cannot represent the voltage ratio measurements for $f > 1$ MHz. It can be due to inaccuracy in measurements due to effect of leads, inaccuracies in the proximity effect or dissipation factors ($\tan\delta$) formulas.

In fact, the qualitatively good agreement of the calculation model assists us to study the internal overvoltages in future work. The least vulnerable winding design seems in this case (500 kVA) to be the pancake winding. Its modular design makes it also easier to repair compared to the two other winding types.

Acknowledgments

Authors greatly appreciate Norwegian Research Center for Offshore Wind Technology (NOWITECH) which is the source of funding. They are also thankful of Møre Trafo Co. for their assistance in manufacturing the 500 kVA transformer test object.

Appendix A.

A.1. KCL and KVL for an arbitrary unit

Fig. 16 shows an arbitrary unit, i, in HV winding and its adjacent units. Performing KVL in this unit gives,

$$V(i) - V(i-1) = z(i,i)I_b(i) + z(i,i-1)I_b(i-1) + z(i,i+1)I_b(i+1) + z(i,m)I_b(m) + z(i,n)I_b(n) + \cdots \quad \text{(A-1)}$$

where $V(i)$ and $V(i-1)$ are voltages of nodes i and $i-1$. The branch current in unit i is introduced by $I_b(i)$. Accordingly, the other branch currents in units are introduced. Unit i has mutual impedance with other units, e.g. unit n as shown in Fig. 16 and brought in (A-1) in the form of $z(i, n)$. Mutual impedances are calculated by means of (A-3). Self-impedance, $z(i, i)$, is calculated by adding the internal resistance (6)–(A-3). Writing KVL for all units in LV and HV result in (1). To perform KCL, an injected nodal current, I, is assumed and connected to node i (see Fig. 16). The sum of all branch currents connected to node i is equal to I.

$$\begin{aligned} I = {} & I_b(i) - I_b(i+1) + (G(i,i-1) + j2\pi fC(i,i-1))(V(i) - V(i-1)) \\ & + (G(i,i+1) + j2\pi fC(i,i+1))(V(i) - V(i+1)) + G(i,m) \\ & + j2\pi fC(i,m))(V(i) - V(m)) + G(i,n) + j2\pi fC(i,n))(V(i) - V(n)) \end{aligned} \quad \text{(A-2)}$$

The branch currents and nodal voltages are shown in Fig. 16. $C(i, i-1)$ and $C(i, i+1)$ are the series capacitances of units i and $i+1$. $C(i, m)$ is the parallel capacitance between units i and m. The conductances can be defined same as the capacitances. Writing KCL for

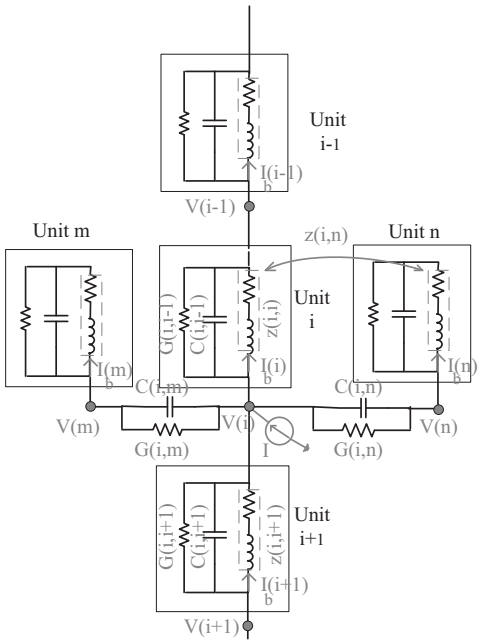

Fig. 16. The layout of unit *i*, an arbitrary unit in HV windings.

all units in LV and HV and doing simple mathematical manipulation result in (2). Besides, Eq. (A-2) shows that the summation of all adjacent capacitors of unit *i* come into the diagonal element of *C* matrix. Since they are all multiplied to *V*(*i*). The matrix *I* in (2) has only one non-zero element, which is the last one. This variable is the HV terminal current. Only the HV terminal is connected to source and other nodes does not have any connection to source in reality. Therefore, their nodal injection currents are zero.

A.2. Computation of the self and mutual impedance

Fig. 17 shows two arbitrary units around the core. The core is assumed as a solid magnetic material with μ_z in the axial direction, μ_r in the radial direction and an isotropic resistivity ρ. Eqs. (A-3)–(A-6) describe the mutual impedance between these two units [19]. (A-5) describes the impedance contribution due to that part of flux which is confined entirely to the core. (A-4) and (A-6) are

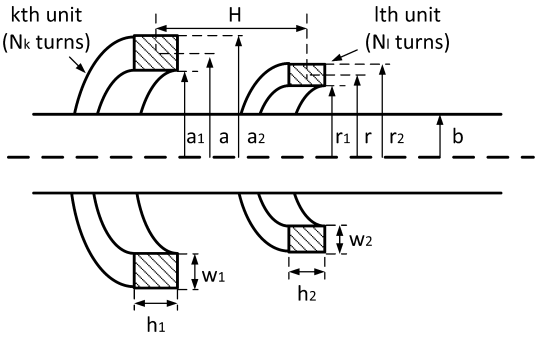

Fig. 17. Dimensions of two arbitrary units for the calculation of self and mutual impedances.

contributions to the impedance arising entirely from the effects of leakage flux. They are also the terms which control differential impedances. The effect of closed core is considered in (A-6) with *N* number of images introduced by opening the core and having parallel infinite plates at the open ends [20].

$$z(k,l) = sL(k,l) + z_1(k,l) + z_2(k,l) \tag{A-3}$$

$$L(k,l) \cong \mu_0 N_k N_l \sqrt{ra}\frac{2}{p}\left[\left(1-\frac{p^2}{2}\right)K(p) - E(p)\right] \tag{A-4}$$

$$z_1(k,l) = sN_kN_l\frac{\pi b^2}{\lambda}\left\{\frac{2\mu_z I_1(mb)}{mbI_0(mb)} - \mu_0\right\} \tag{A-5}$$

$$z_2(k,l) = sN_kN_l\frac{\pi}{\lambda}\left\{\frac{4}{h_1h_2w_1w_2}\sum_{n=1}^{N}P_1(\beta_n\alpha_1,\beta_n\alpha_2) \times P_1(\beta_n r_1,\beta_n r_2)Q_1(\beta_n h_1,\beta_n h_2)\times\frac{I_1(\beta_n b)F_1(\beta_n b)}{K_1(\beta_n b)}\cos(\beta_n H)\right\} \tag{A-6}$$

s is the Laplace transform operator in (A-3). The supporting equations for calculating functions and parameters in (A-3)–(A-6) are described in (A-7)–(A-16). In (A-4), *K*(*p*) and *E*(*p*) are complete elliptic integrals of the first and second kinds respectively, and

$$p = \sqrt{\frac{4ar}{H^2+(a+r)^2}} \tag{A-7}$$

The dimensions *a*, *r* and *H* are specified in Fig. 17. In (A-5), the core skin effect parameter, *m*, is equal to,

$$m = \sqrt{\frac{s\mu_z}{\rho}} \tag{A-8}$$

In (A-6), $\beta_n = 2\pi n/\lambda$, where λ is the length of the magnetic circuit. I_0, I_1, K_0 and K_1 are modified Bessel functions. The functions *P*, *Q*, and *F* used in (A-6), are defined in (A-9)–(A-12).

$$P_1(x,y) = \frac{1}{\beta_n^2}[p_1(x) - p_1(y)] \tag{A-9}$$

$$Q_1(x,y)\frac{2}{\beta_n^2}\left[\cos\left(\frac{x-y}{2}\right) - \cos\left(\frac{x+y}{2}\right)\right] \tag{A-10}$$

$$F_1(\beta_n b) = \mu_0\left\{\frac{\mu_z\cdot f(\beta_n \mathrm{b}) - \mu_0 f(\Gamma_n \mathrm{b})}{\mu_z\cdot g(\beta_n \mathrm{b}) + \mu_0 f(\Gamma_n \mathrm{b})}\right\} \tag{A-11}$$

$$\Gamma_n = \sqrt{\frac{\mu_z}{\mu_r}\beta_n^2 + \frac{s\mu_z}{\rho'}} \tag{A-12}$$

In (A-12), $\rho' = \gamma.|s|$ and γ is defined as fundamental core parameter related to leakage flux and is in the range of 10^{-10}–10^{-8} [19]. The functions *f*, *g* and p_1 are defined by

$$f(\xi) = \xi\frac{I_0(\xi)}{I_1(\xi)} \tag{A-13}$$

$$g(\xi) = \xi\frac{K_0(\xi)}{K_1(\xi)} \tag{A-14}$$

$$p_1(\alpha) = \frac{\pi\alpha}{2}[K_1(\alpha)L_0(\alpha) + K_0(\alpha)L_1(\alpha)] \tag{A-15}$$

In (A-15), $L_k(\alpha)$ is the modified Struve function,

$$L_k(\alpha) = \sum_{n=0}^{\infty}\frac{(0.5\alpha)^{k+2n+1}}{[n+0.5]![k+n+0.5]!} \tag{A-16}$$

It should be mentioned that for self-impedance calculation (*z*(*k*, *k*)), *H* should be set to zero in (A-6) and $H = 0.2235(h+w)$ in (A-7) where *h* and *w* are the height and the width of the coil cross section.

References

[1] F.J.F. de LIMA, C. Machado Jr., W.S. Pinto, Tucurui's generator step-up transformer failures due to very-fast transients in GIS, in: Proc. Int. Conf. Power Systems Transients (IPST), Seattle, WA, 1997, pp. 285–290.

[2] B. Gustavsen, Study of transformer resonant overvoltages caused by cable-transformer high frequency interaction, IEEE Trans Power Del. 25 (2010) 770–779.

[3] T. Adielson, Å. Carlson, H.B. Margolis, J.A. Halladay, Resonant overvoltages in EHV transformers—modeling and application, IEEE Trans. Power App. Syst. PAS-100 (1981) 3563–3572.

[4] A.S. Morched, L. Martí, R.H. Brierley, J.G. Lacke, Analysis of internal winding stresses in EHV generator step-up transformer failures, IEEE Trans. Power Del. 11 (1996) 888–894.

[5] M. Ikeda, T. Inoue, T. Yanari, *V–t* characteristics and probabilistic distribution of partial discharge and breakdown voltages for transformer insulation, Trans. Inst. Elect. Eng. Jpn. 101-B (1981) 571–578.

[6] B. Gustavsen, A.P. Brede, J.O. Tande, Multivariate analysis of transformer resonance overvoltages in power stations, IEEE Trans. Power Del. 26 (2011) 2563–2572.

[7] A.H. Soloot, H.Kr. Hoidalen, B. Gustavsen, Frequency domain investigation of switching transients in offshore wind farms, in: Proc. IEEE Powertech Conference, Trondheim, Norway, 2011, pp. 1–5.

[8] A.H. Soloot, H.Kr. Hoidalen, B. Gustavsen, The assessment of overvoltage protection within energization of offshore wind farms, J. Energy Procedia 24 (2012) 151–158.

[9] A.H. Soloot, H.K. Høidalen, High frequency modeling of transformers in ATP for investigation of resonances in offshore wind park, in: Porc. EEUG Meeting 2010, European EMTP-ATP Conference, Finland, 2010, pp. 164–175.

[10] T. Abdulahovic, Analysis of high-frequency electrical transients in offshore wind parks (Ph.D. Dissertation), Dept. Energy and Environment, Division of Electric Power Eng., Chalmers University of Technology, Göteborg, 2011.

[11] A.H. Soloot, H.J. Bahirat, H.K. Høidalen, B. Gustavsen, B.A. Mork, Investigation of resonant overvoltages in offshore wind farms-modeling and protection, in proc, in: Intl. Conf. Power Systems Transients (IPST), Canada, 2013.

[12] A.H. Soloot, H.Kr. Hoidalen, B. Gustavsen, A study of switching overvoltages in offshore wind farm, in: Proc. 17th International Symposium on High Voltage Engineering, Paper B-30, Hanover, Germany, 2011.

[13] S.A. Ryder, Diagnosing transformer faults using frequency response analysis, IEEE Electrical Insulation Magazine 19 (2003) 16–22.

[14] C. Bengtsson, Status and trends in transformer monitoring, IEEE Trans. Power Del. 11 (1996) 1379–1384.

[15] E. Hanique, H.F. Reijnders, P.T.M. Vaessen, Frequency response analysis as a diagnostic tool, J. Elektotechniek 68 (1990) 549–558.

[16] T. Leibfried, K. Feser, Monitoring of power transformers using the transfer function method, IEEE Trans. Power Del. 14 (1999) 1333–1341.

[17] J.A. Martinez-Velasco, Power System Transients: Parameter Determination, CRC Press-Taylor and Francis Group, New York, 2010, pp. 222.

[18] S.M.H. Hosseini, M. Vakilian, G.B. Gharehpetian, Comparison of transformer detailed models for fast and very fast transient studies, IEEE Trans. Power Del. 23 (2008) 733–741.

[19] D.J. Wilcox, W.G. Hurley, M. Conlon, Calculation of self and mutual impedances between sections of transformer windings, J. Proc. IEE. C 136 (1989) 308–314.

[20] D.J. Wilcox, M. Conlon, W.G. Hurley, Calculation of self and mutual impedances for coils on ferromagnetic cores, J. IEE Proc. A 135 (1988) 470–476.

[21] M.K. Kazimierczuk, High Frequency Magnetic Component, Wiley, West Sussex, 2009, pp. 186.

[22] S.V. Kulkarni, S.A. Khaparde, Transformer Engineering: Design and Practice, Marcel Dekker, New York, 2004, pp. 286.

[23] E. Bjerkan, High frequency modeling of power transformers—stresses and diagnostics (Ph.D. Dissertation), Dept. Elc. Power. Eng., Norwegian Univ. of Science and Technology, Trondheim, 2005.

[24] E. Rahimpour, Hochfrequente Modellierung von Transformatoren zur Berechnung der Übertragungsfunktion (Dissertation), University of Stuttgart, 2001.

[25] A.H. Soloot, H.K. Hoidalen, B. Gustavsen, Modeling of wind turbine transformers for resonant overvoltage —sensitivity analysis, in: Proc. International Conference on Electrical Machines and Systems 2013 (ICEMS 2013), Busan, Korea, 2013.

[26] A.H. Soloot, H.K. Høidalen, B. Gustavsen, The effect of winding design on transformer frequency response with application on offshore wind farm energization, in: Proc. Int. Conference on Renewable Energy Research and Applications (ICRERA), Nagasaki, Japan, 2012.

[27] A.H. Soloot, H.K. Høidalen, B. Gustavsen, Upon the improvement of the winding design of wind turbine transformers for safer performance within resonant overvoltages, in: Proc. CIGRE Joint Colloquium – SC A2/C4, Zurich, Switzerland, 2013.

[28] J. Lammeraner, M. Stafl, Eddy Currents, Iliffe books Ltd., London, 1966, pp. 21.